POLYDIACETYLENE-BASED SUPRAMOLECULAR SYSTEMS: SYNTHESIS, CHARACTERIZATION, AND APPLICATIONS

by
GİZEM BELİKTAY

Submitted to the Graduate School of Engineering and Natural Sciences
in partial fulfilment of the requirements for the degree of
Master of Science

Sabancı University
July 2023

POLYDIACETYLENE-BASED SUPRAMOLECULAR SYSTEMS: SYNTHESIS, CHARACTERIZATION, AND APPLICATIONS

Approved by:

Approval Date: 26.07.2023

ABSTRACT

POLYDIACETYLENE-BASED SUPRAMOLECULAR SYSTEMS: SYNTHESIS, CHARACTERIZATION, AND APPLICATIONS

GİZEM BELİKTAY

Materials Science and Nano Engineering, MSc Thesis, June 2023

Thesis Supervisor: Dr. Eric Meng Meng Tan

Keywords: Polydiacetylenes, Self-assembly, Supramolecular interactions, Colloidal systems, Food sensor

Polydiacetylenes (PDAs) are useful conjugated polymers for studying supramolecular interactions and sensing applications. External stimuli disrupt the planar conjugated backbone of PDAs, resulting in a blue-to-red color transition and activated fluorescent signal. Modifying diacetylene monomers improved resistance to external triggers through enhanced head group interactions or facilitated the detection of specific molecules, thereby increasing sensitivity. This thesis investigates the covalent attachment of bulky *m*BzA (*m*-amino benzoic acid) and linear DETA (diethylenetriamine) molecules to the carboxylic head group of two DA monomers, namely PCDA and TCDA, with different alkyl tail lengths. Their responses were evaluated under various triggers using self-assembled PDA vesicles, enabling three-dimensional exposure to the stimuli. Testing *m*BzA-substituted PDA vesicles under basic conditions and varying photopolymerization duration revealed decreased sensitivity to high pH with prolonged UV irradiation and allowed reversibility in *m*BzA-functionalized vesicles. Furthermore, DETA-functionalized PDA with a shorter alkyl tail initially produced purple-colored vesicles. The effect of the initial intermediate phase was assessed by comparing monocarboxylic and longer alkyl tail monomers under various external triggers, including acid and alcohol. The intermediate phase promoted the purple-to-red color transition despite being thermodynamically more stable than the blue phase. However, exposure to liquid ethanol and acetic acid vapor resulted in the presence of a small fraction of blue phase in poly(TCDA-DETA) vesicles but not in poly(PCDA-DETA) vesicles, indicating the significant role of inter- and intra-chain interactions in strain release through chain distortion and realignment. Electrospun fibers of DETA-functionalized and

monocarboxylic diacetylenes were employed for solid-phase sensor applications. Food spoilage sources such as wine, milk, and chicken were used. The results revealed that amine-substituted PDA/PEO fibers were affected by the spoilage of those products. However, more in-depth analysis is needed to optimize their response to the actual spoilage of the food products.

ÖZET

POLİDİASETTİLEN BAZLI SUPRAMOLEKÜLER SİSTEMLER: SENTEZ, KARAKTERIZASYON VE UYGULAMALAR

GİZEM BELİKTAY

Malzeme Bilimi ve Nano Mühendislik, Yüksek Lisans Tezi, Temmuz 2023

Tez Danışmanı: Dr. Eric Meng Meng Tan

Anahtar Kelimeler: Polidiasetilenler, Kendiliğinden birleşme, Supramoleküler etkileşimler, Kolloidal sistemler, Gıda bozulma sensörü

Polidiasetilenler (PDA'lar) supramoleküler etkileşimleri ve sensör uygulamalarını incelemek için kullanışlı konjuge polimerlerdir. Dış etkiler, PDA'ların düzlemsel konjuge yapısında bir bozulmaya neden olarak maviden kırmızıya renk geçişi ve floresan sinyali vermesi ile sonuçlanır. Diasetilen monomerlerinin modifikasyonu, güçlendirilmiş baş grup etkileşimleri yoluyla tetikleyicilere karşı hareket direnci geliştirir veya belirli moleküllerin algılanmasını kolaylaştırarak hassasiyeti artırır. Bu tezde, ağır *m*BzA ve lineer DETA moleküllerinin, farklı alkil kuyruk uzunluklarına sahip PCDA ve TCDA olmak üzere iki DA monomerinin karboksilik baş grubuna kovalent bağlanması ve dış etkenlere verdiği cevap çalışılmıştır. Kendiliğinden oluşan PDA vezikülleri kullanılarak üç boyutlu maruz kalma sağlanmış ve bu yapılar çeşitli etkiler altında değerlendirilmiştir. Bazik koşullar altında *m*BzA ile modifiye edilmiş PDA vezikülleri fotopolimerizasyon süresinin de değiştirilmesi ile test edilmiştir. Sonuçlar, uzun süreli UV radyasyonuna maruz kalan PDA'ların yüksek pH'a karşı duyarlılıklarının azalmasının yanı sıra bu veziküllerin tersinir renk değişimi cevabı verdiğini ortaya koymuştur. Diğer taraftan, daha kısa alkil kuyruğuna sahip DETA ile fonksiyonlandırılmış PDA vezikülleri başlangıçta mor renkli görünmektedirler. Başlangıçtaki ara fazın etkisi, asit ve alkol gibi çeşitli dış etkenler altında monokarboksilik ve daha uzun alkil kuyruklu monomerler ile karşılaştırılarak değerlendirilmiştir. Termodinamik olarak mavi faza kıyasla daha kararlı olmasına rağmen, ara fazda mordan kırmızıya renk geçişinin hızlandığı görülmüştür.

Bununla birlikte, sıvı etanol ve asetik asit buharına maruz kalma, poli(TCDA-DETA) veziküllerinde küçük bir mavi faz fraksiyonunun varlığına neden olurken poli(PCDA-DETA) veziküllerinde olmamıştır, bu da zincirler arası ve zincir içi etkileşimlerin zincir bozulması ve yeniden kurulması yoluyla gerinim salınımında önemli rol oynadığını göstermektedir. Katı faz sensör uygulamaları için, DETA ile fonksiyonelleştirilmiş ve monokarboksilik diasetilenlerin elektropsun fiberleri kullanılmıştır. Gıda bozulması deneylerinde şarap, süt ve tavuk kaynakları kullanılmıştır. Sonuçlar, amin modifiyeli PDA/PEO fiberlerinin kırmızı faza döndükleri gözlemlenmiştir. Bununla birlikte, gıda ürünlerinin gerçek bozulmasına tepkilerini optimize etmek için daha derinlemesine analizlere ihtiyaç vardır.

ACKNOWLEDGEMENT

I would like to express my deepest gratitude and appreciation to my supervisor, Dr. Hande Cingil Tan, for her continuous support, imparted experience, and motivation throughout my Master's thesis journey. I consider myself fortunate to have had the opportunity to work with her.

I extend my thanks to my co-advisor, Dr. Eric Men Meng Tan, for his unwavering support and his passion for science, which ignited my enthusiasm for academic pursuits in materials science and physics.

I am sincerely grateful to my committee members, Prof. Dr. Turan Öztürk and Dr. Catherine Hirel Arslan, for generously dedicating their time and interest and providing constructive suggestions, which greatly contributed to the development of my research.

I would like to acknowledge the financial support of the Scientific and Technological Research Council of Turkey (TÜBİTAK) received under the 2232 project (Project No: 118C241). Additionally, I am grateful to SUNUM and FENS members at Sabanci University for their invaluable infrastructure and unwavering support.

I am eternally grateful to Tuçe Fidan, my best friend and companion since our undergraduate years, for her unwavering support, advice, and constant presence in my life. Her friendship has been a tremendous source of strength and comfort.

I extend my gratitude to Pelin Duru for her friendship and the significant impact she has had on my life. Her unwavering support and guidance have helped me navigate challenging times and make important decisions.

I would like to thank Aybüke Özer for her continuous support, friendship, and warmth. Every day, my motivation to come to SUNUM was fueled by the companionship of my deskmates, Yelda Yorulmaz, Ceren Mitmit and Alp Yetişgin. I deeply appreciate their support and for making me feel they will always be by my side.

I am thankful to Tayyaba Shaikh and Emirhan Koca for their boundless support and motivation in scientific endeavors. I am truly grateful to have known them.

I would like to thank Öykü Demirel, Selin Öykü Gündoğdu, Mehmet Can Dursun, my tango partner Sarp Kölgesiz, Sena Yüce, Neslihan Şişman, Mehmet Kahraman, Tuna Alp (who patiently answered my various physics questions and contributed to my love for science), Eda Güney, and Dr. İsmail Fidan (who provided technical knowledge in chemical synthesis) for making SUNUM an enjoyable and educational place.

I express my gratitude to Yeşim Tütüncü, Beril Üstünkaya, Belkıs Güneş, Gülşah Yıldız, and Yasemin Akyol for their unwavering support and guidance, which have been instrumental in my academic journey.

To the members of SU-Mems, including Melih Can Taşdelen, Maryam Gols, Özberk Öztürk, Farid Sayer, Osman Şahin, Saygun Güler, Oğuz Albayrak, honorary member Elif Albayrak, and Irmak Kayalan, I am profoundly grateful for their continuous presence in my life and for being an integral part of the beautiful memories I have accumulated throughout this adventure.

I would like to thank Ekin Özek for the support and encouragement that have profoundly impacted my life, leading to positive changes and expanding my horizons.

I am forever grateful to my lifelong friends who have brought immense happiness and support to my life: Damla Gültekin, Nilay Görgün, Gül Karakoç, Nazlı Temel, Rümeysa Kılıç, Meryem Güneş Erşahin, Ali Kaan Sünnetçioğlu, Mustafa Gayret, Hande Işıl Akçay, Elif Aydoğan, and Burçak Çakar. They have constantly supported me and made me feel their unwavering presence.

Finally, I want to express my boundless love and gratitude to my dear family: my mother, Sibel Beliktay; my father, Abdülgafur Beliktay; and my brother, Deniz Beliktay. Your never-ending support and continuous presence in my life are immeasurable. I am incredibly fortunate to have such a loving family, and I am eternally grateful for your presence in my life. Thank you for always being there for me.

Dedicated to my beloved family

TABLE OF CONTENTS

LIST OF FIGURES

LIST OF TABLES

LIST OF ABBREVIATIONS

Polydiacetylene	: PDA
Highest Occupied Molecular Orbital	: HOMO
Lowest Unoccupied Molecular Orbital	: LUMO
light-emitting diodes	: LEDs
Diacetylene	: DA
Ultraviolet	: UV
gamma ray	: γ
Transmission Electron Microscopy	: TEM
Differential scanning calorimetry	: DSC
N-(3-Dimethylaminopropyl)-N'-ethylcarbodiimide hydrochloride/N-Hydroxysuccinimide	: EDC/NHS
10,12-Pentacosadiynoic acid	: PCDA
meta-aminobenzoic Acid	: *m*BzA
Dietyhelenetriamine	: DETA
Volatile organic compounds	: VOCs
Phenylboronic acid	: PBA
10, 12-tricosadiynoic acid	: TCDA
Hydrochloric acid	: HCl
Polyethylene oxide	: PEO
Fourier-Transform Infrared Spectroscopy	: FTIR
Nuclear Magnetic Resonance	: NMR
UV-Visible Spectroscopy	: UV-Vis
Dynamic Light Scattering	: DLS

Scanning Electron Microscopy	: SEM
N-hydroxysuccinimide	: NHS
Dimethyl sulfoxide	: DMSO
Polytetrafluoroethylene	: PTFE
Dichloromethane	: DCM
Dimethylformamide	: DMF
Potassium hydroxide	: KOH
Polyvinylidene fluoride	: PVDF
Attenuated Total Reflectance	: ATR
Radiofrequency	: RF
Nitrogen	: N_2
standard cubic centimeters per minute	: sccm
Polydispersity index	: PDI
Hydrodynamic Radii	: R_h
Colorimetric response	: CR%
Hydroxide	: OH
Acetic acid	: AA
Ethanol	: EtOH

CHAPTER 1. **INTRODUCTION**

Sensors are necessary tools in various fields, building a bridge between people and the environment. They detect and measure physical, chemical, and biological changes, providing a deeper understanding of processes. Chemical sensors using conjugated polymers are particularly notable due to their rapid response. These polymers, known for their exceptional electrical and optical properties, are widely studied in sensing. Their electron delocalization allows for conductivity or fluorescence changes when exposed to specific stimuli, making them highly versatile for detecting various substances and a favored choice in sensor development.

Among these conjugated polymers, polydiacetylene (PDA) stands out due to its unique chromatic behavior when subjected to environmental changes, including variations in solvent,[1] temperature,[2] ions,[3], and analytes.[4] This property has led to the widespread exploration and application of PDAs in electronic and chemical sensors. Typically, PDAs exhibit a deep blue color once polymerized, which changes to red under stimuli. PDAs own this optical transition to their supramolecular interactions, including hydrogen bonding, π-π stacking, and dispersion forces within its polymeric structure. These non-covalent interactions play a crucial role in the assembly (or re-assembly) and the stability of PDAs. By altering the polymeric backbone of diacetylene (DA) monomers by modifying the hydrophobic tail and the head group (see Figure 1.1), these supramolecular interactions can be studied on their formation and response to various stimuli.

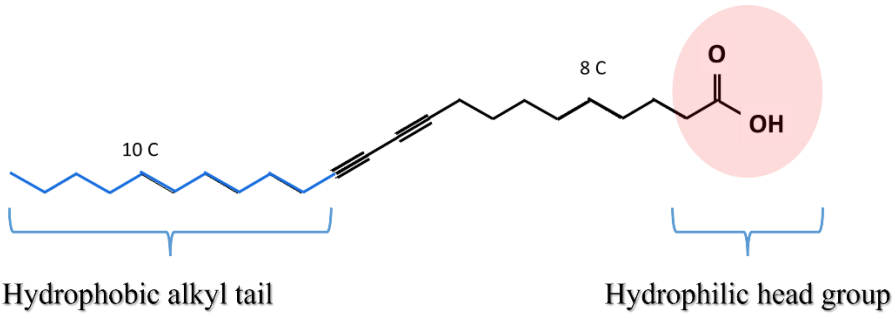

Figure 1.1 Chemical structure of diacetylene monomer

In this master thesis, a comprehensive investigation was conducted on various types of DA monomers prepared by modifying the headgroup structure of DAs having different alkyl tails. These variations were utilized in fine-tuning and understanding the chemical properties of PDA. The self-assembled form in aqueous solutions was predominantly

utilized to explore PDA's response to external stimuli, including acids, solvents, temperature, and pH. The influence of initial conformation on external stimuli was analyzed on amine modified PDA assemblies having different alkyl tails.[5] The photopolymerization dependency and its effect on PDAs having bulky head-group and different alkyl tails under high pH were characterized. Furthermore, along with the vesicle form, fibers were also employed to explore their potential in applied sensor systems. This thesis aims to shed light on the properties and applications of polydiacetylene for potential employment in conjugated polymer-based sensor development.

1.1. Supramolecular Interactions

Supramolecular chemistry deals with the less energetic non-covalent inter- and intra-molecular interactions. Described by Jean-Marie Lehn as "chemistry beyond the molecule"[6], this chemistry field governs many fundamental processes such as self-organization,[7] analyte binding,[8] enzymatic reactions,[9] protein-protein complex assemblies,[10, 11] cellular recognition.[12] Energy range of covalent bonds typically falls within the 100 to 400 kJ mol^{-1}. The secondary noncovalent interactions exhibit relatively weak strengths ranging from less than 5 kJ mol^{-1} to 250 kJ mol^{-1}.[13] These energies are given in the following table.[14]

Table 1. 1. Strengths of several interactions [14]

Type of interaction or bonding	**strength (kJ mol^{-1})**
Covalent bond	100-400
Coulomb	250
Hydrogen bond	10-65
Ion-dipole	50-200
Dipole-dipole	5-50
Cation-π	5-80
π - π	0-50
van der Waals forces	<5
Hydrophobic effects	Difficult to assess
Metal-ligand	0-400

1.2. **Conjugated Polymers**

Conjugated polymers are a class of polymers that exhibit unique electronic properties. The most commonly used conjugated polymers are shown in Figure 1.2. These polymers possess alternating single and double (or triple) bonds in their backbone, leading to π-conjugation. This results in a relatively low energy gap between their highest occupied molecular orbital (HOMO) and lowest unoccupied molecular orbital (LUMO), making them known as semiconductor polymers. Their optical properties allow for specific wavelength absorbance[15] and fluorescent[16] changes, which find applications in fields such as light-emitting diodes (LEDs),[17] photovoltaic cells[18], and sensors[19]. Weak secondary bonds such as π-π stacking and hydrogen bonding play a notable role in emerging those changes. The delocalized π electrons enhance these polymers' electronic and optical characteristics, while secondary interactions contribute to self-assembly, purity, organization, and crystalline structure. By implementing molecular modifications, the supramolecular organization of conjugated polymers can be finely tuned, resulting in control of their physical properties. Due to their weak nature and restricted potential energy surface depth, comprehending the strength and spatial preferences of π-π interactions, hydrogen bonds, electrostatic forces, and hydrophobic interactions is challenging. Therefore, analyzing the response to substituent impact is useful to address this challenge and understand the rational design of supramolecular structures.[20]

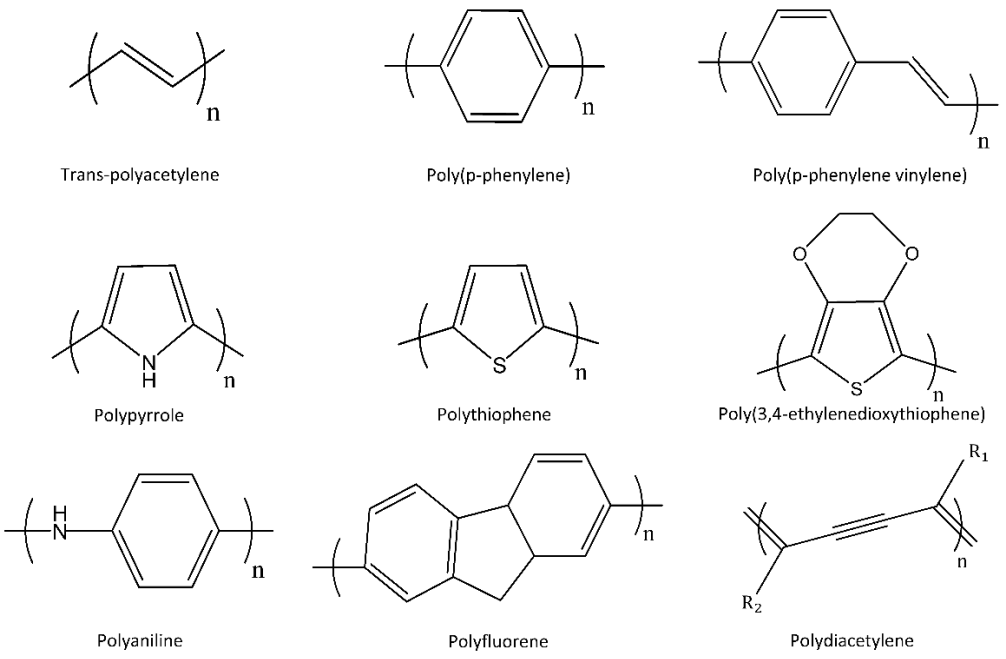

Figure 1. 2 The chemical structures of commonly used conjugated polymers

1.3. **Polydiacetylenes**

PDAs are a class of conjugated polymers that exhibit unique optical properties, making them attractive for applications in colorimetric and fluorometric sensors.[21] These polymers are formed through the self-assembly of amphiphilic DA monomers, forming organized structures with favorable geometric arrangements as shown in Figure 1. 3.[22-24] When exposed to 254 nm UV light, neighboring DA monomers undergo topochemical polymerization via a 1,4-addition reaction, resulting in alternating *ene-yne* polymer chains with a delocalized network of π electrons.[25] The continuous planar arrangement creates overlapping π orbitals, facilitating the movement of loosely bonded π-electrons along the polymeric chain.[26] The delocalization of π-electrons within the PDA structure leads to distinct energy levels known as the HOMO and the LUMO.[27] These energy levels play a crucial role in the electronic behavior of PDAs. The extent of delocalization of the π-electrons determines the effective conjugation length of the polymer chain.[28] The energy gap between the HOMO and LUMO levels falls within the visible spectrum, typically in the orange-yellow region. As a result, PDA exhibits a characteristic blue as a complementary color.[29] The delocalized π-electrons enable efficient charge transport along the polymeric chain, leading to high electrical conductivity.[30]

PDAs exhibit a blue-to-red color transition when exposed to stimuli such as heat,[31] pH,[32] pressure,[33] or chemical[34], and biological[23, 35] recognition events, which the naked eye can easily observe.[36] The blue-to-red color transition is associated with changes in the polymer backbone conformation and is accompanied by a shift in the absorption peak.[37] Red-phase PDAs have an absorption peak at approximately 540 nm.[38] Additionally, blue-phase PDAs are nonfluorescent, while red-phase PDAs exhibit enhanced fluorescence.[39] The on-off fluorescent property can be effectively utilized to detect the presence of an analyte, particularly in biological studies.[40] The polymerization of PDA typically does not require catalysts or initiators, resulting in highly pure materials.[41] PDAs can be fabricated in various forms, including aggregates, films, and powders, through self-assembly processes.[38, 42-44]

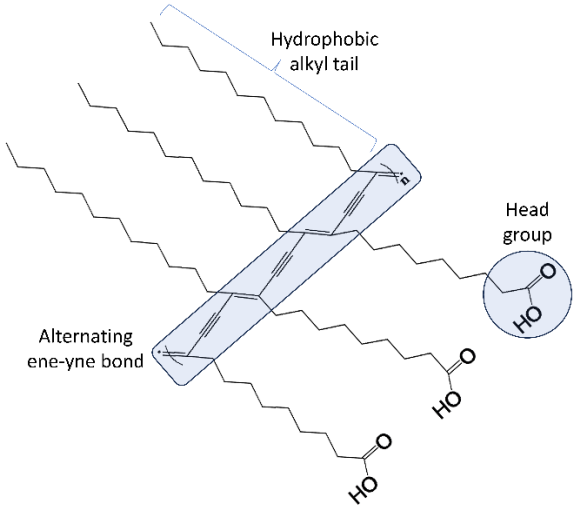

Figure 1. 3 Chemical structure of PDA illustrating the hydrophobic alkyl tail, *ene-yne* bond, and the head group

1.3.1. Self-assembly of DAs and Photopolymerization

The amphiphilic nature of DAs promotes self-assembly through various non-covalent interactions such as hydrogen bonding, π-π stacking, dispersion forces, ionic bonding, and electrostatic interactions.[45] Properly aligned diacetylene monomers with a tilt angle of 45° and a spacing of 5 Å undergo photopolymerization through 1,4 addition reaction under Ultraviolet (UV), gamma ray (γ), or thermal irradiation on various substrates and media as shown in Figure 1. 4.[46-48] These interactions lead to the assembly of PDA molecules into supramolecular ordered structures like films on solid surfaces,[49] vesicles via hydration[50], and blends with other polymers[51]. The resulting polymer has a planar conformity and visible blue color.[46]

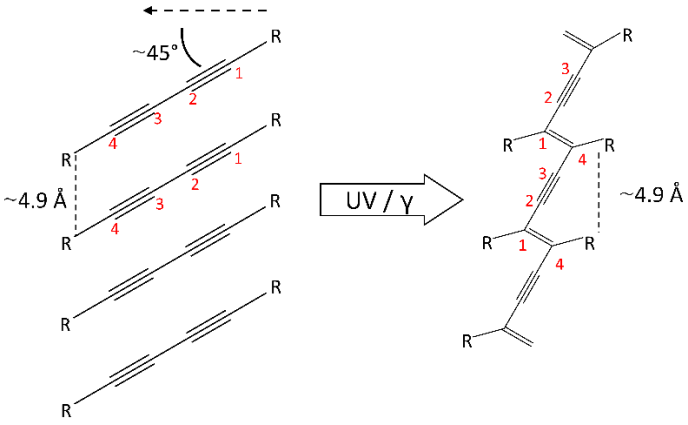

Figure 1. 4 Schematic drawing of 1,4 addition polymerization of PDA

The terms vesicle and liposome are often used interchangeably in the literature. [23] Throughout this thesis, "vesicles" are used. Vesicles are versatile tools due to their straightforward preparation and large volume capacity. Additionally, studying the behavior of vesicles under stimuli allows the evaluation of three-dimensional effects, which can be useful for analysing supramolecular interactions.[34] Bilayer vesicles in an aqueous suspension are obtained by hydrating and sonicating a thin film from dissolved DA monomers above the phase transition temperature.[23] One of the key points is that the ones that properly aligned vesicles can undergo 1,4-addition polymerization upon exposure to UV or γ irradiation, yielding colored solutions.[23, 52] Figure 1.5 illustrates DA lipid monomer, 2D and 3D versions of the polymer vesicle. The absorption of light by vesicles is at different characteristic wavelengths, such as ~640 nm (yielding blue color) and ~540 nm (yielding red color), depending on their length of planarity.[52] Other addition types, 1,2- or 1,3- addition, inhibit photopolymerization. Polymerization of the hydrated bilayer structure remains intact following UV irradiation, as evidenced by Transmission Electron Microscopy (TEM) images,[52, 53] which demonstrated that the integrity of monomeric vesicles is unaffected by exposure to UV light.[54] The self-assembly behavior of monomeric vesicles, as well as the following photopolymerization, are determined by the architectural characteristics of the lipid diacetylenes, which are governed by various non-covalent interactions.[52, 55] Several studies utilized H^+ ions to enhance the efficiency of polymerization by contributing to the correct spatial arrangement.[36, 56, 57]

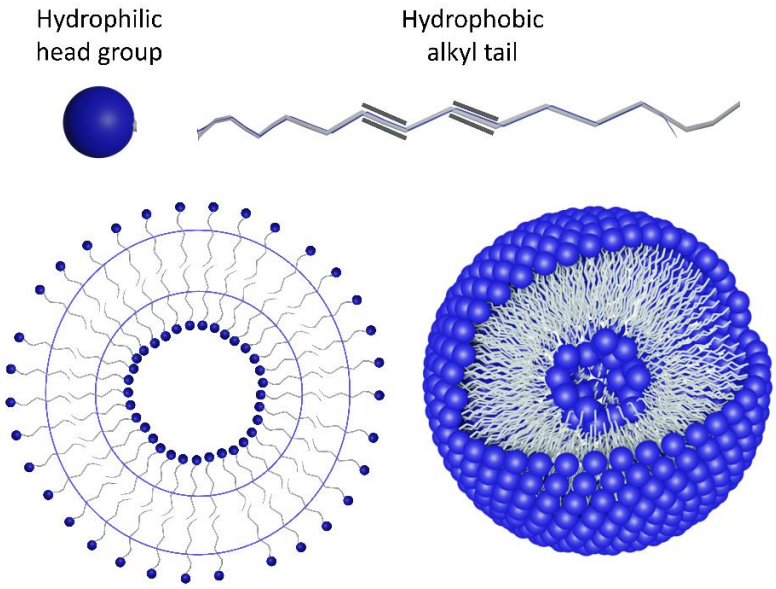

Figure 1. 5 Schematic drawing of an aliphatic DA monomer, 2D and 3D illustration of polymer vesicles

1.3.2. **Molecular recognition and color change mechanism**

PDAs exhibit color change properties driven by the conformational transition and therefore changes in effective conjugation length.[58] The low energy gap between HOMO and LUMO relies on the uninterrupted planarity of the polymer repeating units, determining the effective conjugation length and optical absorption properties.[59] When the polymer is exposed to an external stimulus, the structural arrangement of the backbone transforms from a planar to a twisted ribbon-like structure while creating disorders in conjugation, as shown in Figure 1. 6.[5] In this conformation, the energy gap increases. Hence, the absorption occurs in shorter wavelengths accompanied by a visible color change from blue to red.[46, 48] Additionally, while the rigid planar conformation exhibits no fluorescence, the transition to a semi-rigid twisted backbone gives a fluorescence signal. The disordered structure creates new states where excitons can relax, generating a fluorescent signal. [36, 40, 51, 60]

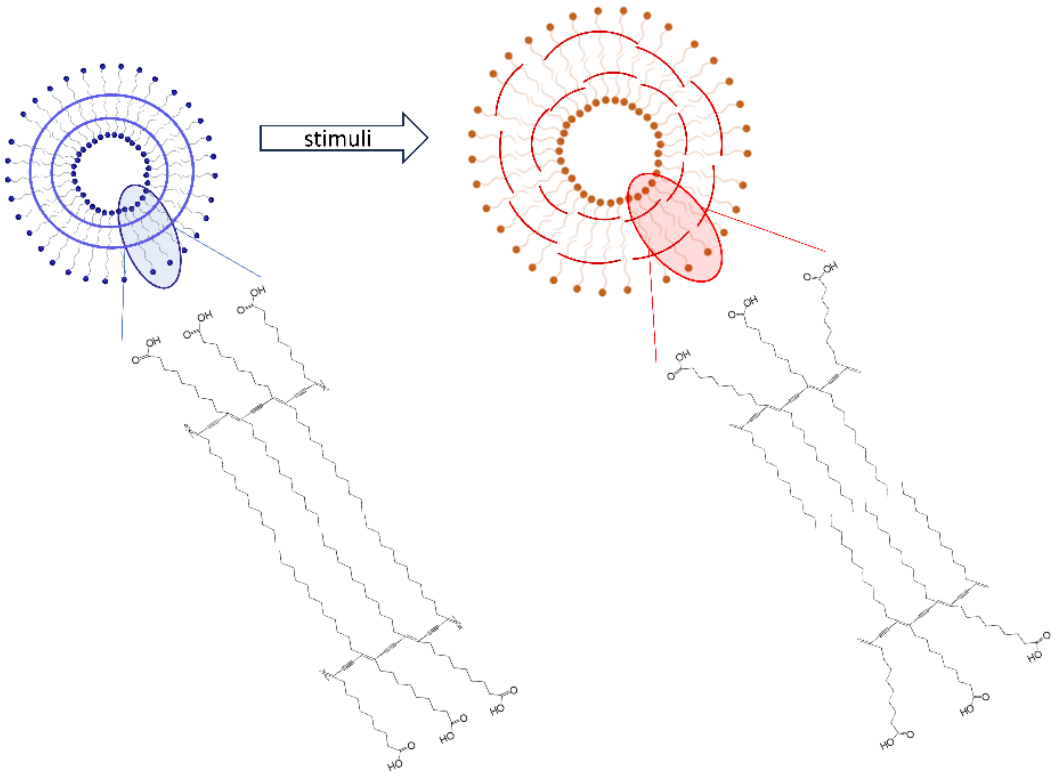

Figure 1. 6 Schematic drawing of blue-to-red conformation transition

1.3.3. Variations in diacetylene monomers

1.3.3.1. Variations in alkyl chain (tail) length

PDAs are amphiphilic molecules with an alkyl spacer positioned between the head group and the diacetylene moiety and an alkyl tail on the hydrophobic side.[61] These spacers play a significant role in inter and intra-chain interactions, ultimately determining the nature of color transitions exhibited by PDAs. Notably, a decrease in the length of the alkyl tail significantly impacts the behavior of polydiacetylenes due to reduced dispersion forces, specifically interchain interactions. It is worth mentioning that the presence of strong head group interactions can render the difference in alkyl tail length negligible, thus resulting in reversible thermochromism of PDA vesicles.[62] Conversely, weak interactions between the head groups amplify the effects of alkyl tail length on the behavior of PDAs under external stimuli, such as temperature or alcohol.[61, 63, 64] The pronounced influence of alkyl tail length on PDAs can be attributed primarily to decreased dispersion forces between the hydrophobic alkyl side, resulting from fewer alkyl chains.[64, 65] In the context of the thermochromic transition, melting plays a pivotal role, as it impacts the flexibility of conformation and subsequent structural rearrangement.[63] Differential scanning calorimetry (DSC) analysis of PDA vesicles with varying alkyl tail segments, both in the hydrophobic region and between the diacetylene moiety and the head group, further supports this notion by demonstrating that shorter alkyl tails yield reduced melting temperatures.[64] These dependencies are closely tied to the alkyl tail in the hydrophobic section. Furthermore, the alkyl segment connecting the hydrophilic head group and the diacetylene moiety, i.e., the alkyl side bonded to the head group, also affects PDAs' packing and transition behavior.[66] In this thesis, two common diacetylene monomers were utilized: 10,12-Tricosadiynoic acid (TCDA) and 10,12-Pentacosadiynoic acid (PCDA) having 23 and 25 carbon, respectively (see Figure 1.7).

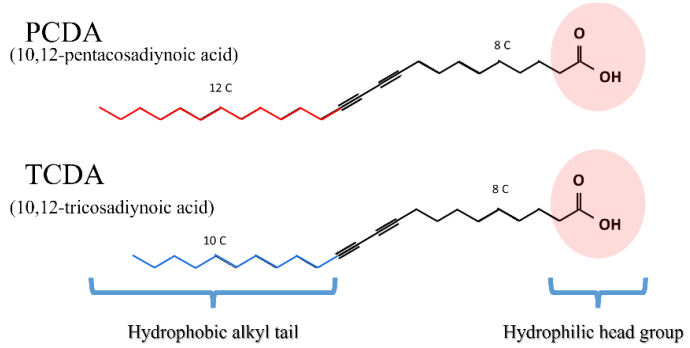

Figure 1. 7 Chemical structures of diacetylene monomers used in this thesis

1.3.3.2. Variations in head group

Diacetylenes provide a versatile platform for functionalization, allowing for the customization of their properties for various applications.[67] Functionalization strategies for target-specific recognition include amide bond formation using EDC/NHS coupling[60, 68] or acyl chloride[62]. The reaction mechanisms are shown in Figures 1. 6 and 1. 7. Esterification reactions with hydroxyl groups expand the versatility of diacetylenes, while solid-phase peptide synthesis is employed for incorporating peptide segments. Functionalization of diacetylenes offers a tailored approach to create receptors, capture biomolecules, detect ions, and achieve reversibility in PDAs.[44]

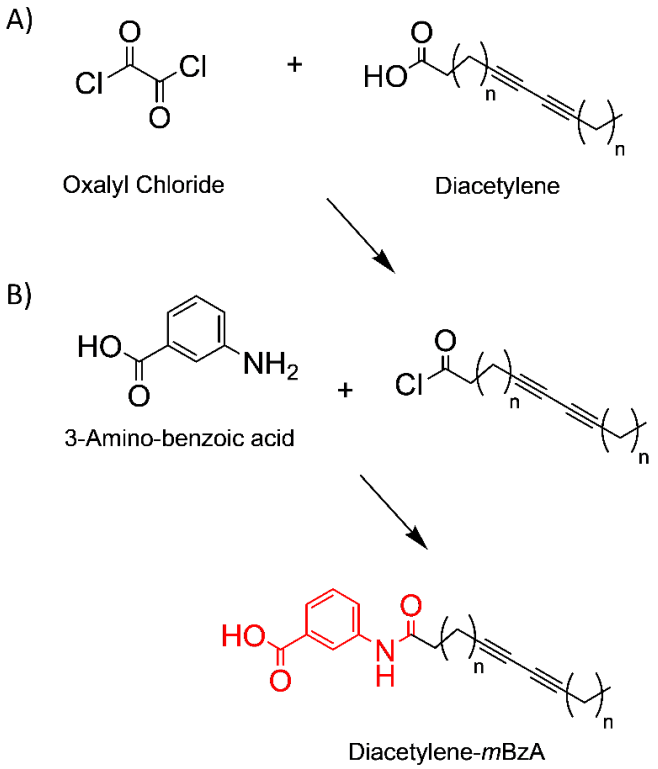

Figure 1. 8 Acyl chloride (A) and -*m*BzA (B) substitution of diacetylene monomer

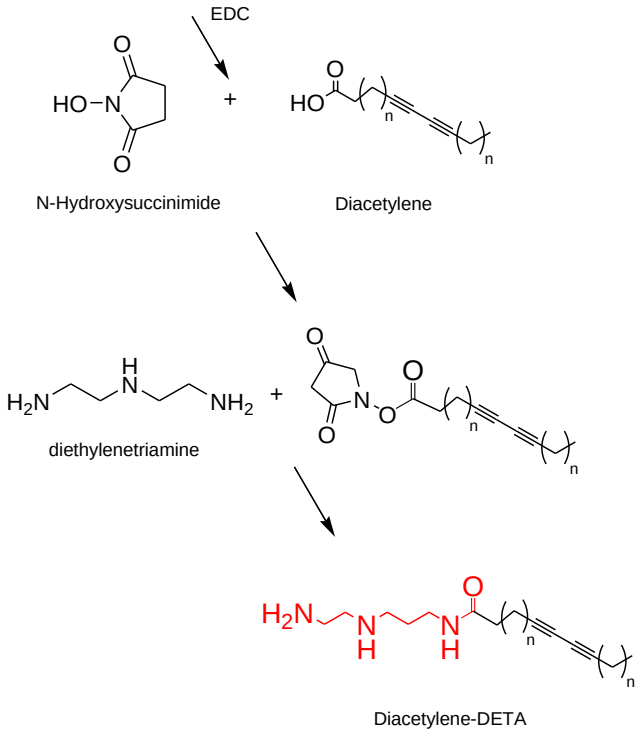

Figure 1. 9 NHS-EDC coupling (A) and DETA (B) substitution of diacetylene monomer

1.3.4. **Polydiacetylene-Based Sensors and Applications**

PDAs exhibit color change to various stimuli such as solvents [61, 65, 69] and VOCs [23], temperature [28, 63, 70-73], pH [74], and various analytes [40, 46, 75]. One of the most studied stimuli affecting the behavior of PDAs is temperature. The double and triple bonds in the side chain induce a strain on the PDAs backbone, preventing the chain's movement. Increasing temperature relieves the strain on the backbone and enhances chain mobility. While analyte detection dominantly depends on the head group function, all PDAs respond to an increase in temperature with a conformation transition, namely a blue-to-red transition.[31] The head group functionality affects the hydrogen bond network, which could generate either an earlier or later response to increasing temperature.[76] Additionally, in applications requiring a reversible response, reversible thermochromic polydiacetylene (PDA) forms can be achieved through nanoparticle introduction,[28, 71, 77-79] head group modification, [31, 80-83] and photopolymerization duration change [84] are employed to obtain reversible thermochromic PDA forms.

Substituting the carboxylic head group of commercial PDAs with other functional head groups allows the detection or enhances the sensitivity towards various analytes and ions. For example, modification of diacetylene monomer with phenylboronic acid (PBA) induced higher sensitivity to hydrogen peroxide than the commercial ones.[85] Structural

modifications that enhance hydrogen bonding can tune the pH response.[36, 56, 80, 86]

Observing colorimetric and fluorescent transitions of a molecule upon exposure to an organic solvent is called solvatochromism. Identifying or differentiating an organic solvent from a medium is important in various chemical, biological, and industrial processes [87]. The solvatochromism of polydiacetylenes depends on the polarity of the solvent to which they are exposed. Although the functionalization of the headgroup allows for making customized PDA-based materials, the development of solvent-specific PDA materials possess a challenge[22], except for several examples[1, 88]. Nevertheless, the structural variations in solvents affect the conformational change of polydiacetylenes, thereby leading to alternative approaches to differentiate the colorimetric changes.[22, 87, 89, 90] For instance, smartphone applications [91] and sensor arrays [92] have been employed as strategies to build a solvent fingerprint database. Also, different forms of PDAs are used to enhance their applicability.[93] Additionally, studying the effect of different solvents could be useful for understanding the structural mechanism of color change and supramolecular interactions.[61, 65, 94, 95]

Conjugating target receptors to diacetylene moieties opens possibilities for the analytical detection of biological molecules.[23] Several reviews on this concept highlight the opportunities that PDA-based materials offer.[22, 35, 96, 97] After the first report of sialic acid-modified PDA-based sensors for detecting influenza, various strategies have been employed for applicable diagnostics.[23, 98, 99] By various functionalization routes, the living organism, protein, or the releasing products could be detected.[35]

CHAPTER 2. MATERIALS AND METHODS

This section provides information on the materials and methods employed in this thesis. Commercial diacetylene monomers, TCDA and PCDA, with alkyl tail lengths of 23 and 25 carbons, respectively, were employed in this research. Their carboxylic terminal groups were altered to obtain monomers with functional groups, *meta*-aminobenzoic acid (*m*BzA) and diethylene triamine (DETA). The preparation of monomer vesicles and photopolymerized vesicles is given in detail.

The polymeric vesicles are then subjected to various stimuli depending on their head group. Hydrochloric acid (HCl), acetic acid, and ethanol in liquid and vapor forms were used on DETA-modified PDA vesicle solutions. The *m*BzA-substituted PDA vesicles were exposed to high pH conditions and extended UV irradiation.

Furthermore, DETA-functionalized diacetylene monomers were used for PDA-based composite electrospun fibers where polyethylene oxide (PEO) served as a matrix polymer. The solution preparation and electrospinning process were described. Real-time food spoilage experiments were conducted using wine, milk, and chicken, along with the vapor phase of ethanol and acetic acid exposure. The effect of humidity was also evaluated on the deterioration of fibers.

The principles of the characterization tools employed in this study are briefly explained. Monomer modification was confirmed by using Fourier-Transform Infrared Spectroscopy (FTIR) and Nuclear Magnetic Resonance Spectroscopy (NMR) characterization methods. UV-Visible Spectroscopy, Fluorescence and Dynamic Light Scattering spectroscopy (DLS) tools were used to monitor the optical and structural changes in PDA vesicles. FTIR characterization was performed to study molecular transitions and Scanning Electron Microscopy (SEM) images were captured to analyze morphological changes in the electrospun fiber mats. Finally, photos were recorded to highlight the visual monitoring of the colorimetric response of PDAs.

1.4. Materials

PCDA (10,12-Pentacosadiynoic acid), TCDA (10,12-Tricosadiynoic acid), N-hydroxysuccinimide (NHS), diethylenetriamine (DETA), oxalyl chloride, tetrahydrofuran, anhydrous tetrahydrofuran, acetic acid, dimethyl sulfoxide (DMSO), polyethylene oxide (PEO) and polytetrafluoroethylene (PTFE) filters (0.45 μm) were purchased from Sigma-Aldrich. 1-(3-(dimethylamino)propyl)-3-ethylcarbodi-imide

hydrochloride (EDC-HCl) was purchased from TCI. Chloroform, ethanol, and diethyl ether were purchased from Isolab Chemicals. Dichloromethane (DCM), anhydrous dichloromethane, dimethylformamide (DMF), and methanol were purchased from Scharlab. Hydrochloric acid (HCl) was purchased from Carlo Erba Reagents. Triethylamine, acetone, and potassium hydroxide (KOH) were purchased from Merck. 3-aminobenzoic acid (*m*BzA) was purchased from AlfaAesar. polyvinylidene fluoride (PVDF) filters (0.45 μm) were purchased from Whatman. All chemicals were used as received unless otherwise stated. Milli-Q water (18.2 Ω) was used as an ultrapure water source.

1.5. Synthesis of diacetylene monomers

This thesis used two end group types to modify the diacetylene monomers: diethylenetriamine (DETA) to see the effect of additional H-bonding due to polyamine groups and *meta*-aminobenzoic acid (*m*BzA) to see the effect of a bulky aromatic head group on structural changes.

1.5.1. Functionalization with *meta*-aminobenzoic Acid (*m*BzA)

Modification of PCDA: The carboxy-substituted anilido diacetylene, PCDA-*m*BzA (3-(pentacosa-10,12-diynamido) benzoic acid) monomer was obtained by slightly altering an earlier protocol. First, PCDA (100.5 mg, 0.27 mmol) was dissolved in 4 mL of anhydrous DCM in a round-bottom flask wrapped up with aluminum foil to provide a dark environment in the reaction vessel. The solution was flushed with nitrogen before adding oxalyl chloride (300 μl) and anhydrous DMF dropwise. The reaction mixture was refluxed under nitrogen and stirred overnight at 45°C. DCM was evaporated via a rotary evaporator to concentrate the solution. The resulting product (PCDA-Cl) was dissolved in 1 ml of anhydrous DCM and combined separately with 3-amino benzoic acid (45.1 mg, 0.33 mmol) in 3 ml of anhydrous THF. Then, the reaction mixture was stirred at room temperature under nitrogen for 24 hours after adding 300 μl of triethylamine. The solvents were evaporated via a rotary evaporator before the product (PCDA-*m*BzA) was fully redissolved in 2.5 ml of THF. To purify PCDA-*m*BzA, a solution mixture containing methanol, acetone, 0.1 M HCl, and Milli-Q (1:1:1:1) volume ratio was prepared. The product was dispersed in 40 ml of this mixture and then centrifuged. After repeating this process 3 times, the precipitate was collected and dried in a vacuum oven at 45°C. Finally,

the monomer was stored in a glass vial wrapped in aluminum foil at 4°C. (PCDA-*m*BzA, 48.6 mg). 13C NMR (176 MHz, DMSO-d6, 295 K): δ= 174.51, 171.92, 171.48, 167.21, 139.50, 131.22, 128.92, 123.75, 123.03, 119.71, 78.01, 77.99, 65.36, 36.71, 36.41, 34.76, 33.66, 32.34, 31.33, 29.03, 28.97, 28.88, 28.74, 28.69, 28.63, 28.53, 28.40, 28.36, 28.34, 28.22, 28.20, 28.18, 27.73, 27.70, 25.04, 24.67, 24.48, 22.13, 18.29, 18.28, 13.99. ^{1}H NMR (700 MHz, DMSO-d6, 295 K): δ= 10.05 (s, 1H), 8.22 (s, 1H), 7.81 (d, 1H), 7.59 (d, 1H), 7.40 (t, 1H), 2.27-2.18 (m, 6H), 1.60-1.23 (m, 32H), 0.85 (t, 3H) ppm.

Modification of TCDA: The same method was used to convert TCDA into TCDA-*m*BzA (3-(tricosa-10,12-diynamido) benzoic acid), yielding 56.3 mg. 13C NMR (176 MHz, DMSO-d6, 295 K): δ= 174.51, 171.92, 171.53, 171.44, 167.20, 139.55, 139.45, 131.19, 128.92, 123.75, 123.09, 122.99, 119.75, 119.66, 78.01, 65.36, 36.71, 36.41, 36.36, 34.76, 33.65, 32.34, 31.32, 29.03, 28.94, 28.90, 28.80, 28.79, 28.73, 28.69, 28.62, 28.52, 28.41, 28.36, 28.22, 28.19, 27.73, 27.71, 25.04, 24.67, 24.48, 22.12, 18.28, 13.99. ^{1}H NMR (700 MHz, DMSO-d6, 295 K): δ= 10.05 (s, 1H), 8.22 (s, 1H), 7.81 (d, 1H), 7.59 (d, 1H), 7.40 (t, 1H), 2.27-2.18 (m, 6H), 1.60-1.23 (m, 30H), 0.85 (t, 3H) ppm.

1.5.2. Functionalization with diethylene triamine (DETA)

***Modification of PCDA*:** Firstly, PCDA was converted to PCDA-NHS (pentacosa-10,12-diynoic acid 2,4-dioxo-pyrrolidin-1-yl ester) by using a slightly different method.1, 2 A round-bottom flask containing PCDA (100 mg, 0.27 mmol) dissolved in 3 mL of DCM was wrapped up with aluminum foil to a dark environment. The solution was flushed with nitrogen before adding NHS (50 mg, 0.43 mmol) and EDC (104 mg, 0.54 mmol) dissolved in 5 mL of DCM in a separate flask. The reaction mixture was stirred overnight, and then the DCM was removed by evaporation under nitrogen. The resulting product was extracted using diethyl ether and washed with water three times. The diethyl ether was removed, and the remaining substance was dried at room temperature in a vacuum oven overnight to give 60.6 mg of PCDA-NHS, yielding 40.4%.

Then, PCDA-NHS (60.6 mg, 0.13 mmol) was dissolved in 8 mL of DCM, followed by dropwise addition of 1 mL of DETA. The mixture was stirred overnight. The solvent was then removed using a nitrogen stream. The resulting product was extracted with diethyl ether, washed with water three times, and dried at room temperature. Finally, the product was placed in a vacuum oven, resulting in the formation of N-(2-(pentacosa-10,12-diynoyloxy) amino) ethyl) ethane-1,2-diamine (PCDA-DETA) with a yield of 169.7 mg.

(PCDA-DETA) (169,7 mg).[13]C NMR (125 MHz, CDCl3): δ= 173.43, 65.36, 52.03, 48.70, 41.80, 39.24, 37.25, 36.95, 32.92, 32.07, 30.18, 29.85, 29.63, 29.50, 29.40, 29.33, 29.25, 29.08, 29.02, 28.92, 28.51, 28.45, 25.88, 22.84, 19.35, 14.27 ppm. [1]H NMR (500 MHz, CDCl3): δ= 3.33-3.37 (q, 3H), 2.66-2.82 (t, 6H), 2.15-2.25 (m, 6H), 1.25-1.58 (m, 30H), 0.84-0.89 (t, 3H) ppm.

***Modification of TCDA*:** The same method was used to convert TCDA into TCDA-NHS and then into TCDA-DETA (N-(2-(tricosa-10,12-diynoyloxy) amino) ethyl) ethane-1,2-diamine), which gave a yield of 142.7 mg. 13C NMR (126 MHz, CDCl3): δ= 173.43, 65.52, 52.03, 48.70, 45.48, 41.79, 39.23, 36.95, 32.04, 30.20, 29.86, 29.71, 29.63, 29.45, 29.40, 29.33, 29.25, 29.08, 29.01, 28.92, 28.51, 28.45, 25.88, 22.83, 19.34, 14.27 ppm. 1H NMR (500 MHz, CDCl3): δ= 3.33-3.37 (q, 3H), 2.66-2.82 (t, 6H), 2.15-2.25 (m, 6H), 1.25-1.59 (m, 30H), 0.83-0.89 (t, 3H) ppm.

1.6. Equipment

Rotary Evaporator: The rotary evaporator functions by lowering the boiling temperatures of solvents under low pressure and selectively removing solvents from mixtures. A rotating flask in the heat bath enhances the surface area of the solvent and ensures even heat distribution along the flask wall. Because of these characteristics, the rotary evaporator is a significant solvent extraction and purification instrument in various study domains. In this thesis, Heidolph-Vap Core is used.

***UV Lamp* Source:** UV Lamp has two different wavelengths, 254 nm and 361 nm, corresponding to UVC and UVB radiation, respectively. These two wavelengths are specific regarding their capabilities for various biological tools. The photopolymerization of PDAs was achieved at 254 nm exposure with CAMAG ® UV Cabinet 4 (8 W).

ATR-FTIR: Fourier-Transform Infrared Spectroscopy (FTIR) is a versatile analytical technique used to detect the vibrational modes of molecules. Molecules have their vibrations, including stretching, bending, and scissoring. By applying Fourier Transforms to analyze the specific frequencies a substance absorbs, the vibrational modes are identified, enabling the determination of the functional groups and chemical bonds present. Typically, these vibrational modes are between 4000 and 400 cm^{-1}.[100] Attenuated Total Reflectance (ATR) is an accessory for FTIR to measure samples such as liquids. The high-refractive-index crystal enables multiple reflections of IR radiation to reach the sample and minimizes the amount of sample required for analysis.[101] In this thesis, Shimadzu, IRAffinity-1S equipped with an ATR accessory from Pike Technologies is

used. All the ATR-FTIR spectra were recorded over the 4000-1000 cm^{-1} range with a resolution of 4 cm^{-1} and 20 total scans.

NMR: Nuclear Magnetic Resonance (NMR) is an analytical tool for studying atomic nuclei. It measures the magnetic field of nuclei by aligning their spins in the presence of a strong magnetic field. Appling radiofrequency (RF) pulses causing transitions of nuclei to different energy states. Then returning to their original alignment emits a signal in RF which is detected and analyzed. NMR is commonly used in organic chemistry to validate the synthesis and identify the structure of molecules. Two main protons are concerned, 1H and 13C, to identify the chemical shifts in the samples.[102] In this thesis, 1H NMR and 13C NMR spectra were recorded on a Bruker AVANCE NEO 700 NMR Spectrophotometer.

UV-Vis: UV-Visible Spectroscopy is a popular analytical technique for determining the optical characteristics of materials in the ultraviolet and visible light ranges. The Beer-Lambert rule, which relates the absorbance (A) of light to the concentration (c) of the material, the path length (l) of the sample holder cuvette, and the molar absorptivity (ε) of the material, is the fundamental principle of UV-Vis spectrometry. UV-Vis spectroscopy is frequently used to determine the concentration of solutes in solution, the presence of nanoparticles and molecules and for sensory applications where the material's optical property changes with stimuli. Furthermore, since the absorption spectrum reflects the energies of electronic transitions, UV-Vis spectroscopy can be used to analyze the electronic structure of materials.[103] In this thesis, the UV-Vis absorption spectra were collected using a PG Instruments T80+ spectrophotometer for monitoring the optical response of PDA-based vesicles.

Fluorescence Spectroscopy: Fluorescence spectroscopy measures the electromagnetic radiation emitted by the molecule in an excited state when irradiated with light. The fluorescence signal is one of the photoluminescence events that is the emitted radiation from a singlet state when the molecule absorbs a specific energy. The emitted light has a longer wavelength compared to absorbed light. Fluorescence has many practical advantages in various fields. For instance, monitoring the fluorescence intensity changes is used to understand and control the detection or activation of biological samples.[104] The fluorescence emission measurements were performed on a Shimadzu RF-6000 fluorescence spectrometer.

DLS: Dynamic Light Scattering (DLS) was employed as a characterization method to determine the size of colloidal particles within a solution. By illuminating the sample with

laser light, the instrument analyzes the particles' behavior in the solution, particularly their Brownian motion. Based on this analysis, the instrument generates a size distribution profile that provides information about the intensity, volume, and number of particles.[105] In this thesis, DLS experiments were conducted using the Malvern Zetasizer NANO ZS apparatus at an angle of 173°, with a 633 nm laser, to monitor the changes in size and distribution profiles of the PDA vesicles under the influence of external stimuli.

SEM: Scanning Electron Microscopy (SEM) is a useful tool to visualize the surface features of samples closely. A primary electron beam interacts with the specimen, creating secondary and backscattered electrons within the interaction volume. The secondary electrons are emitted from a few tens of nanometers which gives information about surface morphology.[106] In this thesis, Leo Supra 35VP is used and operated at 15 kV for imaging PDA-PEO electrospun fibers. Before SEM measurements, all fibers were coated with gold-palladium (Au/Pd) coating of 3 layers using Cressington Sputter Coater.

1.7. Methods

1.7.1. Polymerization

Vesicle preparation: The vesicles were prepared by hydrating the dissolved diacetylene monomers in an appropriate solvent, followed by sonication. Specifically, a nitrogen (N_2) purging process was employed to obtain a thin white film at the bottom of a glass vial from the dissolved diacetylene monomers. Milli-Q water at 80°C was added, and the resulting solution was sonicated for one hour at 80°C. The amount of Milli-Q water was adjusted to obtain a concentration of 1 mM. A 0.45 μm syringe filter was utilized to prevent agglomeration between the dissolving and solvent evaporation steps. The vial was covered with aluminum foil to ensure darkness and prevent undesired photopolymerization. Following the sonication step, the glass vials were kept at 4°C overnight to facilitate the formation of monomeric vesicles. The next day, the solutions were directly transferred to a glass petri dish and exposed to a 254 nm UV light source for a definite period (the UV exposure duration was varied for *m*BzA-substituted diacetylenes, and for fixed at 10 minutes for DETA-substituted diacetylenes). The solvents and the type of filters used in this study are summarized in Table 2.

Table 2. 1. Solvents and type of filters used during vesicle preparation.

Monomer	Solvent	Filter
PCDA	THF	0.45 μm PVDF

TCDA	Ethanol	0.45 μm PVDF
PCDA-*m*BzA	DMSO	0.45 μm PTFE
TCDA-*m*BzA	DMSO	0.45 μm PTFE
PCDA-DETA	Chloroform	0.45 μm PVDF
TCDA-DETA	Chloroform	0.45 μm PVDF

Electrospun Fibers: The electrospinning procedure involved the direct mixture of the DA monomer and PEO matrix. The DA monomers were dissolved in chloroform and subsequently mixed with the PEO matrix polymer, also dissolved in chloroform. The mixing ratio was maintained at a mass ratio of 7.2:1 for PEO to DA. The solution was stirred overnight before the spinning process to ensure homogeneity. The electrospinning parameters were set as follows: an applied voltage of 25 kV, a solution flow rate (injection speed) of 0.5 ml/h, and a distance of 15 cm between the needle tip and the aluminum foil substrate. The monomers PCDA, TCDA, PCDA-DETA, and TCDA-DETA were utilized in this study. After unpolymerized DA-containing PEO fibers are obtained, the fiber mat is exposed to UV irradiation at 254 nm for 10 minutes and blue-colored fiber mats are obtained from poly(PCDA)-PEO, poly(TCDA)-PEO, and poly(PCDA-DETA)-PEO whereas poly(TCDA-DETA)-PEO showed a hue characterized by a combination of purple and blue tones.

1.7.2. Exposure Experiments

Liquid Exposure Experiments: The *m*BzA functionalized PDA vesicles were subjected to high pH conditions. A titration process was employed using solutions of 0.05 M, 0.1 M, and 0.5 M KOH to obtain high pH values. For the PDA-DETA vesicle solutions, the titration was performed using either 0.1 M HCl or 0.1 M acetic acid until the desired acidic pH level was reached. They were also exposed to excess ethanol by adding 600 μL of absolute ethanol to 200 μL (1 mM) of PDA vesicle solution. The same procedures were conducted in all experiments on monocarboxylic poly(PCDA) and poly(TCDA) samples to compare the head group functionality.

Vapor Exposure Experiments: The vapor from a volatile liquid was generated with a vapor delivery setup consisting of a 15 cm glass bubbler, a mass flow controller (GMC1200, Atovac), an N_2 stream (99.9%) regulated to 1.5 bar pressure, tubes, and a syringe. 10 ml of liquid solvent (ethanol or acetic acid) (99.9%) was prepared and placed inside the glass bubbler. The output of the bubbler was connected to a syringe via a tube.

PDA solutions were exposed to solvent vapor by inserting a needle. With the help of nitrogen as the carrier gas, solvent vapor from the bubbler was directed to the PDA solution inside a plastic microcentrifuge vial. A mass flow controller controlled the input flow of nitrogen at 50 standard cubic centimeters per minute (sccm). Solvent vapor continued to flow into the sample for 5 and 10 minutes for acetic acid and ethanol vapors, respectively. The same procedure was applied for ethanol and acetic acid exposure to PDA-PEO electrospun fibres.

Food Spoilage Experiments: Wine, milk, and chicken were employed as the test materials. For the milk and wine spoilage experiments, glass vials containing milk and wine were used with fibers cut in 1 cm x 1 cm dimensions and stuck to the inner side of each vial's lid. The lids were subsequently closed, and the fibers were monitored periodically for over two days. Photos were recorded at definite time intervals, and FTIR spectra was used to assess the structural changes.

Regarding the chicken spoilage experiment, a fresh chicken and a humidity sensor were placed in a chamber. PDA-PEO fibers in 1 cm x 1 cm dimensions were cut and attached to the inside of the lid. Photos were recorded at definite time intervals by using a digital camera. The experimental setup is given in Figure 2.1.

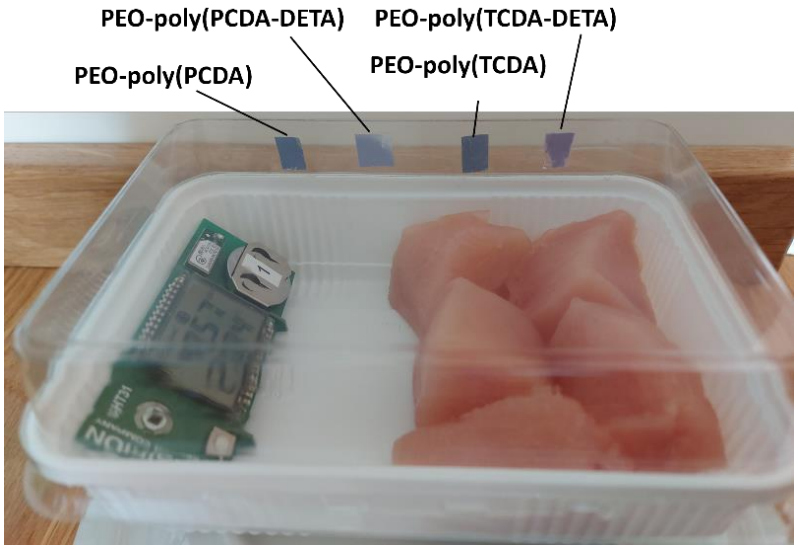

Figure 2. 1. Experimental setup to detect chicken spoilage with PDA-based colorimetric sensors.

CHAPTER 3. PDAs with *m*BzA HEAD GROUP

This chapter presents the photopolymerization time influence on mBzA-substituted PDA vesicles and their response to high pH conditions. Firstly, the head group modification of diacetylene monomers is evaluated by NMR and FTIR spectra. Then, PDAs prepared at different photopolymerization durations were evaluated for their high pH response, structural changes and reversible colorimetric response. Methods such as UV-Visible and fluorescence spectroscopy were employed to monitor optical responses. Dynamic light scattering is used to evaluate the change in the polymer vesicle sizes prepared at different photopolymerization durations and after exposure.

1.8. Characterization of *m*BzA-DA Monomers

The proton nuclear magnetic resonance spectroscopy (^{1}H NMR) and the carbon nuclear magnetic resonance (^{13}C NMR) spectroscopy are employed to evaluate the protons of substituted functional groups of *m*BzA to diacetylene monomers.

The ^{1}H NMR spectra of PCDA-*m*BzA are provided in Figure 3. 1**Figure 3. 1**. **Figure 3. 1** ^{1}H NMR spectrum of PCDA-*m*BzA with the interval 7.4 – 12.0 ppm as an inset.The distinctive protons associated with PCDA are observed at chemical shift values of δ 0.85 ppm, δ 1.60-1.23 ppm, and δ 2.27-2.18 ppm, which correspond to a triplet signal arising from the hydrophobic tail end, multiplet signals from the alkyl chain, and multiplet signals from protons close to the C=O bond and diacetylene moiety, respectively. The emergence of new peaks within the range of δ 7.40 ppm to δ 12.0 ppm confirms the occurrence of chemical bonding between the *m*BzA functional group and PCDA. The terminal carboxylic acid proton appears as a singlet at δ 10.05 ppm. The proton of the secondary amide appears as a singlet at δ 8.22 ppm. Lastly, the peaks observed as a doublet, doublet, and triplet at δ 7.81 ppm, δ 7.59 ppm, and δ 7.40 ppm, respectively, can be attributed to the benzene ring of the *m*BzA functional group.[26]

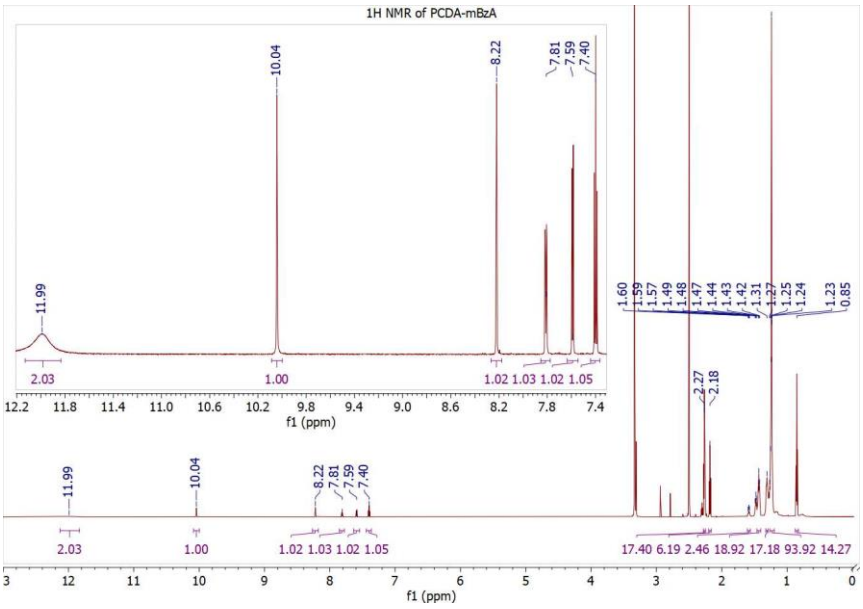

Figure 3. 1 ^{1}H NMR spectrum of PCDA-*m*BzA with the interval 7.4 – 12.0 ppm as an inset.

The carbon nuclear magnetic resonance (^{13}C NMR) result of PCDA-*m*BzA is given in Figure 3. 2, where the emergence of new peaks between 115.0 ppm and 173.0 ppm confirms the *m*BzA substitution to PCDA monomer.[62]

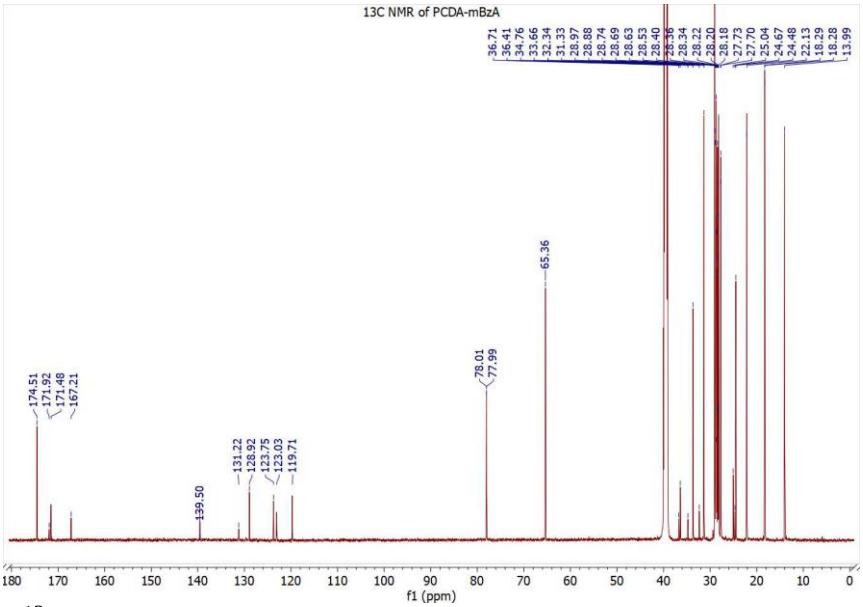

Figure 3. 2 ^{13}C NMR spectrum of PCDA-*m*BzA with the interval 7.4 – 12.0 ppm as an inset.

The ^{1}H NMR and ^{13}C NMR data obtained from modifying TCDA monomer with *m*BzA are presented in Figure 3. 3 and Figure 3. **4**, respectively. Similarly, the appearance of triplet, doublet, and doublet signals at chemical shift values of δ 7.40 ppm, δ 7.59 ppm, and δ 7.81 ppm, respectively, confirm the presence of a benzene ring. Furthermore, the proton chemical shift at δ 10.0 ppm indicates the OH group at the carboxylic terminal.

The new peaks between 115.0 and 173.0 ppm in ^{13}C NMR also validate the chemical modification of TCDA with *m*BzA.

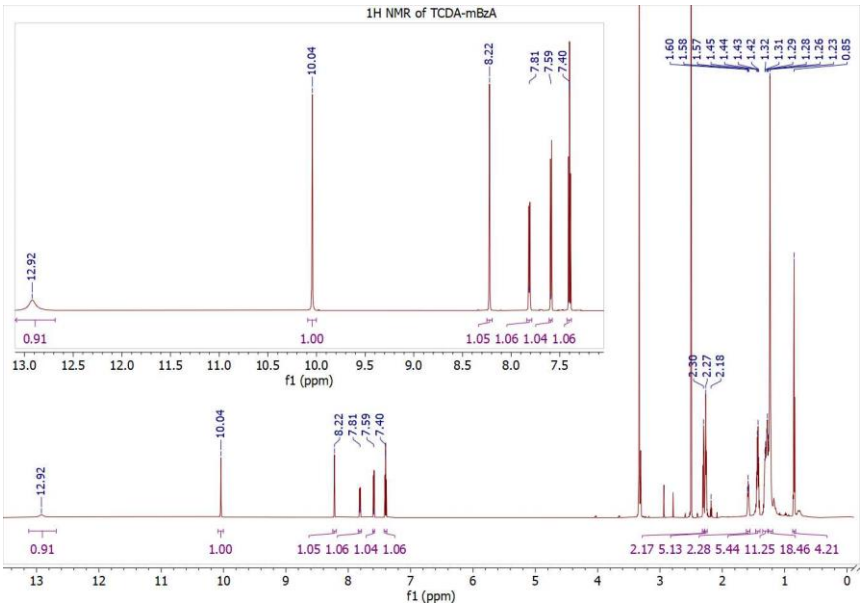

Figure 3. 3 ^{1}H NMR spectrum of TCDA-*m*BzA with the interval 7.4 – 13.0 ppm as an inset.

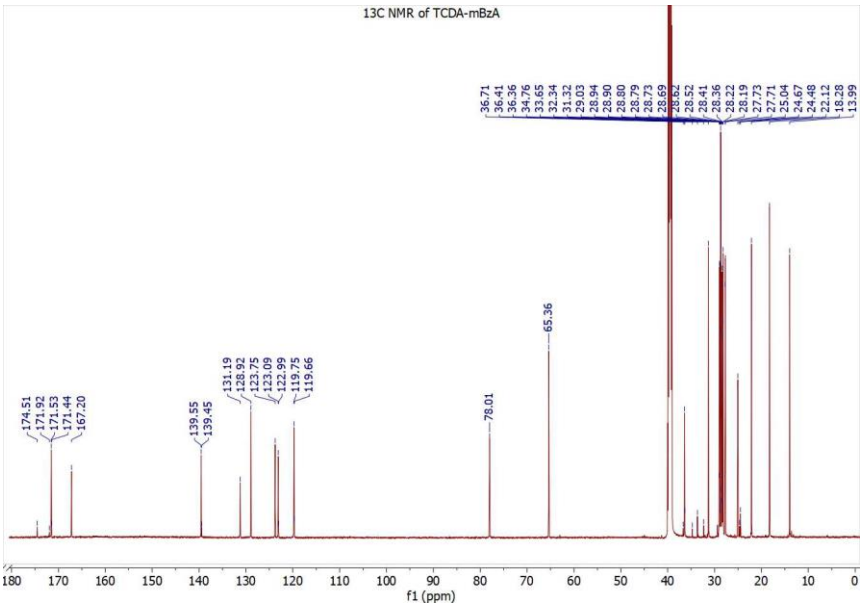

Figure 3. 4 ^{13}C NMR spectrum of TCDA-*m*BzA with the interval 7.4 – 12.0 ppm as an inset.

FTIR Spectroscopy is used to assess the vibrational bands present in *m*BzA functional group and to evaluate the band shifts in the chemical structure of diacetylenes.

The spectra of the *m*BzA functionalized monomers are demonstrated in **Figure 3. 5**. The commercial DA monomers are included again for a clear comparison. All monomers' symmetric and asymmetric stretching vibrations of alkyl side chains are around ~2847 cm^{-1} and ~2918 cm^{-1}, respectively. The carbonyl stretching vibrations located at ~1692

cm^{-1} and ~1657 cm^{-1} are assigned to the terminal carboxyl group of unmodified DA monomers and the amide group of *m*BzA substituted ones, respectively. In the *m*BzA-modified DA monomers, the new bands at ~1593 cm^{-1} and ~1543 cm^{-1} show the presence of the phenyl group and the CNH vibrations, respectively.[107]

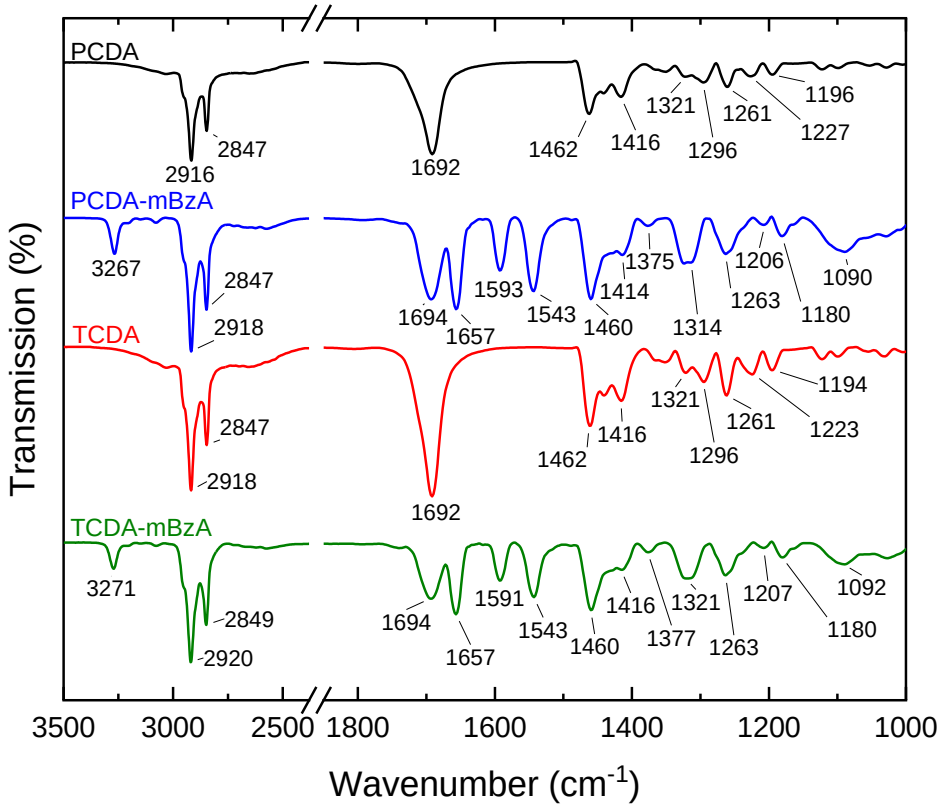

Figure 3. 5 FT-IR spectra of (A) PCDA, (B) PCDA-*m*BzA, (C) TCDA, and (D) TCDA-*m*BzA monomers

1.9. **The Effect of Photopolymerization Duration on PDA vesicles**

1.9.1. **Optical Properties of Vesicles – Studied by Visual Imaging and UV-Visible Spectroscopy Method**

The absorption spectra are used to assess the optical response of PDA vesicles to increased UV photopolymerization duration. The monomer vesicles were irradiated for 1-, 3-, 5-, 10-, 15-, and 20-minutes with 254 nm UV light and subsequently, their absorption spectra were recorded by UV-Vis spectroscopy.

The photopolymerization of DA monomer vesicles under 1 minute of UV irradiation leads to polymer vesicle solutions at different tones of blue. Among the commercial diacetylene monomers, PCDA and TCDA, the latter attains a darker blue color upon photopolymerization. The *m*BzA-substituted diacetylene monomer vesicle solutions

yield lighter blue color solutions after photopolymerization. A shorter alkyl chain length promotes the higher packing of TCDA monomers due to the weak van der Waals interactions. Therefore, darker blue color of poly(TCDA) vesicle solution than the rest is observed indicating higher polymerization efficiency.[29, 108] **Figure 3. 6** illustrates the absorption spectra of four PDAs, each characterized by an excitonic peak at approximately 640 nm and a vibronic shoulder at around 590 nm.[24] The absorption profiles of all PDA vesicle solutions exhibit a similar trend, demonstrating an increasing intensity with prolonged UV irradiation. This trend is visually apparent in PDA solutions.

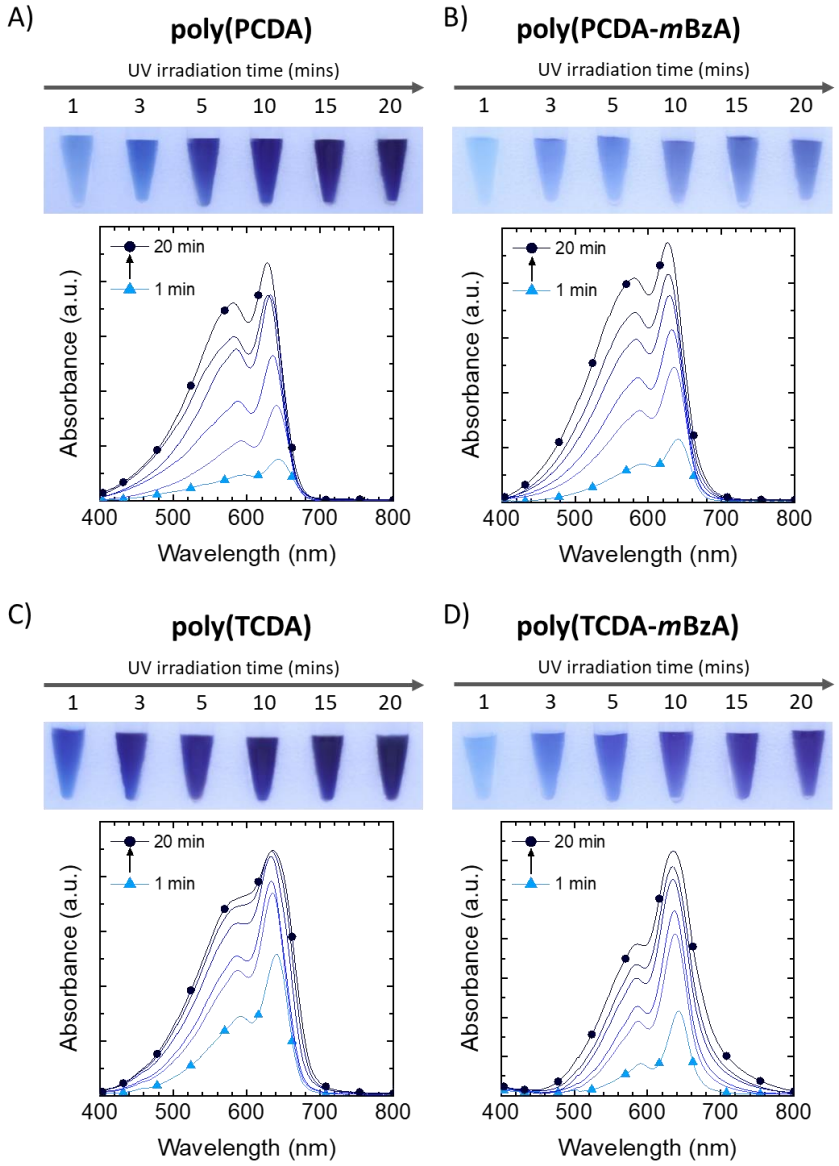

Figure 3. 6 Absorption spectra of PDA vesicle solutions as a function of irradiation time, with corresponding photographs indicating each spectrum.

For better comparison, the intensity and absorption wavelength profiles are plotted in Figure 3. 7 as a function of UV irradiation time. The maximum absorption intensity

experiences a significant rise within the first 5 minutes of UV exposure, while further increments in UV irradiation time (from 5 to 20 minutes) result in a comparatively smaller increase (Figure 3. 7. A.). With the initiation of UV exposure, the vesicle solutions contain monomers, oligomers, and polymers.[109] Polymer conversion proceeds with the continued UV irradiation. The intensity profile suggests that the photopolymerization of monomeric vesicles is nearly complete after 5 minutes of UV irradiation.[84, 109-111] Prolonged exposure time continues to facilitate the photopolymerization of the vesicles, although at a comparatively slower conversion rate.[24, 109, 111, 112] It can be inferred that PDAs with shorter alkyl tails exhibit higher photopolymerization efficiency.[113]

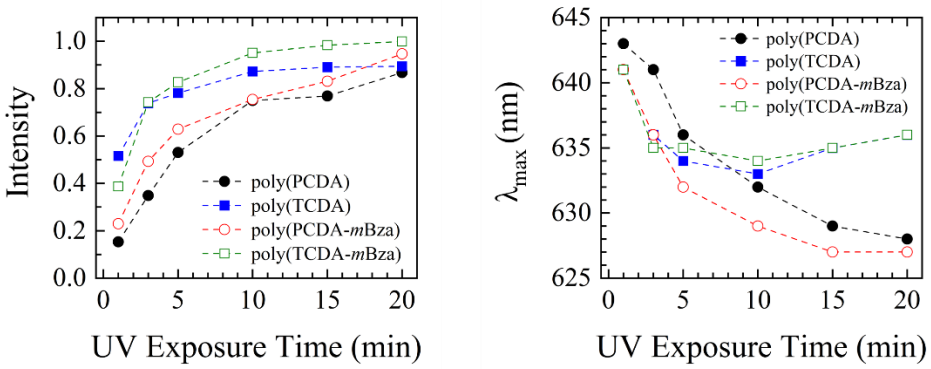

Figure 3. 7 The changes in absorption intensity (A) and maximum (λ_{max}) (B) of PDA vesicles photopolymerized at different times.

Figure 3. 7. B shows the initial maximum absorption of PDA vesicles. The λ_{max} of poly(PCDA) was 643 nm after 1 minute of UV irradiation, while the rest were at 641 nm. This difference could be due to various experimental processes.[85, 114] Along with the difference in hydrophobic tail length and structure of the headgroups, the vesicle preparation process, including the type of organic solvent used, sonication time, and storage conditions, also affects the packing of the monomers. All PDA solutions exhibited similar colorimetric behavior. The general decrease in absorption wavelength up to 10 minutes indicates that the polymerized, blue-colored vesicles are affected by UV light irradiation, resulting in a change in electronic properties. While poly(PCDA) and poly(PCDA-*m*BzA) showed a continuous shift towards shorter wavelengths, poly(TCDA) and poly(TCDA-*m*BzA) remained unchanged from 10 to 20 minutes of irradiation. As the polymer chain length increases, greater rotational freedom and a tendency for conformational transitions are observed.[59, 115] Both poly(PCDA) and poly(PCDA-*m*BzA) have longer hydrophobic tail lengths compared to their counterparts. Increasing photoirradiation leads to longer polymer chains,[84] which enhances chain

mobility. Increased mobility leads to rearrangement of the backbone causing interrupted conjugation length and a blue shift.[59] Additionally, due to the high energy of UV light, the PDAs might experience degradation and chain scission along the conjugated backbone, leading to a rearrangement of the PDA lipids, which could contribute to the blue shift in λ_{max}.[23, 116, 117] However, this structural rearrangement does not dominate the system, as the observed color of the solutions is still blue, and the absorption in the red phase does not exceed the blue phase absorption wavelength. The following section of the thesis discusses the effect of longer photoirradiation time on an external stimulus, pH, and its reversibility properties on PDA vesicle solutions.

1.9.2. **Size of Vesicles – Studied by Dynamic Light Scattering Method**

The structure of PDA vesicles as a function of UV duration is evaluated using the dynamic light scattering method. **Figure 3. 8** presents the size distribution of PDA vesicles under varying durations of UV light exposure (1, 3, 5, 10, 15, and 20 minutes). 1-minute photopolymerization forms a vesicle solution with distinct populations ranging in mean sizes of 46 nm, 73 nm, 67 nm, and 150 nm for poly(PCDA), poly(TCDA), poly(PCDA-*m*BzA), and poly(TCDA-*m*BzA), respectively. The initial polydispersity index (PDI) values, ranging from 0.2 to 0.3, are demonstrated in **Figure 3. 9** B. Prolonged UV irradiation shows a subtle decrease in vesicle size for all PDAs except for poly(TCDA-*m*BzA), which exhibits more reduction in size from 150 nm to 125 nm (see **Figure 3. 9** A). While photopolymerization proceeds, the formation of *yne-ene* conjugation induces an attraction among DA monomers, which might decrease vesicle size. [84, 112, 118] Furthermore, the vesicles maintained their respective single-size populations, except for poly(PCDA), which exhibited minor populations at 8 nm and 2 nm with prolonged UV irradiation, which can also be seen in plotted PDI values. The DLS results suggest that variations in hydrophobic packing and head group interactions are instrumental during the self-assembly of monomer vesicles (Figure 3.8 E). Once the vesicles are formed, UV exposure to light for up to 20 minutes does not significantly alter the size distribution profile.

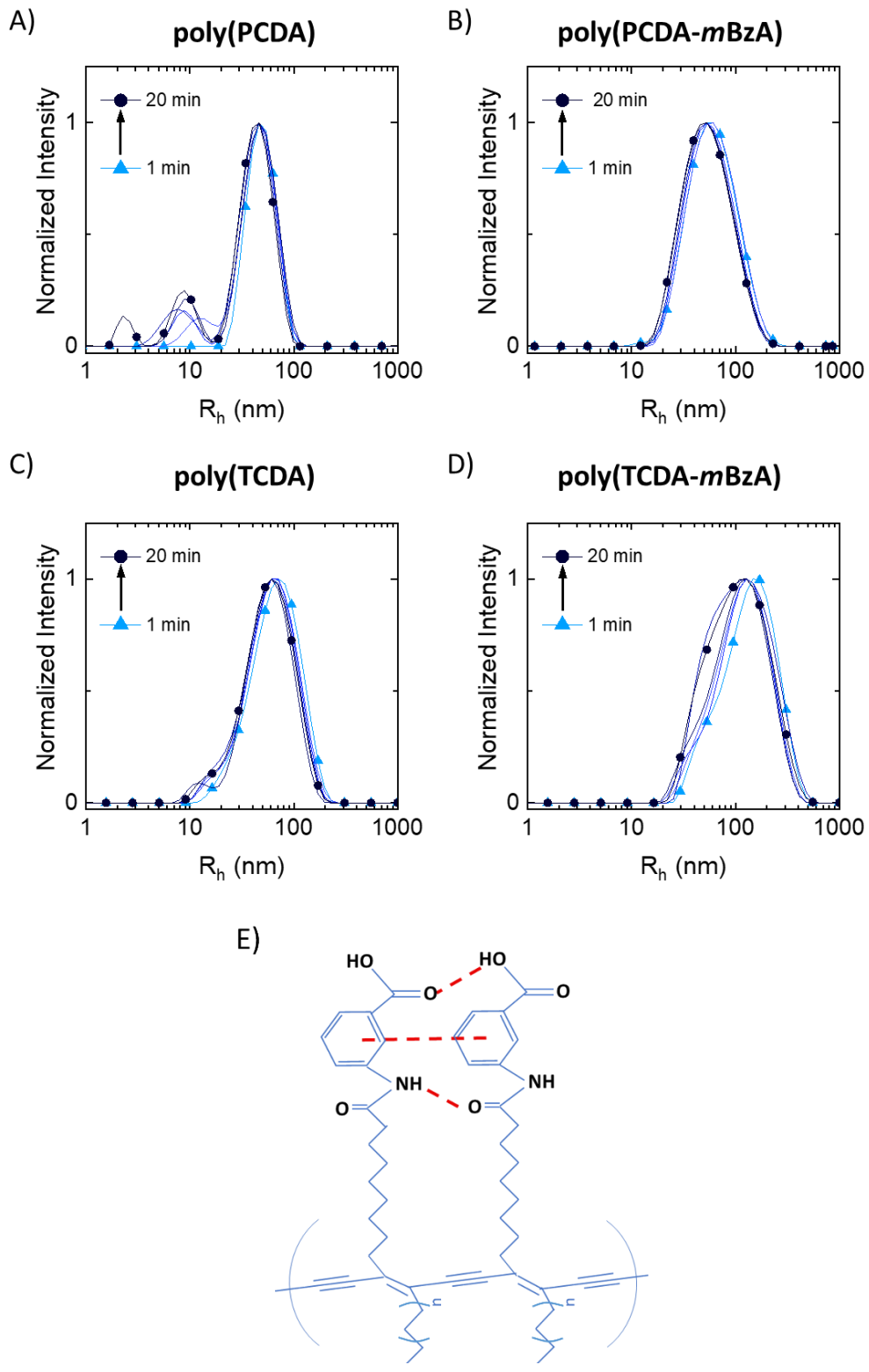

Figure 3. 8 (A-D) Size profiles of PDA vesicles irradiated for 1, 3, 5, 10, 15, and 20 minutes and E) schematic non-covalent interactions on *m*BzA-substituted diacetylene head group

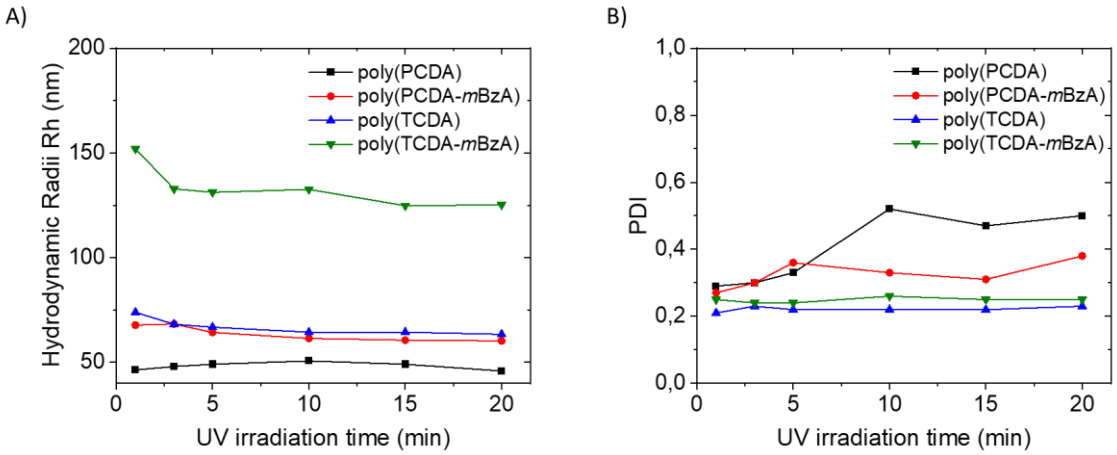

Figure 3. 9 Hydrodynamic Radii (R_h) (A) and PDI values (B) of PDA vesicles as a function of irradiation time

1.10. **Colorimetric Response of PDAs to High pH Conditions**

The preceding section examined the influence of UV irradiation time on polymer conversion in solution. The results revealed that prolonged exposure to UV irradiation, specifically up to 20 minutes, increased polymer conversion. The current section explores the effect of prolonged UV irradiation on the colorimetric transition of *m*BzA-substituted polydiacetylene (PDA) vesicles as the pH increases. Short (3 minutes) and long (20 minutes) UV irradiation durations were chosen as representative time frames for comparison. The visual appearance, absorption, fluorescence profiles, and size changes of the vesicles were evaluated to assess the differences.

The response to pH can be observed at increasing pH levels since commercially available and modified PDAs contain a carboxylic acid head group. In a neutral environment, the vesicle solutions are stable due to the non-covalent interactions, including hydrogen bonds, electrostatic interactions between the head group, and the dispersion forces between the alky chains of PDA lipids.[113] Introducing OH^- ions to the system deprotonates the carboxylic acid forming negatively charged carboxylate ions.[74, 119, 120] This acid-base reaction breaks the hydrogen bonds in the head group and induces Coulombic repulsion due to the formed carboxylate ions.[121] The formed stress on the backbone results in a structural realignment to obtain relaxation, and the red phase forms.[5] The visual appearances of vesicle solutions irradiated for 3 and 20 minutes to increase pH level are given in Figure 3. 10. The vesicles irradiated for 3 minutes appear light blue color at pH 7, whereas the ones irradiated for 20 minutes appear dark blue color. Adding KOH to the solutions allows a transition from blue to red to be visually followed.

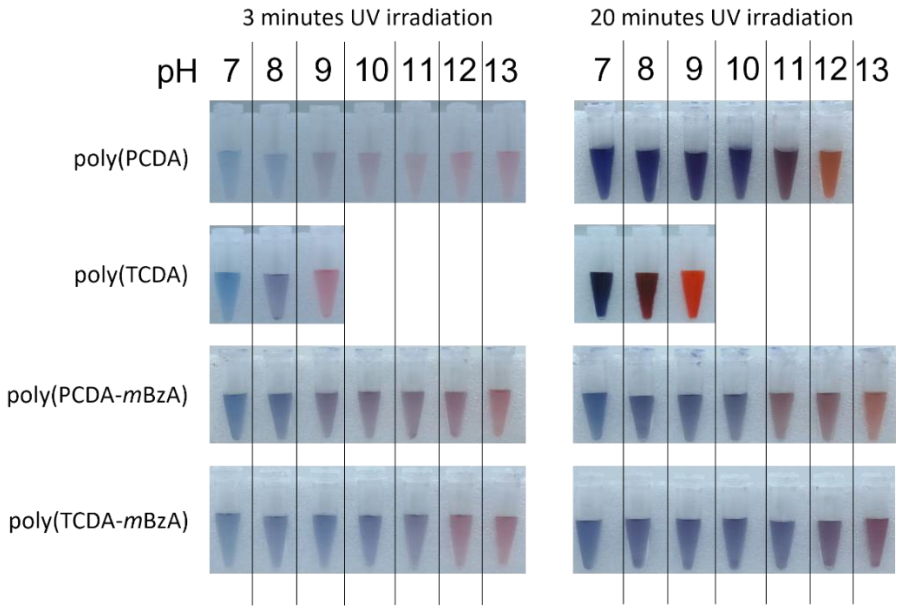

Figure 3. 10 Photos of vesicle solutions photopolymerized for 3 and 20 minutes to high pH

Structural transitions from planar to twisted (non-planar)[93] are characterized by absorption and fluorescence spectroscopy, as shown in Figure 3. 11, 3. 12, 3. 13, and 3.14. The vesicles photopolymerized for 3 minutes exhibited a characteristic blue phase peak at around 640 nm with a vibronic shoulder at 590 nm.[80] As pH increases, the characteristic red phase peak at around 540 nm emerges, eventually dominating the system.[62] The blue phase peak disappears completely when the pH increases to 12 and 9 for poly(PCDA) and poly(TCDA), respectively. However, poly(PCDA-*m*BzA) and poly(TCDA-*m*BzA) turned to the red phase at higher pH values and still exhibited the blue phase even at very high pH levels (pH=13). As expected, the PDAs with long alkyl tails turned to red phase at a higher pH level than those with shorter hydrophobic tails.[64]

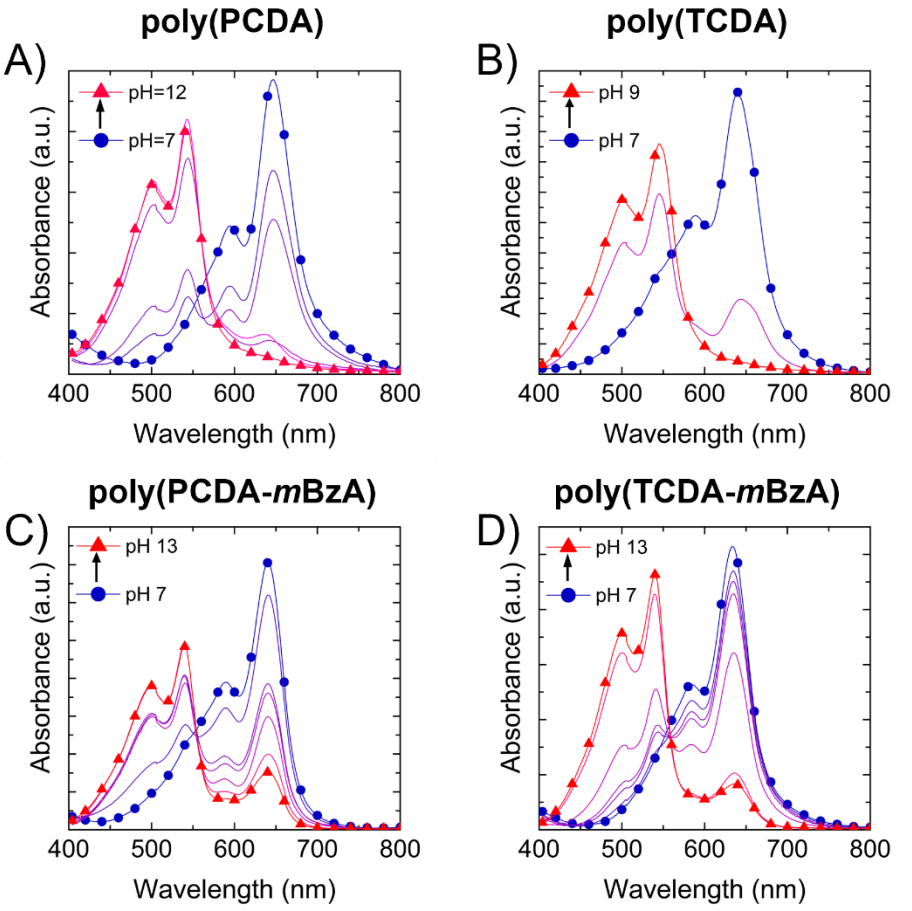

Figure 3. 11 UV-Vis spectra of 3 minutes UV irradiated A) poly(PCDA), B) poly(TCDA), C) poly(PCDA-*m*BzA), D) poly(TCDA-*m*BzA) upon increasing of pH

Since poly(PCDA) vesicles have stronger dispersion forces between DA molecules, they resist more to the introduction of OH^- ions. The *m*BzA substituted ones however, resist the present OH^- ions in the system through their strong head group interactions constituting hydrogen bonds and aromatic interactions.[61] The unusual response of poly(TCDA-*m*BzA) can be seen from visual images and absorption spectra compared to poly(PCDA-*m*BzA) vesicles. Even though both modified polymer vesicles have the same headgroup, the shorter alkyl chain containing PDA, namely poly(TCDA-*m*BzA), experiences a later response to pH compared to the longer alkyl tail poly(PCDA-*m*BzA). This unique behavior is similar when both vesicles undergo 20 minutes of photopolymerization before exposure to basic conditions. This behavior suggests that the presence of a bulky head group dominated the weak dispersion forces resulting from shorter hydrophobic tail and the system becomes more resistive to conformational transitions.[61] The 20 minutes irradiated vesicle solutions generally showed a transition from blue to red at higher pH values compared to their 3 minutes irradiated counterparts. Since the longer photopolymerization results in more conversion from monomer to

polymer, the fluidity of the solution decreases and a more stable polymer solution is obtained.[112] Therefore, the interactions between the PDA membrane and OH^- ions become difficult to exert strain on the polymer backbone.

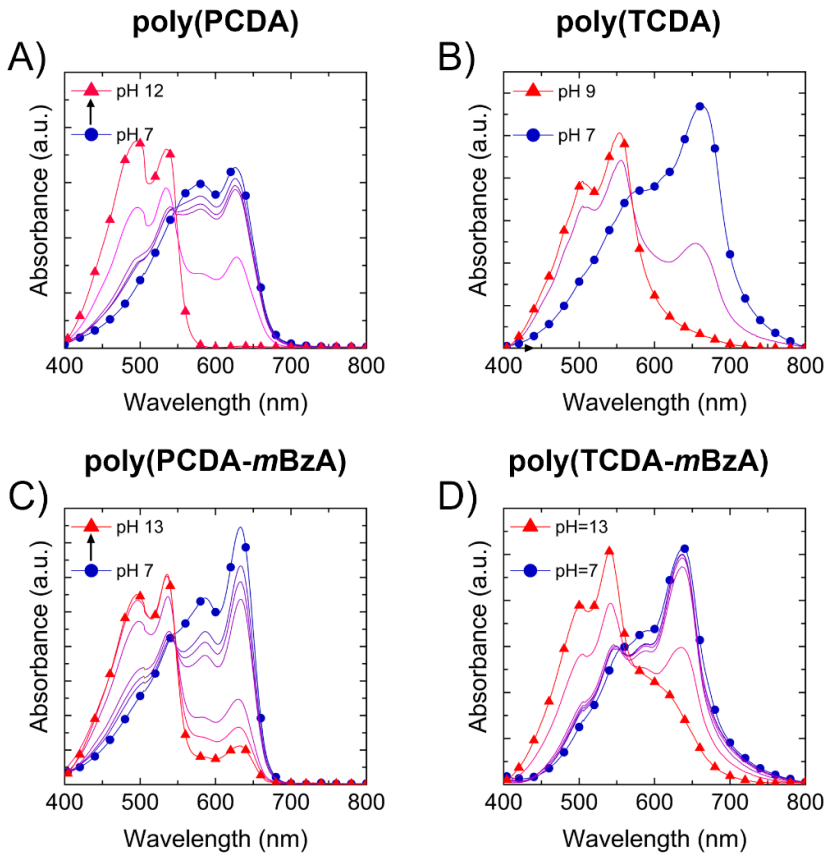

Figure 3. 12 UV-Vis spectra of 20 minutes UV irradiated A) poly(PCDA), B) poly(TCDA), C) poly(PCDA-*m*BzA), D) poly(TCDA-*m*BzA) upon increasing pH

The fluorescence spectra of PDA vesicles exhibited an off-to-on response upon adding KOH. The conformational transition on the backbone creates additional energy states where an excited electron from the HOMO level could emit a photon to those states, releasing a fluorescence signal. The rate of increments in the intensity of the fluorescence signal is parallel with the rate of the blue-to-red color transition.

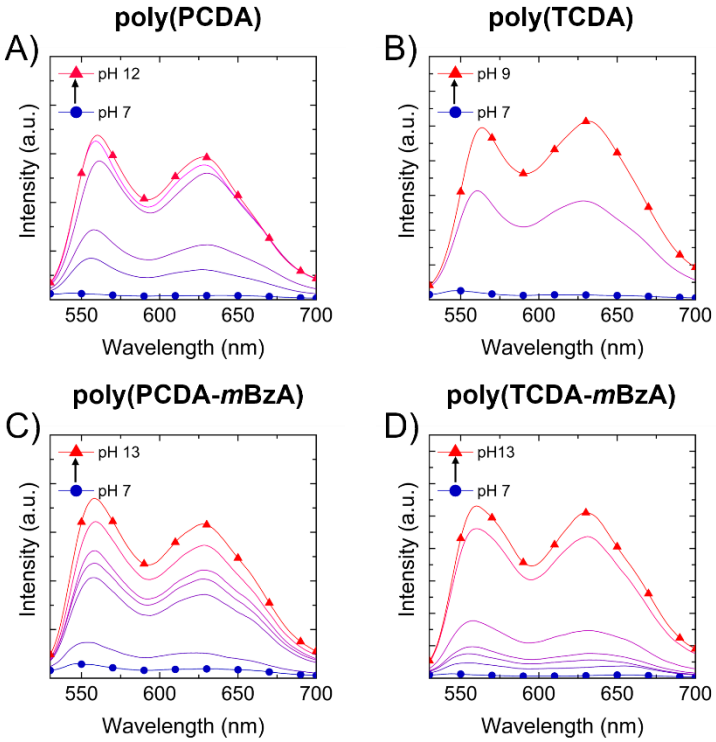

Figure 3. 13 Fluorescence spectra of 3 minutes UV irradiated A) poly(PCDA), B) poly(TCDA), C) poly(PCDA-*m*BzA), D) poly(TCDA-*m*BzA) upon increasing of pH

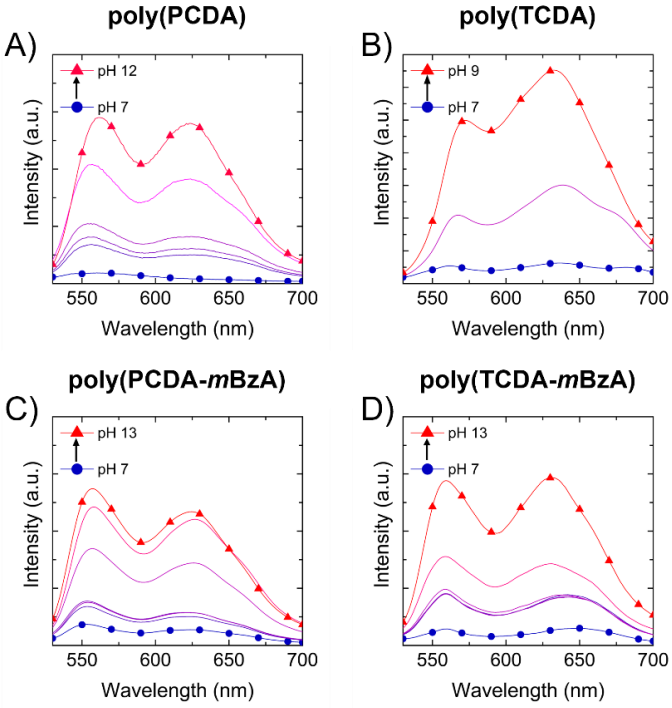

Figure 3. 14 Fluorescence spectra of 20 minutes UV irradiated A) poly(PCDA), B) poly(TCDA), C) poly(PCDA-*m*BzA), D) poly(TCDA-*m*BzA) upon increasing of pH

The delayed response can also be attributed to the PDA vesicles' stronger non-covalent interactions. The calculated colorimetric response (CR%) and maximum absorption

wavelength values are plotted in Figures 3. 15 and 3.16 for all the PDA vesicle solutions. The poly(TCDA) vesicles are not affected by longer photopolymerization compared to the rest since both short and long UV irradiated vesicles turned completely to the red phase at pH 9. This behavior might be due to the weak dispersion forces that could not resist the insertion of OH^- ions into the system.[64, 74]

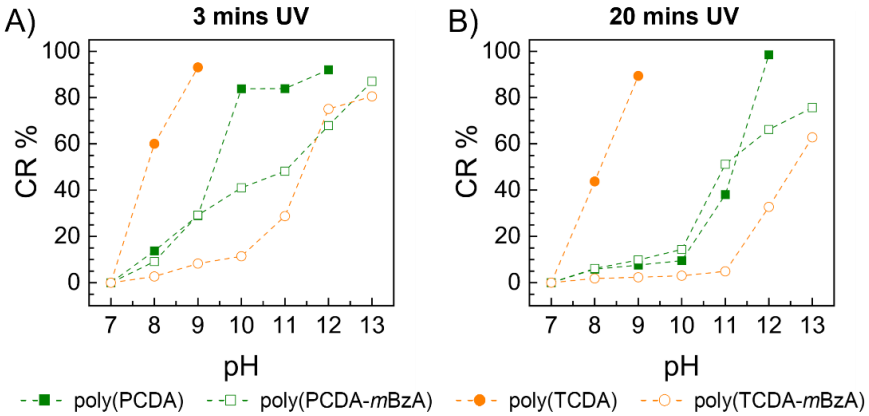

Figure 3. 15 CR% of PDA vesicles UV irradiated for A) 3 minutes and B) 20 minutes as a function of pH

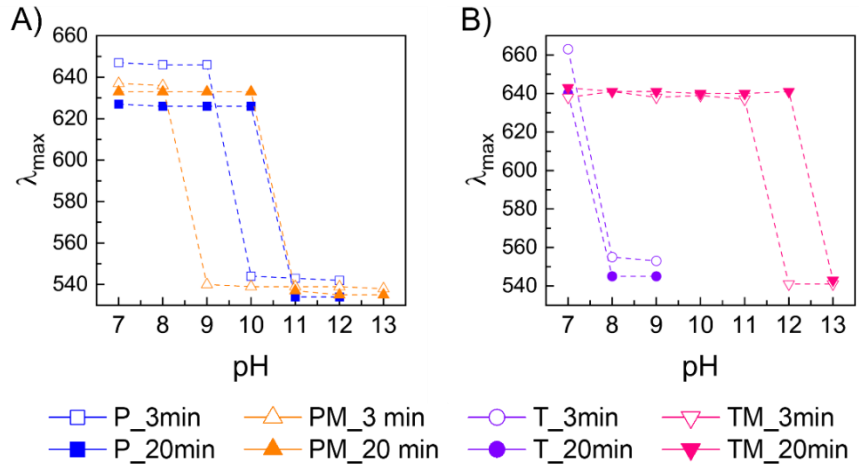

Figure 3. 16 λ_{max} comparison of PDA vesicles irradiated for 3 minutes and 20 minutes with corresponding labels at the bottom

The hydrophobic tail, hydrogen bonding, and aromatic interactions affect the self-assembly behaviour and photopolymerization of PDA vesicles.[113] Adding KOH to the solution showed an increasing trend in vesicle sizes. Figure 3. 17 and Figure 3. **18** show the size distribution response of PDA vesicles irradiated short (3 minutes) and long (20 minutes) UV duration to increase pH.

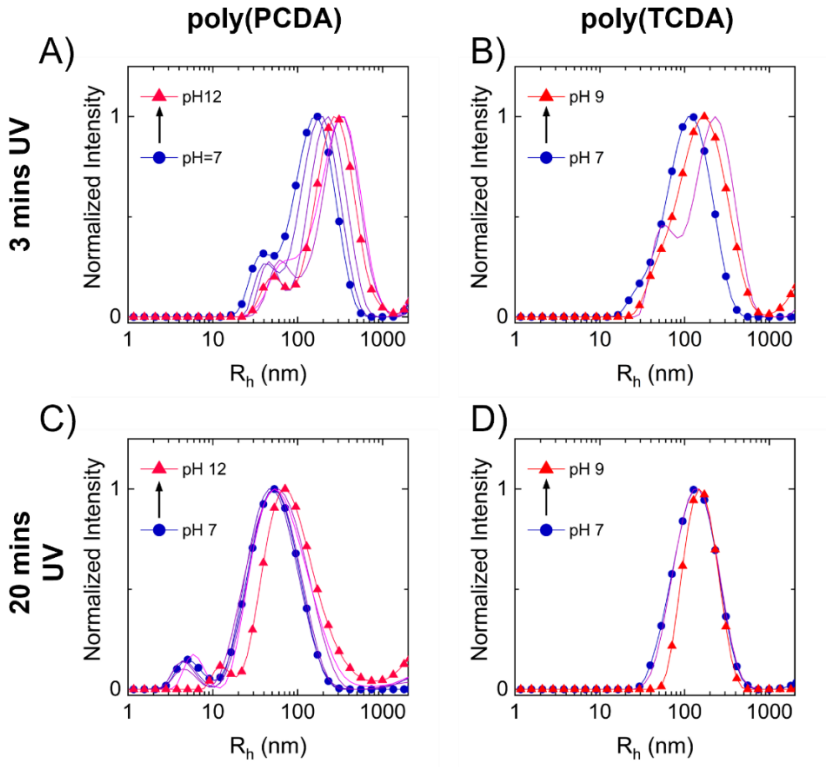

Figure 3. 17 Size distribution profiles of poly(PCDA) and poly(TCDA) vesicles UV irradiated for 3 and 20 minutes upon increasing pH

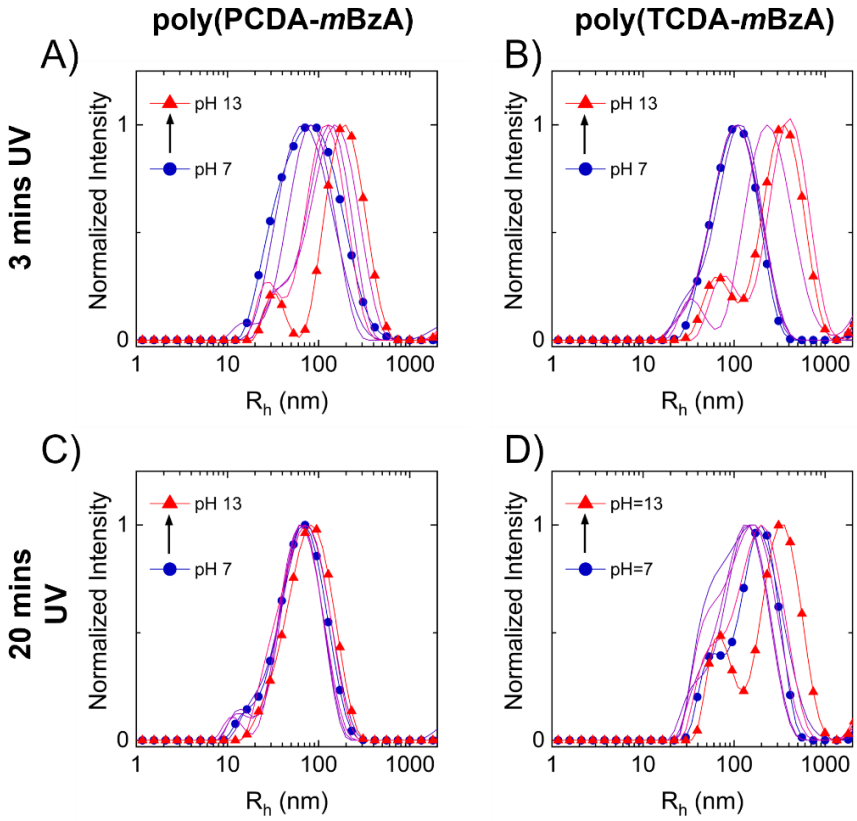

Figure 3. 18 Size distribution profiles of poly(PCDA-*m*BzA) and poly(TCDA-*m*BzA) vesicles UV irradiated for 3 and 20 minutes upon increasing pH

The insertion of hydroxide ions (OH^-) to the system deprotonates the carboxylic headgroup.[118, 120] Thus, the electrostatic repulsion between the DA monomers creates spatial disturbances, thus increasing of vesicle size and transition from blue to red phase.

1.11. **Reversible Colorimetric Response of PDAs**

A study for the reversibility of the modified PDA vesicles was conducted under both short and long UV irradiation durations, to explore the inter and intra-chain interactions of the system. The optical response was assessed using UV-Vis spectroscopy.

The conformation transition of commercial PDAs from the planar blue phase to the twisted, non-planar red phase when exposed to an external trigger is irreversible. Upon removal of the trigger, the rearrangement does not occur since the thermodynamically stable phase is the red phase.[45] The coulomb interaction forces the weak hydrogen bonds that fail to restore to their original state and permanently distort PDAs' backbone. [26, 80, 84] Several studies reported the effect of functional head groups such as amide, aromatic or carboxylic acid attached to DA monomer on the reversible chromatism, especially on thermochromism.[62, 82] Results indicated the necessity of cooperative, stable, and strong hydrogen bonding among head groups to obtain reversibly chromatic PDAs.[32, 62, 71, 80] Therefore, the -*m*BzA substituted PDA vesicles were tested for their reversibility properties. Initially, blue-colored PDA vesicles were titrated with KOH to reach pH 13 and then turned back to pH 7 by adding HCl. To evaluate the effect of UV irradiation time on reversibility, the 3- and 20 minutes UV photopolymerization durations were selected as short and long exposure durations. The colorimetric reversibility tests of poly(PCDA-*m*BzA) and poly(TCDA-*m*BzA) were summarized in Figure 3. 19 andFigure 3. **20** for both irradiation durations. As can be seen in **Error! Reference source not found.**, the PDA vesicles irradiated for 3 minutes did not show any recovery of the blue phase when HCl was added to the solution. Instead, a slight drop in intensity for both poly(PCDA-*m*BzA) and poly(TCDA-*m*BzA) vesicles is seen due to the dilution effect. Additionally, the agglomeration is visible in poly(TCDA-*m*BzA) vesicles due to the salt formation.[32, 36, 56] When the same reversibility test was conducted on 20 minutes irradiated vesicles, some of the red phases of PDA returned to the blue phase accompanied by an intensity drop (see Figure 3. 20). The recovery of the blue phase in poly(PCDA-*m*BzA) is dominating the system. In contrast, the red and blue phase intensities in poly(TCDA-*m*BzA) are almost even, giving both vesicles a purple color. This behavior suggests that the prolonged photopolymerization contributes to the degree of freedom of the PDA

backbone, where

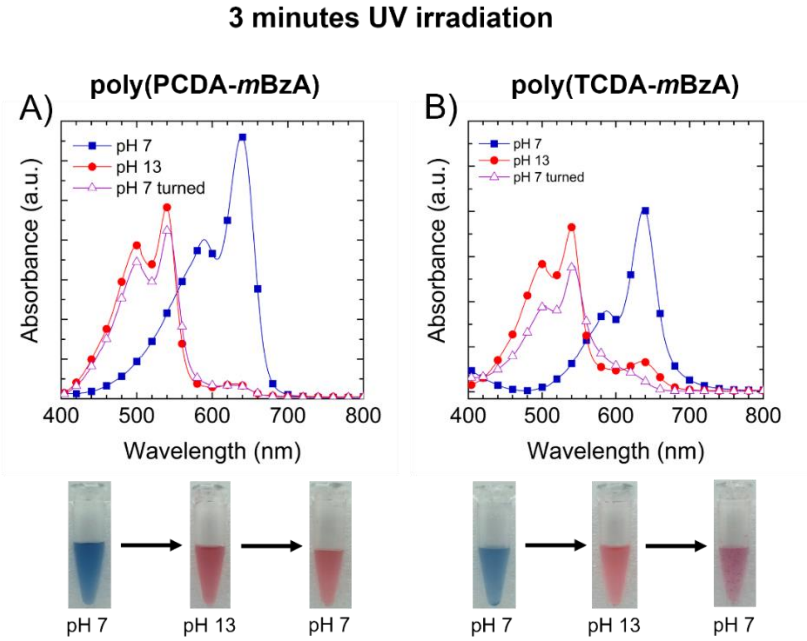

Figure 3. 19 Absorption spectra and corresponding photographs of poly(PCDA-*m*BzA) vesicles irradiated for A) 3 minutes and B) 20 minutes during reversibility test; initial state (pH 7), increasing of pH to 13 and decreasing back to pH 7

neutralization of the solution allows some of the vesicles to return to their original blue state.[57] Even though poly(TCDA-*m*BzA) has later transitioned to the red phase upon increasing pH, the acidification process is not as effective as in poly(PCDA-*m*BzA).

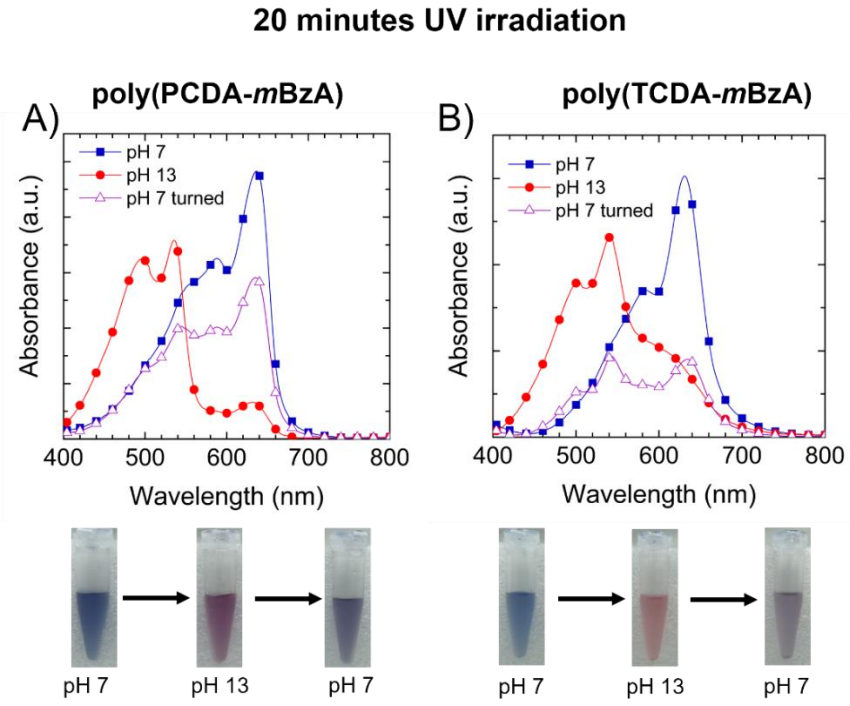

Figure 3. 20 Absorption spectra and corresponding photographs of poly(TCDA-*m*BzA) vesicles irradiated for A) 3 minutes and B) 20 minutes during reversibility test; initial state (pH 7), increasing of pH to 13 and decreasing back to pH 7

This indicates either the system experiencing resistance to complete conformational transition from planar to non-planar twisted form or the strain relaxation of the chain is managed somehow that prevents the further realignment from exerting the strain. Thus, unlike thermochromic reversibility, prolonged UV irradiation contributes to the pH reversibility of PDA vesicles ones the headgroup interactions are enhanced.[21, 84]

CHAPTER 4. PDAs with DETA HEAD GOUP

This chapter presents the influence of initial conformation on DETA-modified PDA vesicles and the alkyl tail length to various external triggers, including low pH, ethanol and acetic acid. The modification of diacetylene monomers is evaluated by NMR and FTIR spectra. Then, the effect of initial conformation on PDA vesicles to the stimuli was evaluated by analysing the UV-Vis spectroscopy, DLS, and visual appearance.

1.12. **Characterization of Modified DA Monomers**

The proton nuclear magnetic resonance spectroscopy (^{1}H NMR) and the carbon nuclear magnetic resonance (^{13}C NMR) spectroscopy are employed to evaluate the protons of substituted functional groups of DETA to diacetylene monomers.

The ^{1}H NMR and ^{13}C NMR spectra of both PCDA-DETA and TCDA-DETA are provided in Figure 4. 1 andFigure 4. **4** . The characteristic protons of PCDA were observed at chemical shift values of δ 0.84-0.89 ppm, δ 1.58-1.25 ppm, and δ 2.25-2.15 ppm in Figure 4. 1, as previously evaluated. New peaks emerged between δ 2.81-2.67 ppm and δ 3.33-3.37 ppm, confirming the presence of ethylene diamine (DETA) at the polar head of the PCDA monomer.

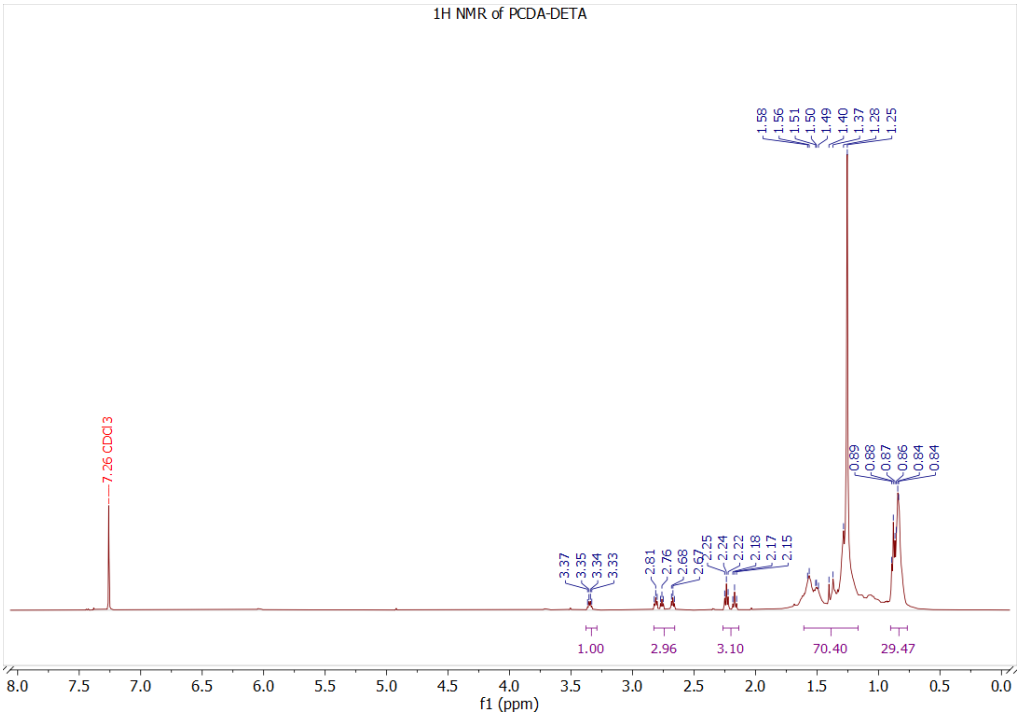

Figure 4. 1 ^{1}H NMR spectrum of PCDA-DETA

The ^{13}C NMR in Figure 4. 2 the new peaks at 40 ppm and 60 ppm indicate the chemically

bonded DETA to PCDA.

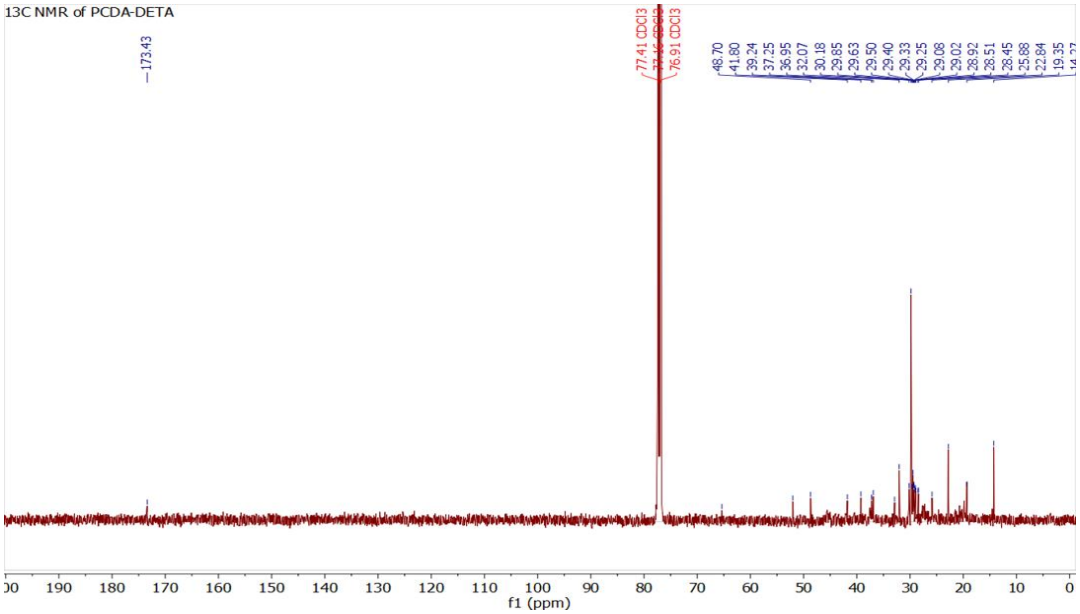

Figure 4. 2 ^{13}C NMR spectrum of PCDA-DETA

Similarly, the characteristic TCDA protons appeared at δ 0.83-0.89 ppm, δ 1.59-1.25 ppm, and δ 2.25-2.15 ppm and the newly emerged peaks between δ 2.82-2.66 ppm and δ 3.33 – 3.37 ppm in Figure 4. 3 and 40-60 ppm in Figure 4. 4 confirms the successful modification of TCDA-DETA.[122]

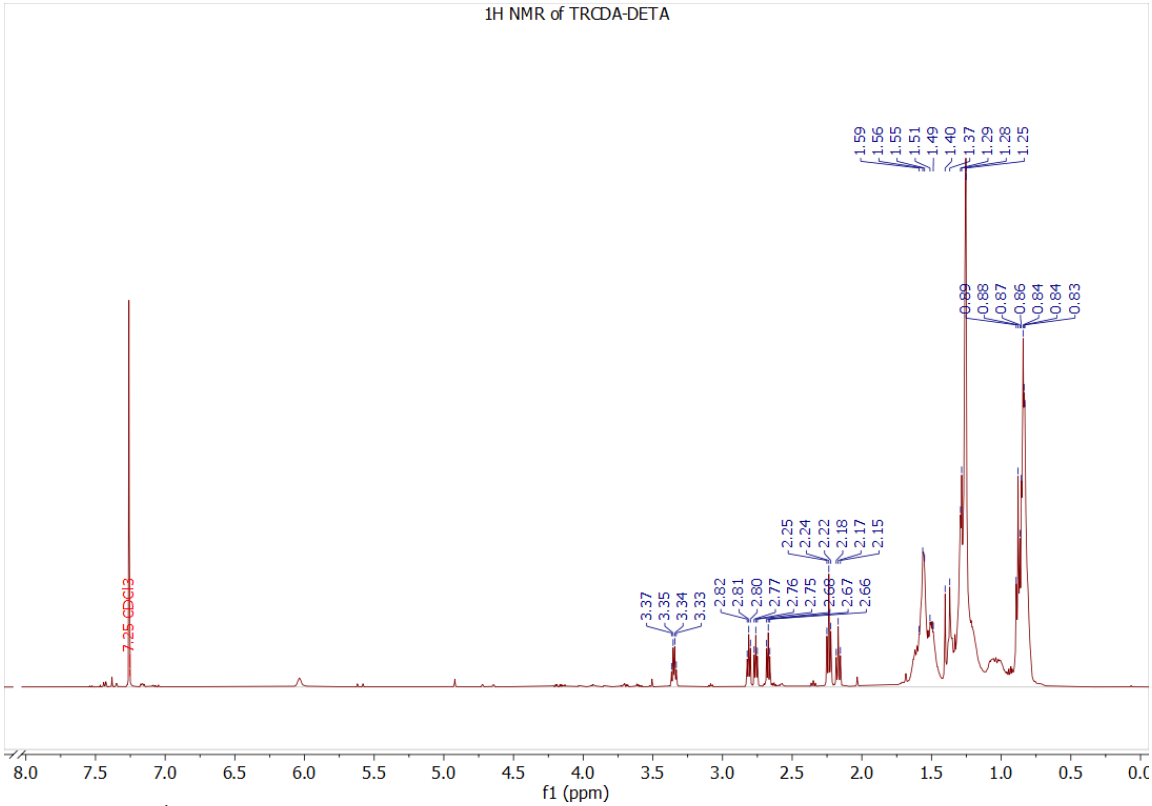

Figure 4. 3 ^{1}H NMR spectrum of TCDA-DETA

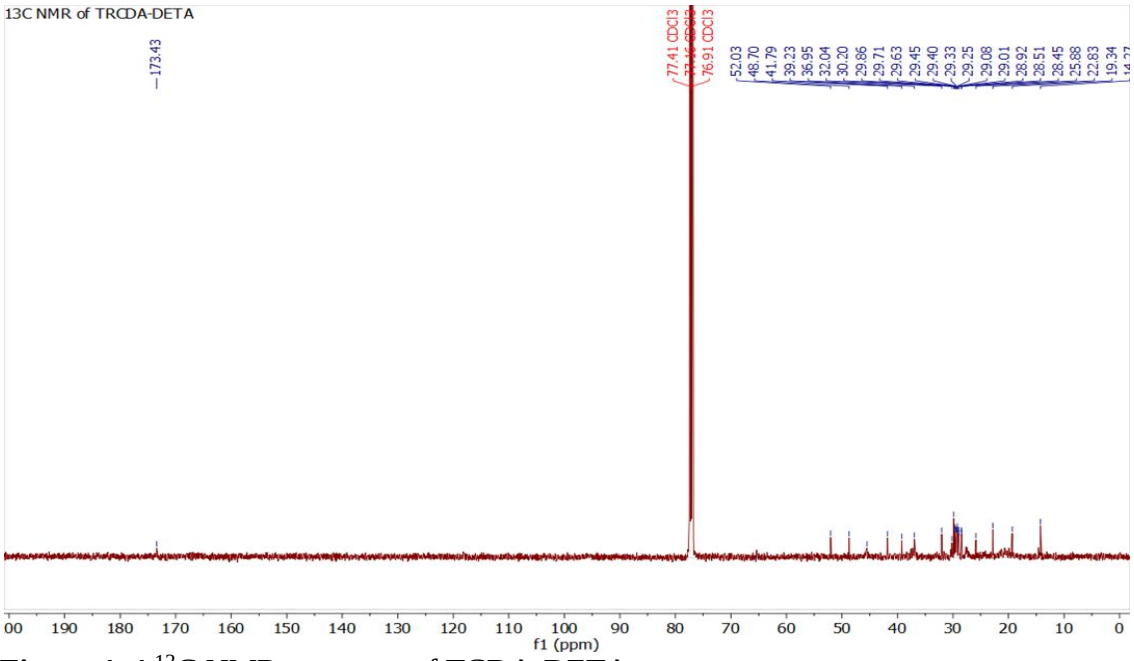

Figure 4. 4 ^{13}C NMR spectrum of TCDA-DETA

FTIR Spectroscopy is used to assess the vibrational bands present in DETA functional group and to evaluate the band shifts in the chemical structure of diacetylenes.

The FTIR spectra are demonstrated in Figure 4. 5 for the commercial and DETA-substituted DA monomers. DETA- substituted DA monomers show a new peak at around 3300 cm^{-1} corresponding to N-H stretching vibrations. The unmodified ones give almost identical spectra where the bands at 2916 cm^{-1} and 2846 cm^{-1} correspond to symmetric and asymmetric stretching vibrations of alkyl chains (CH_2).[64, 77, 123] These bands showed a small shift to higher wavenumber in alkyl side chains of DETA functionalized DA monomers. The carbonyl stretching vibration in the carboxylic head group shows a distinct peak at 1691 cm^{-1} for PCDA and TCDA, whereas DETA-substituted monomers show the carbonyl stretching in the amide bond at around 1643 cm^{-1} with a lower wavenumber domain than the commercial ones. The enhanced hydrogen bonds between the polyamine head group might be contributed to this shift. The new peaks appear at around 1546 cm^{-1} and 1110 cm^{-1} for modified DA monomers corresponding to N-H bending and C-N stretching, respectively. The methylene scissoring bands of alkyl side chains are between 1461 cm^{-1} and 1416 cm^{-1}.[124]

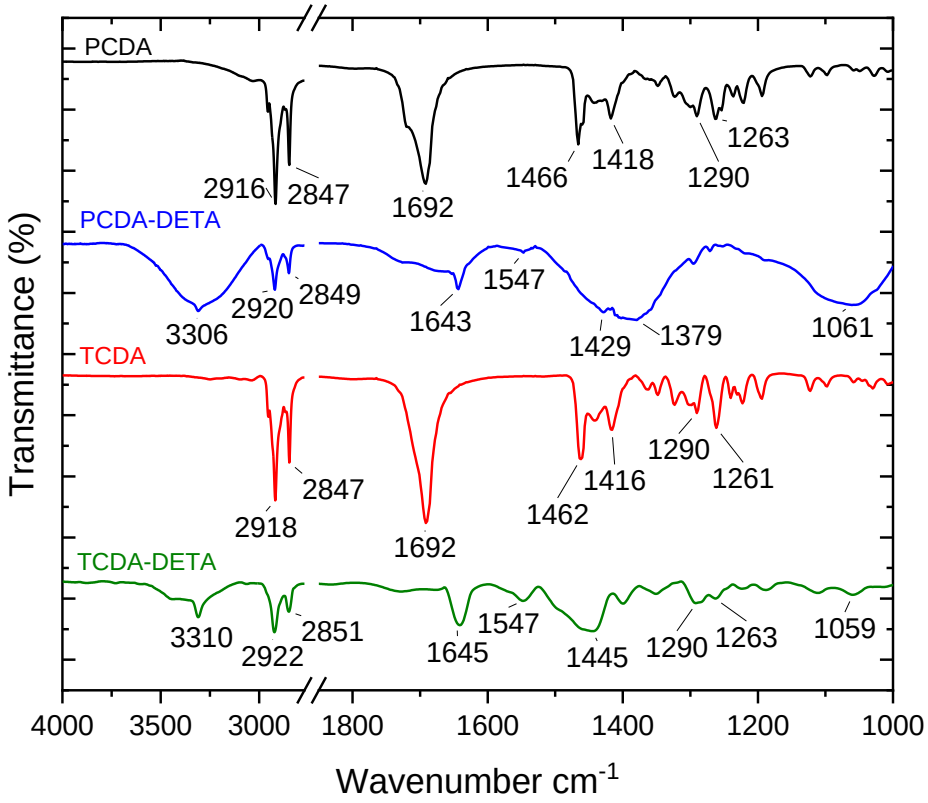

Figure 4. 5 FT-IR spectra of (A) PCDA, (B) PCDA-DETA, (C)TCDA, and (D) TCDA-DETA monomers

1.13. **Colorimetric Response of PDAs to Low pH Conditions**

The presence of a carboxylic head group does not promote any acid-base reaction on the polydiacetylene chain when the pH is lowered.[74] So, the commercially available PCDA and TCDA polymers do not show a conformational change, thus a colorimetric response. However, modification of the head group with amine-containing moiety favors the ionic interactions between hydrogen ions and the amine group. The consequent structural changes affect the electronic state of polydiacetylene showing a blue-to-red phase transition and becoming fluorescent.[120]

1.13.1. **Optical Properties of Vesicles – Studied by Visual Imaging and UV-Visible Spectroscopy Method**

In this section, two different acid sources, one of them being strong acid, HCl, and the other as an organic acid with an alkyl chain containing carboxylic acid, acetic acid were used to obtain predetermined pH. Their absorption spectra were recorded by UV-Vis spectroscopy to evaluate the optical transition in PDA vesicles.

As previously mentioned, the non-covalent interactions affect the efficient packing of the monomers. A proper alignment gives blue-colored polydiacetylenes. Variations in this alignment yield either purple or red polydiacetylenes or no change of color indicating unsuccessful packing. As demonstrated in Figure 4. 6**Error! Reference source not found.**, poly(TCDA-DETA) initially yields purple color which means that the effective π-electron delocalization is interrupted at some locations on the planar backbone leading to an intermediate phase consisting of blue and red phase vesicles.[5] Comparison of chromatic transitions of initially blue and purple PDA vesicles provides useful information about how the thermodynamically intermediate phase allows the rearrangement of conjugated backbone in the presence of external stimuli.

The absorption spectra of PDA vesicle solutions upon exposure to hydrochloric acid and acetic acid are given in Figure 4. 6 and **Figure 4. 7**. The titrations were performed to reach the pH values of 4 and 3 for all exposures. The color transition occurs in modified vesicles by protonating the terminated amine molecules with H^+ ions to form NH_3^+. The electronic repulsion between these positively charged ammonium ions is causing rearrangement of the conjugated backbone transitioning to the red phase.[119, 125] Initially, poly(PCDA-DETA) exhibited blue-colored vesicles with maximum absorption at 630 nm. By lowering the pH to 4 with acetic acid, a new peak emerged at around 540 nm, indicating the presence of a red phase. The blue and red peaks show almost equal intensities, suggesting that pH 4 can be considered an intermediate phase with a purple colour visually appearing. Further addition of acetic acid diminishes the blue phase in poly(PCDA-DETA) without complete elimination. The already emerged red peak at 540 nm dominates the system indicating the significant interruption of the planarity of the conjugated backbone.[80] Initially, purple-colored poly(TCDA-DETA) exhibited similar color transition behavior with poly(PCDA-DETA) upon exposure to acetic acid. Nevertheless, due to the system being in the intermediate phase, the peak at 540 nm already starts dominating the system at pH 4. Lowering the pH to 3 almost eliminates the blue phase. Both vesicle systems contain polyamine terminated polar group; however, shorter alkyl tail length of poly(TCDA-DETA) results in weaker dispersion forces between hydrophobic tails of PDA lipids which promotes the rearrangement of the backbone in poly(TCDA-DETA) more than poly(PCDA-DETA).[29] This indicates that PDA systems with an already organized [59] nonplanar intermediate phase require a lower amount of external stimuli compared to PDAs with a planar conformation to form structural rearrangement on the backbone.[5]

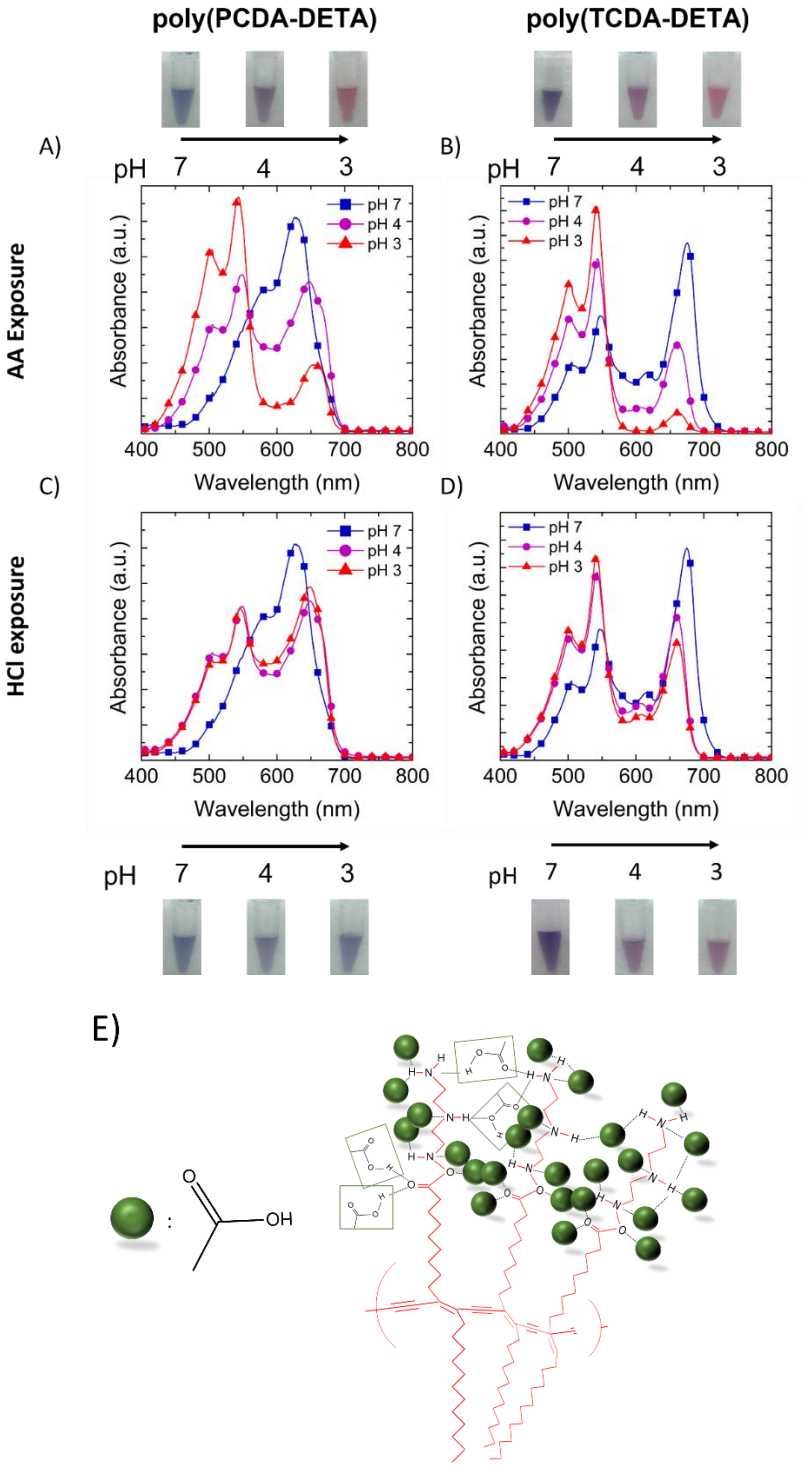

Figure 4. 6 UV-Vis absorption spectra of poly(PCDA-DETA) to (A) HCl and (C) acetic acid addition; poly(TCDA-DETA) to (B) HCl and (D) acetic acid addition with photographs attached above each spectrum, (E) schematic illustration of introduction of acetic acid into the DETA-substituted diacetylene monomers

Absorption spectra of PDA vesicles were measured following the addition of HCl as shown in Figure 4. 6. C-D. Interestingly, diatomic acid produced unusual colorimetric transition in polyamine-modified vesicle systems despite being stronger than acetic acid.

The emergence of a new peak at around 540 nm was observed, accompanied by a bathochromic shift of the blue phase in poly(PCDA-DETA) vesicles, indicating some resistance on the conjugated backbone to H^+ ions.[113] The response of poly(TCDA-DETA) vesicles to adding HCl resembled that of acetic acid, where the absorption in the red phase gradually increased as the pH lowered. Nonetheless, the blue phase remained in this system without showing a bathochromic shift. These unusual results indicate that the introduction of diatomic acid might not cause relaxation on the conjugated backbone like acetic acid. This can be attributed to the swelling of the PDA vesicles where the alkyl tail of acetic acid is more likely to enter the hydrocarbon region of PDA lipids compared to Cl^- ions when HCl is used as an H^+ ion source.[113, 120] Previous studies have shown that diacetylenes with amine headgroups can impede photopolymerization due to the shortening of the distance between DA units[36, 56] To overcome this, HCl is introduced to the system before polymerization leading to the formation of salt through electrostatic interactions on the headgroup.[113] This rearrangement of the self-assembled DA monomers facilitates the alignment, forming blue-colored PDAs upon UV irradiation. The observed red-shift in poly(PCDA-DETA), indicating an increase in effective conjugation length, may be attributed to this phenomenon.[113] The addition of HCl seems to affect the backbone configuration increasing the conjugation of the PDA backbone.

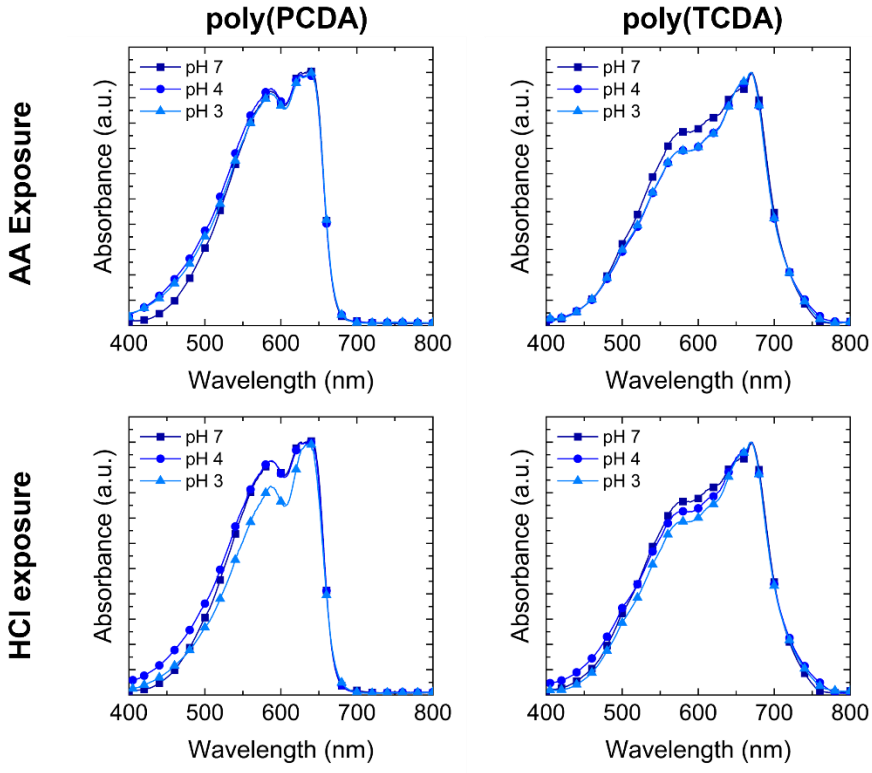

Figure 4. 7 UV-Vis absorption spectra of poly(PCDA) to (A) acetic acid and (B) HCl

addition; poly(TCDA) to (C) acetic acid and (D) HCl addition.

Expectedly, poly(PCDA) and poly(TCDA) did not develop any red phase upon the addition of both acid types indicating that they retain their conformation during acid addition as shown in Figure 4. 7.[74, 119] The slight decrease in absorption intensity can be attributed to the dilution effect and the agglomeration of PDA.[120]

1.14. Ethanol Exposure to PDA Vesicles

Alcohol molecules have been observed to penetrate the head group of PDA layers, leading to a conformational change.[65] To examine the effect of amine-substituted head groups on this insertion, ethanol is used. The analyses were conducted on two forms of PDA vesicles, blue and red phases. To obtain the red phase ethanol was added in excess based on the experimental procedure and literature[65]; however, the addition was kept the same for exposure to each vesicle.

1.14.1. Optical Properties of Vesicles – Studied by Visual Imaging and UV-Visible Spectroscopy Method

The absorption spectra of PDA vesicles were recorded to assess the transitions between HOMO and LUMO levels of blue and red phase PDA vesicles.

Figure 4. 8 shows the UV-Vis spectra of PDA vesicles before and after the excess addition of ethanol, with corresponding images placed at the top of each spectrum. The absorption at 633 and 640 nm of blue phase vesicles significantly declined when ethanol was added, while these peaks showed a blue shift to 540 and 545 nm for poly(PCDA) and poly(TCDA), respectively. The swelling of vesicles leads to the rearrangement of the conjugated backbone and causes an increase in the HOMO-LUMO energy gap.

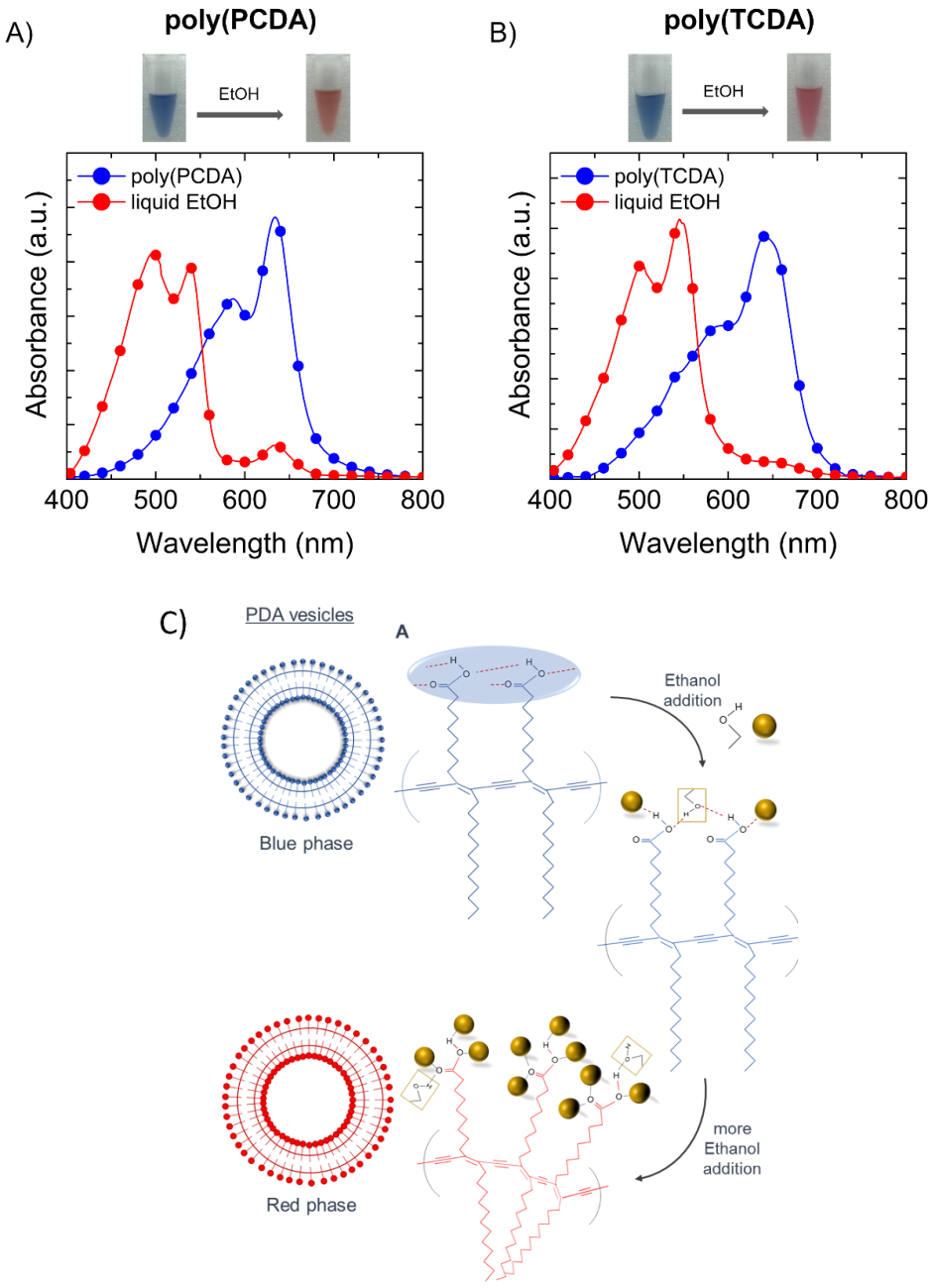

Figure 4. 8 UV-Vis absorption spectra of A) poly(PCDA), B) poly(TCDA) vesicles before (blue) and after (red) addition of liquid ethanol and corresponding photographs of vesicle solutions, C) schematic drawing of introduction of ethanol molecule into the monocarboxylic diacetylene lipids.

With the same amount of ethanol addition, the reduction of the blue phase is more in the poly(TCDA) vesicle system than the poly(PCDA) vesicle system. This behavior could be attributed to the stronger dispersion forces between the hydrophobic alkyl tail of poly(PCDA) resisting the movement. The UV-Vis spectra and images reveal that there is not any loss of intensity despite the excess addition of ethanol, suggesting that the agglomeration, which might be due to the changes in polarity, is negligible.[61, 65]

The absorption spectra of amine-substituted PDA vesicles before and after liquid ethanol addition are demonstrated in Figure 4. 9. The absorption of the blue phase at 625 nm in poly(PCDA-DETA) vesicle system transformed to red phase with the emergence of the peak at 542 nm. The UV-Vis spectrum shows the complete disappearance of the blue phase with a considerable intensity drop due to dilution with ethanol. With the same amount of liquid ethanol addition, the structural realignment, thus the red phase, is observed for both monocarboxylic and amine-tethered PDA vesicles, suggesting that the swelling of vesicles does not mainly depend on the head group's structure. However, with the same vesicle molar concentration and the same amount of ethanol addition, the poly(PCDA-DETA) system experienced a significant intensity drop. Thus, the response depends on the number of ethanol molecules introduced. Contrary to the addition of HCl, the poly(PCDA-DETA) vesicles do not show a bathochromic shift supporting the contribution of H ion to the alignment of the side chains.

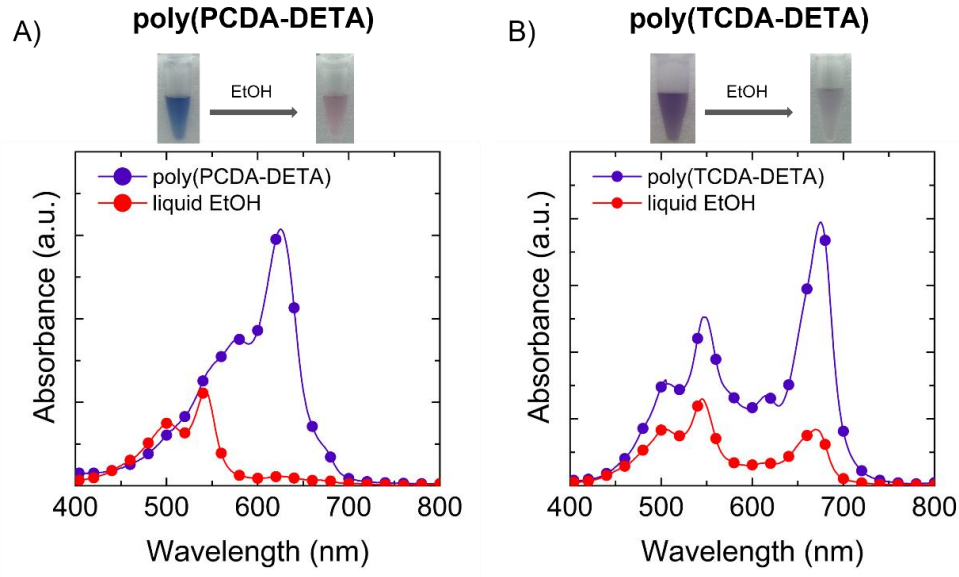

Figure 4. 9 UV-Vis absorption spectra of A) poly(PCDA-DETA), B) poly(TCDA-DETA) vesicles before (blue) and after (red) addition of liquid ethanol and corresponding photographs of vesicle solutions.

Based on the absorption spectra, purple poly(TCDA-DETA) vesicles initially exhibit a similar intensity drop with dominant absorption at 545 nm attributed to the red phase. The vesicle image taken after the excess liquid addition implies that ethanol dilutes the system considerably. Nevertheless, the UV-Vis profile still shows the blue and red phases as intermediate phases. A similar profile was obtained when the pH was lowered to 3 by adding acetic acid. Despite the clear red color on the appearance of the vesicle, the absorption spectra still showed an absorbance intensity at the blue phase. (See Figure 4.

7) Similarly, the blue phase has not completely disappeared after adding ethanol in excess. The poly(TCDA-DETA) vesicles are believed to have interrupted the conjugated backbone due to a twisted ribbon-like shape. Therefore, even though the dispersion forces are weakest, after the external trigger, poly(TCDA-DETA) vesicles either exhibit resistance against a fully conformational transition or the system releases the strain through some other way. Consequently, the twisted side chains provide enough freedom to release the strain created by the perturbation of ethanol or acetic acid molecules.[61]

1.14.2. **Size of Vesicles – Studied by Dynamic Light Scattering Method**

The swelling behavior is observed with dynamic light scattering and the color change of PDA vesicles is assessed.

Figure 4. 10 shows the DLS spectra of poly(PCDA) and poly(TCDA) vesicles before and after ethanol addition in excess with the corresponding vesicle images at the top. The poly(PCDA) size profile shows two distinct peaks before adding ethanol, a major population with Rh=60 nm and a minor population with Rh=127 nm. On the other hand, the size profile of poly(TCDA) becomes singular with Rh=70 nm in the blue phase.

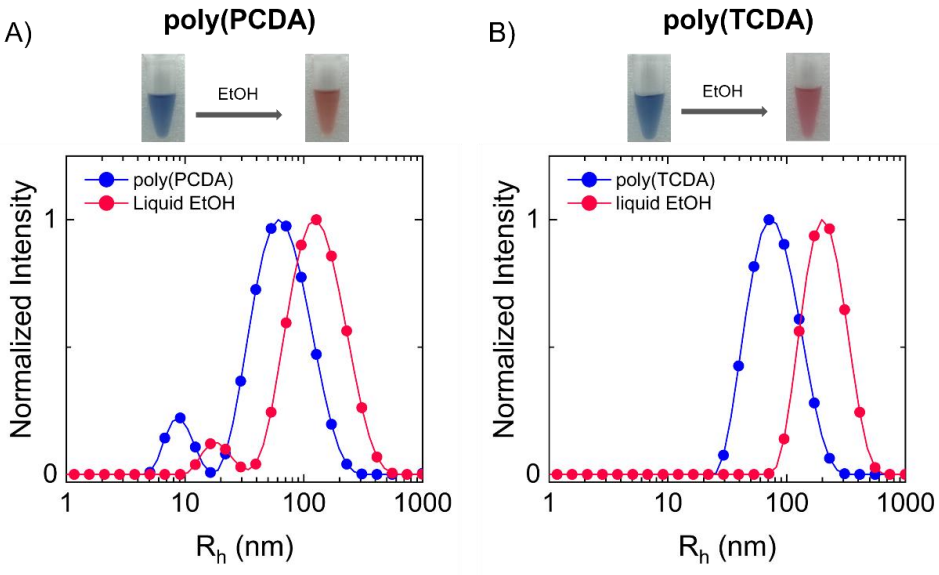

Figure 4. 10 Size distribution profiles of A) poly(PCDA), B) poly(TCDA), before (blue) and after (red) addition of liquid ethanol and corresponding photographs of solutions

In both cases, the shape of the size distribution profiles remains unchanged, with no growth of an additional peak when ethanol in excess is added into aqueous suspensions. Studies related to alcohol and surfactant exposure to PDA vesicles suggest that the ethanol molecules penetrate the inner layer of PDAs from their alkyl tail side. In contrast, the hydrophilic –OH group disturbs the hydrogen bonding of the outer layer of PDAs to minimize the energy. The insertion of ethanol molecules causes a strain relief within the

side chains leading to swelling of the vesicles. The reorganization of conjugated structure emerges in the red phase vesicles. The size profiles are increased almost three-fold, with R_h=127 nm and R_h=200 nm for poly(PCDA) and poly(TCDA) vesicles, respectively. The initial vesicle concentrations are kept at 1 mM, which is relatively high compared to the study in the literature. Therefore, even if the polarity of the aqueous medium is changed with the excess addition of ethanol, the vesicles resist disruption, which might be due to high vesicle concentration.[5, 65]

Figure 4. 11 illustrates the size distribution histograms of amine-substituted poly(PCDA-DETA) and poly(TCDA-DETA) vesicle solutions. In poly(PCDA-DETA), the DLS results showed the conversion of two-size profiles into one single-size profile when ethanol is added in excess to the solution. The hydrodynamic radii are 39 nm and 170 nm for blue and 230 nm for red phases. The size profile of poly(TCDA-DETA) followed a similar trend as the poly(PCDA) and poly(PCDA-DETA), where a minor population with R_h=53 and a major population with Rh=260 nm was observed before ethanol exposure.

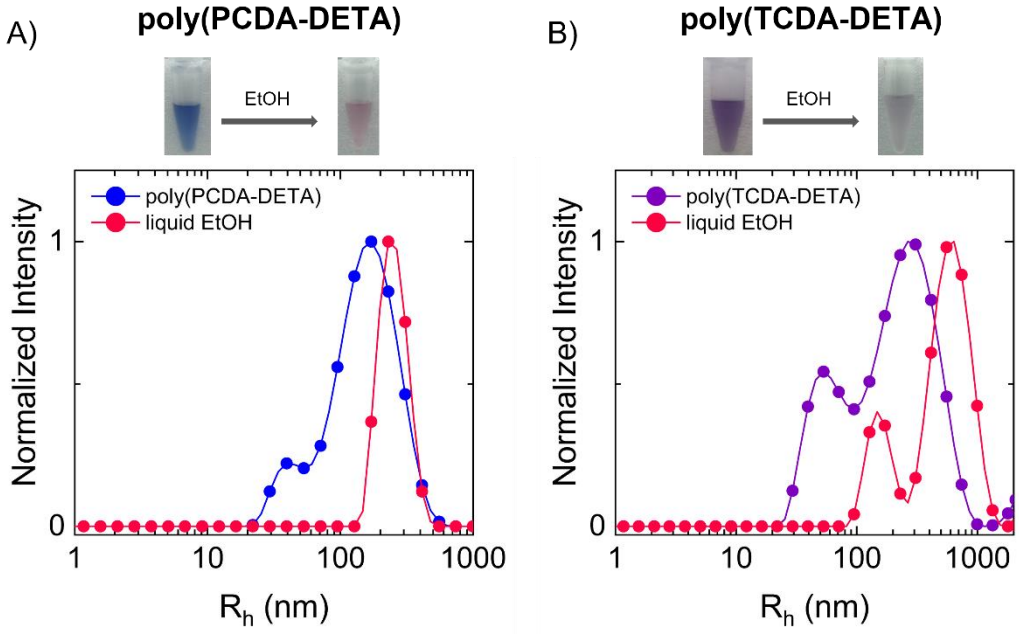

Figure 4. 11 Size distribution profiles of A) poly(PCDA-DETA), B) poly(TCDA-DETA), before (blue) and after (red) addition of liquid ethanol and corresponding photographs of solutions

It is clear from the corresponding vesicle images that the vesicle concentration in the poly(PCDA-DETA) system is highly declined, while this reduction is even more pronounced in the poly(TCDA-DETA) system making the DLS spectra in the red phase unreliable that could not fit the modelling in the instrument. The ethanol molecules and vesicle surface interaction could differ greatly from the monocarboxylic poly(PCDA) and

poly(TCDA). While the ethanol addition to all vesicle solutions is kept the same, the shrinkage of amine-substituted PDA vesicles suggests that these vesicles' swelling ability is less than the monocarboxylic ones. The ethyl spacers in DETA functional group might be making the penetration of ethanol molecules to the hydrophobic layers of PDA difficult. Instead, the excess addition of ethanol distorts the polarity of the suspension medium, which could disrupt amine-tethered vesicles. The intensity and conjugated length profiles of PDA vesicles are further evaluated by analyzing the UV-Vis spectra in the following section.[65]

1.15. Vapor Exposure to PDA Vesicles

DETA-functionalized PDA vesicles are subjected to vapor forms of acetic acid and ethanol to assess the difference in forms of stimuli with the conformational and structural response of PDA vesicles.

1.15.1. Optical Properties of Vesicles – Studied by Visual Imaging and UV-Visible Spectroscopy Method

The optical absorption spectra of PDA vesicles upon exposure to ethanol and acetic acid was analysed using UV-Vis spectroscopy to assess the conformational transition on the conjugated backbone.

The UV-Vis spectra of monocarboxylic PDA vesicle solutions, before and after exposures to acetic acid and ethanol vapor, are depicted in Figure 4. 12. Additionally, the excess liquid ethanol addition results are included for visual comparison. The initial planar conjugated backbone of poly(PCDA) and poly(TCDA) vesicles exhibited maximum absorption at 631 nm and 641 nm, respectively, resulting in visually blue color. As anticipated, the bubbling of acetic acid into either vesicle solution did not induce the strain necessary for the structural reorganization of the PDA backbone. The visual appearance remained blue after 5 minutes of acetic acid bubbling. The absorption spectra of these vesicles also indicated that no additional electronic states were formed upon exposure to acetic acid vapor, as the spectra remained nearly unchanged.

However, exposure to ethanol vapor again did not exhibit any spectral changes in the UV-Vis plots. The visual appearance of the vesicles maintained their blue color. The low concentration of ethanol molecules cannot penetrate the inner layers of the monocarboxylic PDAs. The interactions likely occur primarily on the surface of the

vesicles, which does not exert sufficient strain to induce structural realignment in the polymer backbone, as seen in the case of excess ethanol addition.[5]

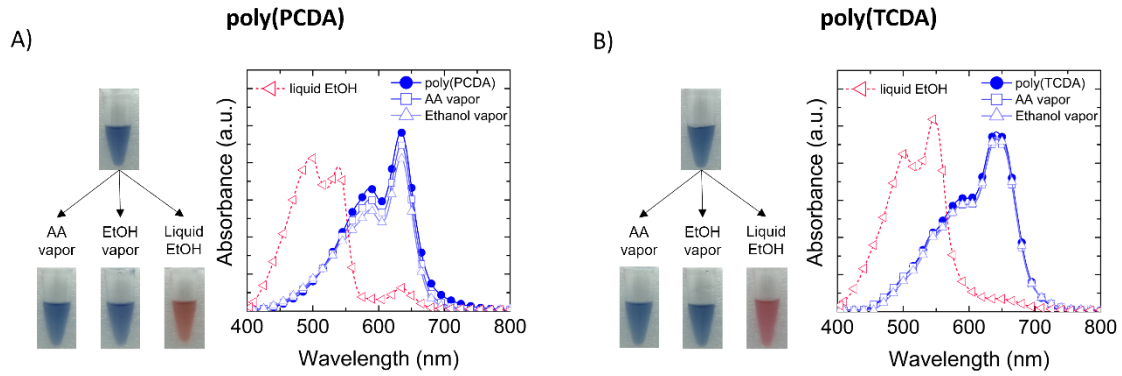

Figure 4. 12 UV-Vis spectra of A) poly(PCDA) and B) poly(TCDA) vesicles upon exposure to acetic acid (AA) vapor, ethanol (EtOH) vapor, and liquid ethanol with the corresponding images on the left of each spectra.

The absorption spectra of DETA-functionalized PDA vesicles, before and after acetic acid and ethanol vapor exposures, are illustrated in Figure 4. **13**, along with the spectra of liquid ethanol addition for comparison. Initially, the blue form of poly(PCDA-DETA) absorbed light at 626 nm, but this peak disappeared completely after exposure to acetic acid vapor. Instead, a new peak at 543 nm emerged, indicating the presence of a red phase. The poly(TCDA-DETA) vesicles in an intermediate purple phase comprising a blue phase fraction that absorbed light at 675 nm and a red phase fraction that absorbed light at 546 nm. Exposure to acetic acid vapor significantly reduced the intensity of the blue phase and resulted in visually red color due to the dominance of the red phase. This suggests a strong interaction between the amine groups and acetic acid, even with a low concentration of acetic acid molecules during vapor exposure.

Interestingly, similar behavior was observed with acetic acid vapor exposure in poly(TCDA-DETA) vesicles, as seen with the addition of excess liquid ethanol. Despite the weaker dispersion forces between the hydrophobic alkyl tails of poly(TCDA-DETA), the blue phase peak was not eliminated but remained a small fraction after exposure to acetic acid vapor. In contrast, the blue phase disappeared completely in poly(PCDA-DETA) upon exposure to acetic acid vapor despite the stronger dispersion forces in the hydrophobic tail. This suggests that the poly(TCDA-DETA) vesicle solution finds a dissipative pathway to release strain without converting to a fully twisted ribbon-like conformation, possibly due to its initial intermediate phase. Additionally, the blue phase of poly(PCDA-DETA) absorbed light at 626 nm, while the blue phase fraction in poly(TCDA-DETA) was present at 675 nm, indicating that the blue phase in poly(TCDA-

DETA) vesicles has a longer conjugated length, which may contribute to the incomplete disappearance of the blue phase.

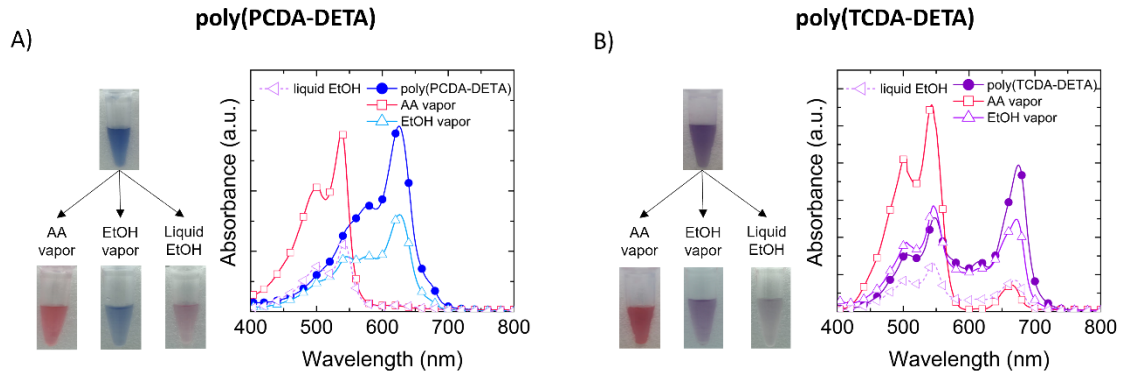

Figure 4. 13 UV-Vis spectra of A) poly(PCDA-DETA) and B) poly(TCDA-DETA) vesicles upon exposure to acetic acid (AA) vapor, ethanol (EtOH) vapor, and liquid ethanol with the corresponding images on the left of each spectra.

As observed in the vesicle images, exposure to ethanol vapor of amine-substituted vesicles tended to decrease the intensity of the absorption spectra. In the case of poly(PCDA-DETA), along with the decreased intensity, a small increment in the peak at 543 nm was observed, indicating the emergence of the red phase. Similarly, in poly(TCDA-DETA), where the blue phase dominated before exposure, the red phase became dominant after 10 minutes of ethanol vapor exposure, indicating a conformational change in the backbone. However, since the concentration of ethanol molecules is lower during vapor exposure, the perturbation of ethanol molecules may be limited to the surface of the vesicles and could not penetrate deeper into the inner layers of the PDA. Nonetheless, the swelling of ethanol molecules is more pronounced in poly(TCDA-DETA) vesicles, as evidenced by the DLS results showing a doubling in vesicle size, likely due to weaker dispersion forces (See Figure 4. 15).

Furthermore, despite the similar spectra observed after exposure to ethanol vapor for monocarboxylic PDAs, DETA-functionalized PDA vesicles exhibited more pronounced conformational transitions, highlighting the susceptibility of the ethanol molecules by the amine groups.[5, 61, 65]

1.15.1. **Size of Vesicles – Studied by Dynamic Light Scattering Method**

The swelling behavior of PDA vesicles upon vapor exposure to ethanol and acetic acid is evaluated using dynamic light scattering.

When exposed to acetic acid and ethanol vapor, the size distribution of PDA vesicles is illustrated in Figure 4. 14The DLS spectra and vesicle image of excess liquid ethanol

addition were also included for visual comparison. Similar to exposure to liquid acetic acid, the monocarboxylic poly(PCDA) and poly(TCDA) exhibited no visible color change upon exposure to acetic acid vapor. The DLS results further demonstrate that the 5-minute bubbling of acetic acid did not cause any rearrangement in the vesicle structure, as the size distribution profiles of the PDA vesicles before and after exposure remained similar.

The colorimetric response of monocarboxylic PDA vesicles to the addition of excess liquid ethanol was evaluated in the previous section. The form of ethanol introduced to the systems is important regarding the stimulus concentration. The liquid ethanol was added at a concentration approximately three times that of the vesicle solution. However, in the case of ethanol vapor, the ethanol concentration in the vesicle solution is lower, resulting in a weaker disruption ability of hydrogen bonding in the polar head and a lack of structural transition.[5] The swelling of the vesicles was not observed when exposed to ethanol vapor.

Even after 5 and 10 minutes of vapor bubbling, the size distribution profiles remained unaffected, suggesting the absence of any mechanical forces that could induce conformational transitions.

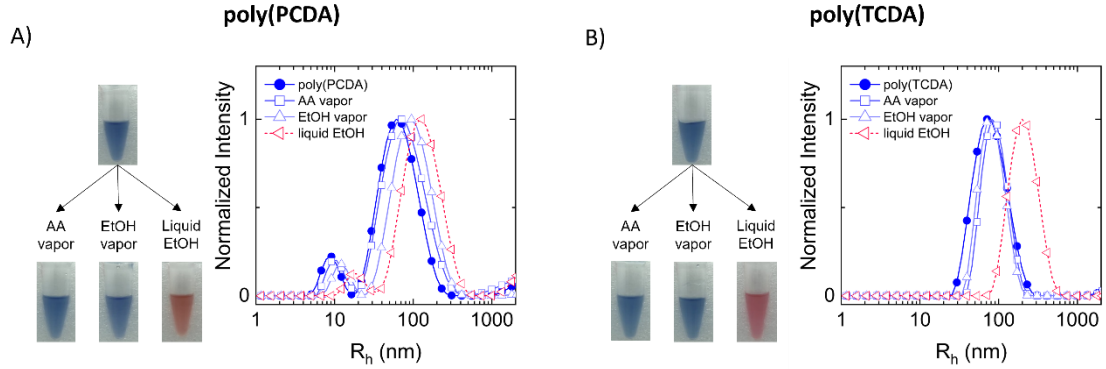

Figure 4. 14 DLS spectra of A) poly(PCDA) and B) poly(TCDA) vesicles upon exposure to acetic acid (AA) vapor, ethanol (EtOH) vapor, and liquid ethanol with the corresponding images on the left of each spectra.

The size distribution profiles of DETA-substituted PDA vesicles and their visual appearances are presented in Figure 4. 15. Additionally, the results of liquid ethanol addition are included. The poly(PCDA-DETA) vesicles exhibited two populations: a minor population at 40 nm and a major population at 170 nm prior to the triggering exposure. After 5 minutes of bubbling with acetic acid, a colorimetric transition from blue to red was induced, accompanied by an interesting change in the size distribution. The major population shifted to 53 nm, while the minor population appeared at 182 nm. On

the other hand, the poly(TCDA-DETA) vesicles initially displayed two distinct size populations, with the minor population at 53 nm and the major population at 265 nm. Similarly, exposure to acetic acid vapor caused a switch in the populations, with the 53 nm hydrodynamic radius vesicles becoming the major population. The mean Rh values remained nearly the same. The visual observations before and after exposure to acetic acid vapor revealed a transition from purple to red.

Upon adding excess liquid ethanol, the PDA backbone undergoes a conformational transition due to vesicle swelling, similar to the monocarboxylic poly(PCDA) and poly(TCDA) vesicles. However, a 10-minute exposure to ethanol vapor did not result in any color change or structural rearrangement in the poly(PCDA-DETA) vesicles. Poly(TCDA-DETA), on the other hand, doubled its size with a minor population in 147 nm and a major population at 660 nm, indicating the swelling of the poly(TCDA-DETA) lipid structure, but a visible color change could not be observed.[61, 65]

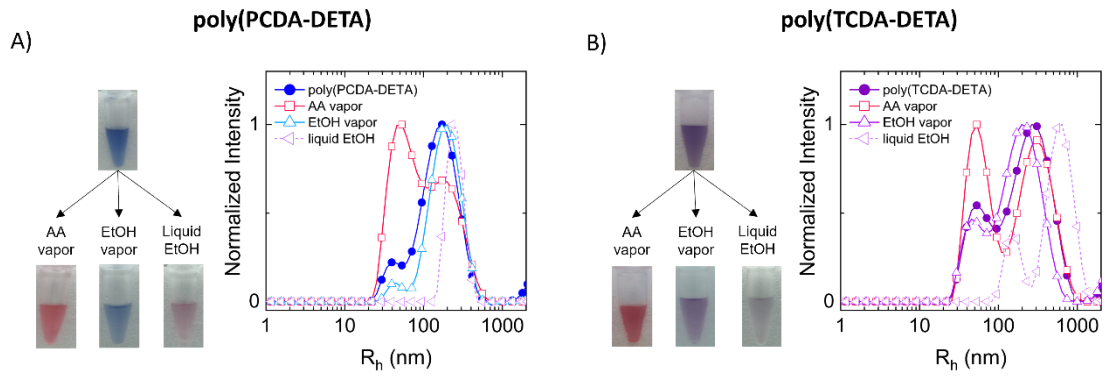

Figure 4. 15 DLS spectra of A) poly(PCDA-DETA) and B) poly(TCDA-DETA) vesicles upon exposure to acetic acid (AA) vapor, ethanol (EtOH) vapor, and liquid ethanol with the corresponding images on the left of each spectra.

CHAPTER 5. PDA ELECTROSPUN FIBERS

This chapter explores the potential of using PDA-based electrospun fibers instead of PDA vesicles in colorimetric detection of food spoilage. The DETA-substituted DA monomers were chosen as the sensing material, and polyethylene oxide (PEO) served as matrix material in the polymer blend used to produce fibers. Fibers were produced with the electrospinning method and characterized with FTIR spectroscopy. Electrospun fibers were tested for their colorimetric response upon acetic acid and ethanol exposure. Fibers were also exposed to various food sources such as milk, wine and chicken spoilage conditions. The fiber color and structure changes were analyzed with visual and spectroscopic tools.

1.16. Characterization of PDA Fibers

PDA-based fibers were obtained by photopolymerizing white color DA-PEO fiber mats under 254 nm UV exposure for 10 mins. The color of the electrospun fiber mat was converted to blue, confirming the successful polymerization. FTIR spectra of PEO powder and fibers produced with different DAs were recorded to check whether electrospun fibres consist of PEO and the DA monomer. Figure 5. 1 shows the FTIR spectra of PEO powder and fibers obtained by mixing PEO with four different DA monomers. The polymer blend that produces fibers contains significantly higher PEO concentrations than PDA. Therefore, the characteristic IR vibrations of PEO dominate the spectra in terms of intensity. The peak at 2880 cm^{-1} is attributed to the stretching of methylene (H-C-H) with no specific shift upon mixing with PDA, and a carbonyl group (C-O) vibration peak appears at 1097 cm^{-1}.[126] To assess the presence of characteristic IR bands of DAs, specific wavenumber intervals of the spectra are being focused in **Figure 5. 2**. The amine bands of DETA-substituted DA monomers appear around 3296 cm^{-1} and 3298 cm^{-1} for PEO-poly(PCDA-DETA) and PEO-poly(TCDA-DETA), respectively (Figure 5.2A). These regions have no observable IR transmission in the spectra of PEO and monocarboxylic PDA/PEO fibers. Mixing DA with PEO cause no changes in the methylene stretching vibrations of all components, as shown in Figure 5. 2 B. The ester (C=O) band of PEO-poly(PCDA) and PEO-poly(TCDA) appears at 1692 cm^{-1}, whereas it is at 1722 cm^{-1} in the spectra of DETA modified DA monomers (Figure 5. 2C). The difference can be attributed to the stronger carbonyl bond, indicating that the hydrogen bonds are reduced when polyamine is attached to a diacetylene monomer.[126] Figure 5. 2D

shows the C=C bond appearing at 723 cm^{-1} and 731 cm^{-1} for commercial DAs and DETA-substituted ones, respectively.[126]

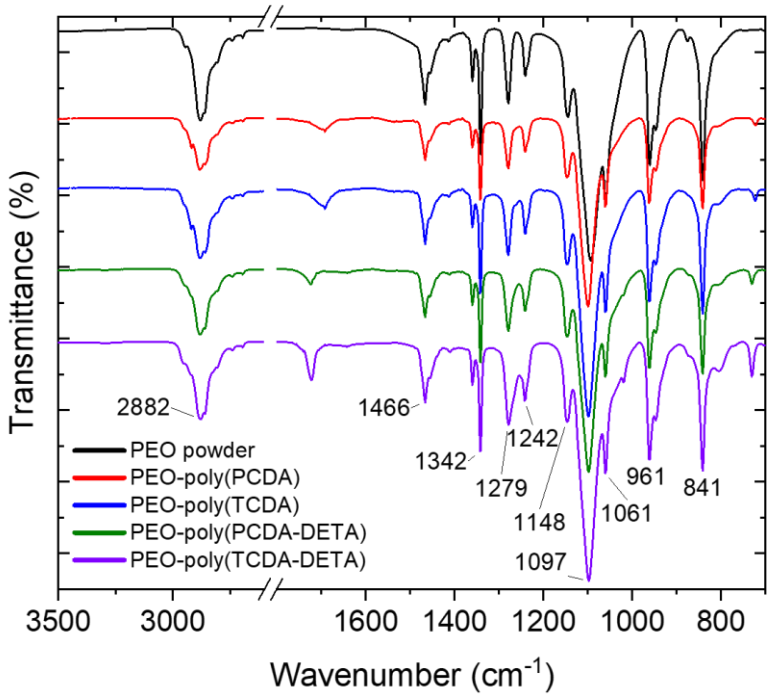

Figure 5. 1 From top to bottom: FTIR spectra of PEO powder (black); electrospun fibers of PEO-poly(PCDA) (red), PEO-poly(TCDA) (blue), PEO-poly(PCDA-DETA) (green), and PEO-poly(TCDA-DETA) (purple).

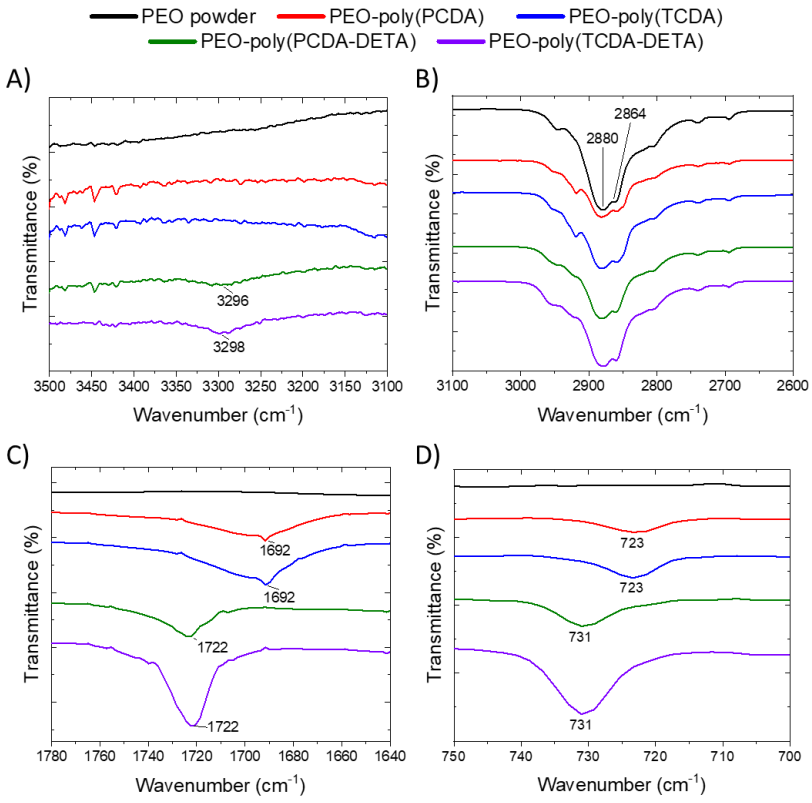

Figure 5. 2 Specific intervals of FTIR spectra of PEO powder and electrospun fibers.

1.17. **Colorimetric Response of PDA-based Fibers to Volatiles**

The electrospun fibers were exposed to ethanol and acetic acid vapors to assess their colorimetric response. The detailed experimental procedure was given in the Methods Section of this thesis. The color change in fibers was monitored visually from the recorded images, as shown in Figure 5. 3. Unlike the response of PDA vesicles to ethanol vapor exposure presented in Chapter 4 of this thesis, the electrospun fibers did not show a visually observable colorimetric response to ethanol vapor exposure.

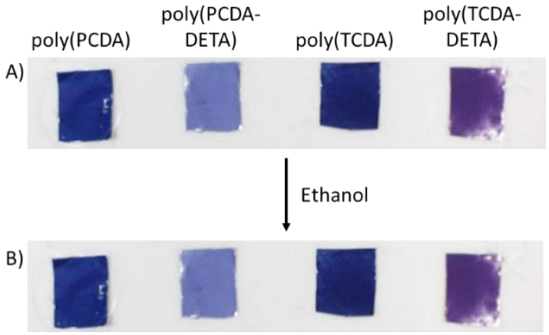

Figure 5. 3 Images of PEO-PDA electrospun fibers A) before and B) after ethanol vapor exposure.

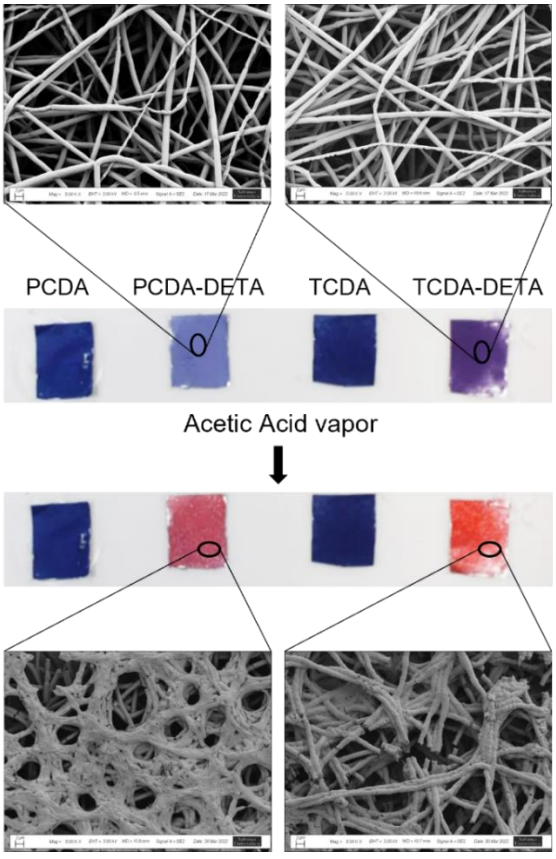

Figure 5. 4 SEM images of PEO-poly(PCDA-DETA) and PEO-poly(TCDA-DETA) electrospun fibers before and after acetic acid vapor exposure with corresponding visual images in the middle.

When fibers are exposed to acetic acid vapor, a colorimetric response as a color change from blue to red is observed for DETA-substituted PEO-PDA electrospun fibers (Figure 5. 4). The SEM images were recorded for the fibers before and after the color change. After exposure to acetic acid vapors and transitioning from blue to red, the top layer of fibers lost their fiber structure but attached as if they were dissolved.

1.18. **Colorimetric Response of PDA-Fibers during Food Spoilage**

Fibers were exposed to spoilage conditions of various food sources such as milk, wine and chicken by attaching to the inner wall of the food containers, as shown in **Figure 5. 5**A for the wine spoilage experiment. The changes in fiber color were visually monitored for a definite time. Figure 5. 5B shows the colorimetric changes in fibers constituted of DETA-substituted DAs. After 1 day, poly(PCDA-DETA) containing fibers were purple colored, whereas the transition from purple to red phase is almost completed in poly(TCDA-DETA)-containing fibers. At the end of the second day, the poly(PCDA-DETA) containing fibers were purple, while poly(TCDA-DETA) containing fibers were converted to red.

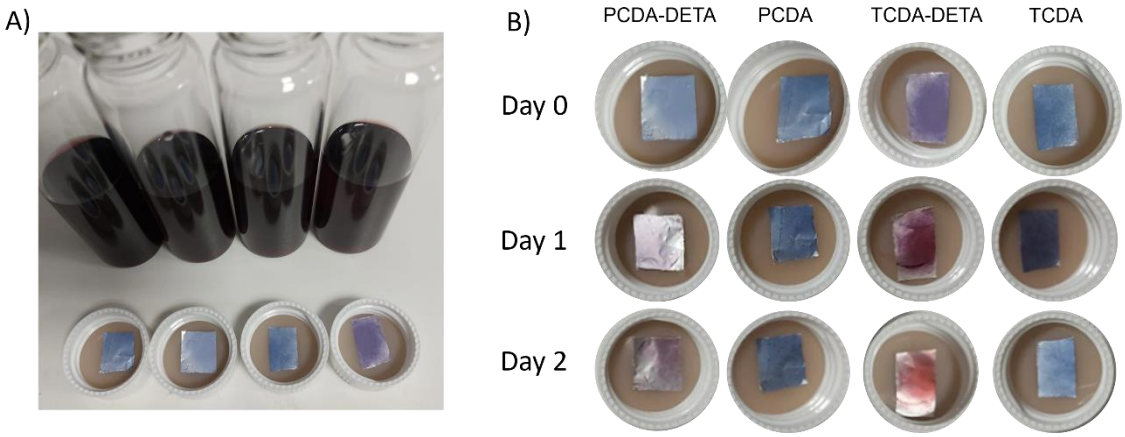

Figure 5. 5 A) Image of PEO-PDA electrospun fibers attached to the cover of the bottles that contain equal amounts of red wine and B) their monitored images for 2 days

Fibers consisting of monocarboxylic PDAs did not exhibit colorimetric response to volatiles of wine, indicating that specific interactions between released vapor from wine and the polyamine headgroup of DETA-substituted DA-containing fibers lead to the color change. Red wine spoilage at room temperature occurs over days, sometimes weeks.[127, 128] Considering the short duration of two days for a red wine to spoil at room temperature, the colorimetric response obtained from fibers cannot indicate spoilage. Instead, it indicates the presence of volatiles, which are already imminently present upon opening

the wine bottle and also increase slowly with the spoilage of wine. One of the volatile in wine is acetic acid.[129] In conclusion, fibers with DETA-substituted DAs are highly sensitive to acetic acid volatiles in wine and can be utilized for colorimetric detection of acid content in wine as a future work.

Milk spoilage was also studied using the same approach, as shown in Figure 5. 6. During milk spoilage, lactic acid is produced. Results in Figure 5. 6B indicate that DETA-substituted DA-containing fibers can also detect the lactic acid presence in the system, contrary to the carboxylic DA-containing fibers. The color changes from blue to purple in the poly(PCDA-DETA)-containing fibers and purple to burgundy in the poly(TCDA-DETA) containing fibers. Thus, the colorimetric response of fibers to lactic acid presence is not as pronounced as to acetic acid. This might be due to lactic acid's lower vapor pressure than acetic acid. The amount of molecules interacting with PDA chains and exerting force on the backbone to lead to a conformational transition is limited. The experiment was stopped after two days at room temperature since it was more than enough time, usually ~ 2 hours, for milk to spoil at room temperature. In conclusion, DETA-substituted DA-containing fibers can detect a poor volatile compound such as lactic acid; however, without further in-depth study on improving its sensitivity to detect spoilage within hours, it cannot be used for milk spoilage detection.

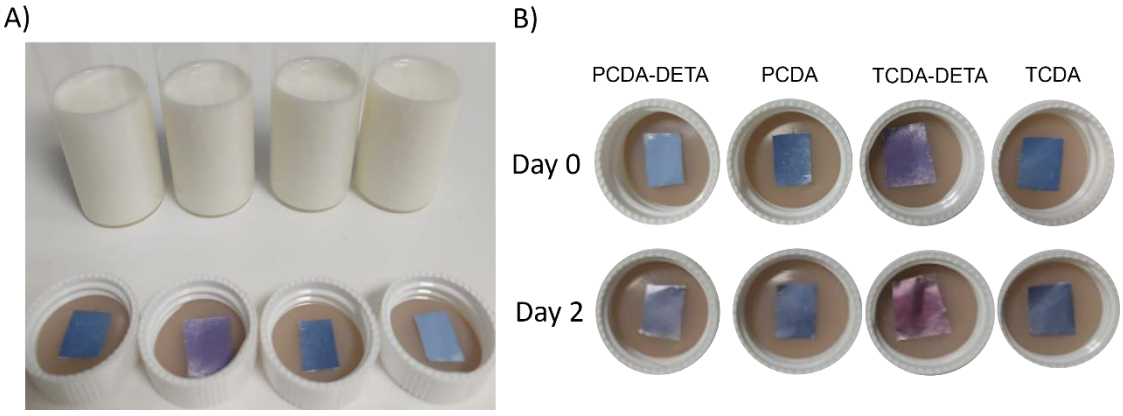

Figure 5. 6 A) Image of PEO-PDA electrospun fibers attached to the cover of the bottles that contain equal amounts of milk and B) Their images were taken on day 0 and day 2.

The chicken spoilage experiments also showed that poly(TCDA-DETA)-containing electrospun fibers turned red from their initial purple color quickly after 3 hours. On the contrary, a visible color change from blue to red is not observed in PEO-poly(PCDA-DETA) electrospun fiber. SEM images showed no fibers after the exposure to chicken spoilage as if there was only a dissolved (melted) top layer (Figure 5. 7B). This might be

due to the increased humidity levels during the chicken spoilage in the closed container. The water vapor might have condensed on the fiber surface and caused dissolution. This raise concerns that an additional measure should be put in place for applications in high humidity conditions to protect the active sensing fiber layer.

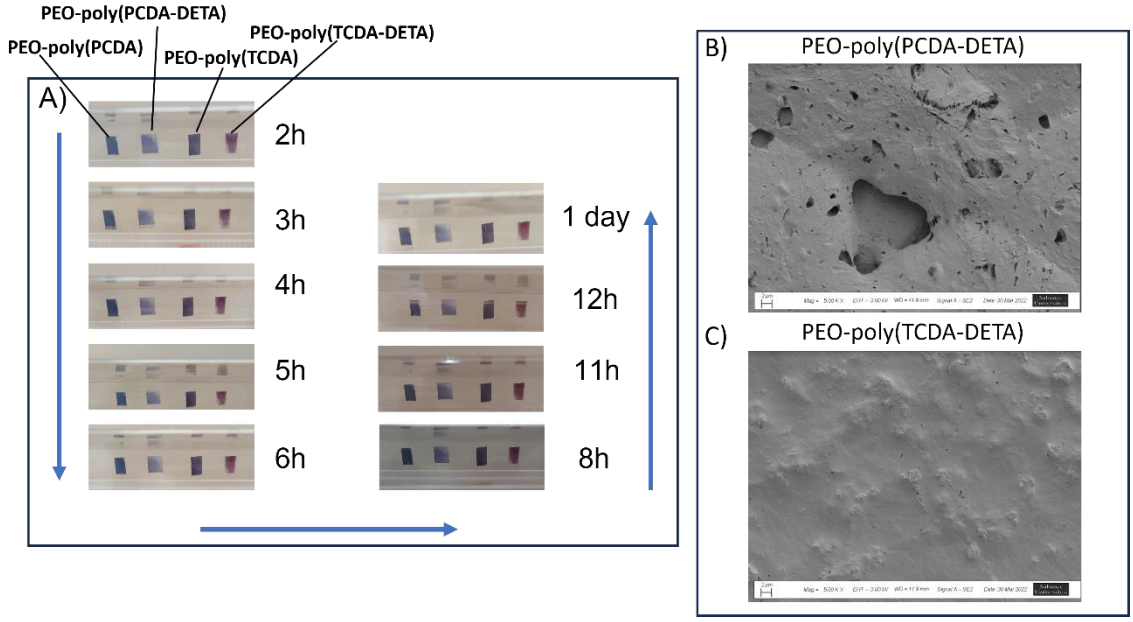

Figure 5. 7 A) Images of fibers monitored for 1 day at various intervals, B and C) SEM images taken at the end of the 1 day.

FTIR spectra of fibers after spoilage experiments were recorded to assess whether these structural deformations observed in SEM images occur due to a change in chemical structure or it is only physical. Figure 5. 8 the peak at 1722 cm^{-1} shifted for 2 units in all experiments of poly(PCDA-DETA)/PEO fibers indicating a small increase in mobility of the C=O bond. This peak disappeared when the poly(TCDA-DETA)/PEO fibers were exposed to acetic acid vapor, milk and wine experiments, as shown in Figure 5. 8B. The band's disappearance suggests a structural rearrangement in those fibers where the C=O bond is either shifted or completely disrupted after the experiment. On the contrary, the C=O bond at 1722 cm^{-1} remained present after chicken experiments suggesting that the present vapor inside the medium is not strong enough to induce such a shift or disruption. The structural rearrangement reveals itself in colorimetric response but not in vibrational modes, causing a change in the energy of the C=O bond.[126]

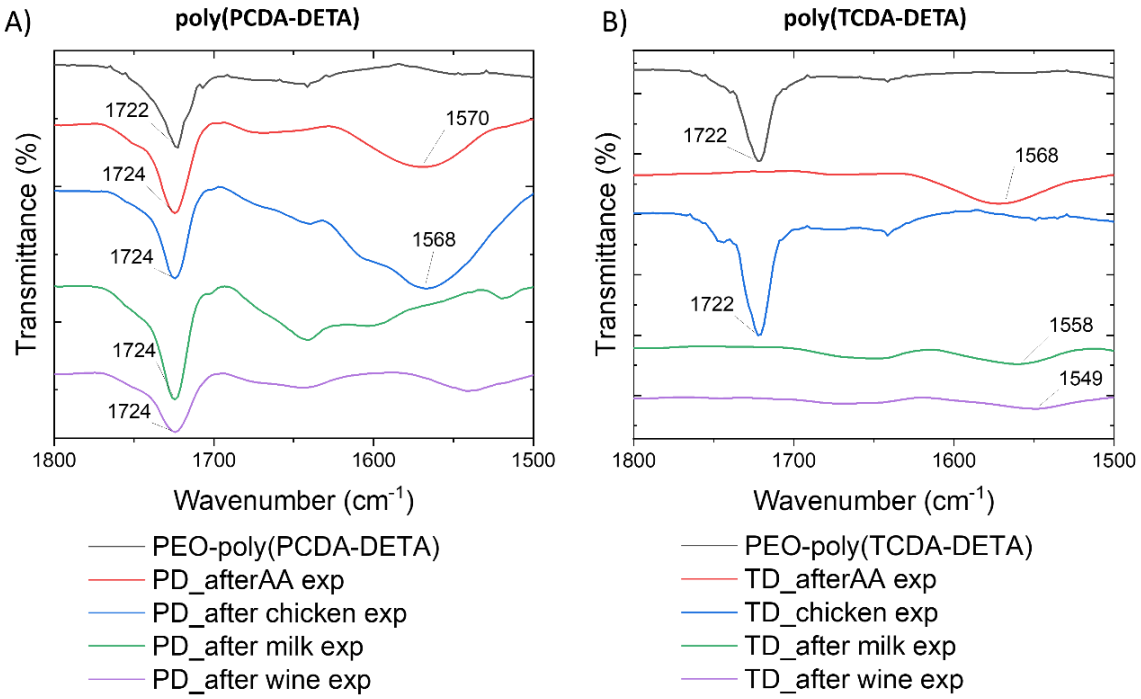

Figure 5. 8 FTIR spectra of A) PEO-poly(PCDA-DETA) and B) PEO-poly(TCDA-DETA) electrospun fibers under different conditions.

CHAPTER 6. CONCLUSION

Polydiacetylenes (PDAs) are valuable conjugated polymers investigating supramolecular interactions and biosensing applications. This master thesis focuses on the response of modified PDAs to various external stimuli to explore the potential for use in sensor applications. Two functional groups are chemically bonded to diacetylene monomers with 23 and 25 carbon in their alkyl chain. Chapter 3 and Chapter 4 evaluated the vesicle forms of PDAs; Chapter 5 focused on the PDA-based electrospun fibers to test the capabilities of solid-state applications, mainly in food spoilage.

While previous literature has extensively studied the thermal and chemical chromism of *m*BzA-functionalized PDAs, the influence of photopolymerization duration on these properties has been overlooked. In Chapter 3, the optical response of vesicle forms of bulky *m*BzA-substituted PDAs is evaluated in high pH conditions by changing the photopolymerization time. Results revealed that varying the UV irradiation time tunes the pH response of polydiacetylene (PDA) vesicles. Prolonged photopolymerization delays the color transition pH of poly(PCDA), poly(PCDA-*m*BzA), and poly(TCDA-*m*BzA) vesicles. This delay is attributed to the reduced fluidity of OH^- ions due to higher polymer conversion resulting from longer photoirradiation. Notably, the monocarboxylic poly(TCDA) formed by shorter alkyl tail monomers did not show any difference in pH response when the UV irradiation increased, likely due to the weak dispersion forces.

Poly (TCDA-*m*BzA) vesicles demonstrate higher resistance to high pH levels than poly(PCDA-*m*BzA) vesicles, regardless of the irradiation time. Despite weaker dispersion forces between TCDA-mBzA layers with the same bulky head group, the red phase is obtained at higher poly(TCDA-mBzA) pH values. This observation suggests enhanced head group interactions may create a dissipation pathway for releasing the strain induced by OH ions, which dominates the weak dispersion forces between TCDA-*m*BzA layers. The pH reversibility of poly(PCDA-*m*BzA) vesicles were already; however, the present study demonstrates that short-time irradiated PDA vesicle systems cannot restore the head group's hydrogen bond network, resulting in an irreversible pH response. In contrast, prolonged UV irradiation facilitates these restorative interactions, inducing partial planarity on the conjugated backbone. The reversibility is more pronounced in poly(PCDA-*m*BzA) vesicles than poly(TCDA-*m*BzA), indicating that strong dispersion forces contribute to the realignment of DA layers, while weaker dispersion forces stabilize the system in an intermediate purple phase.

In Chapter 4, the response of amine-modified PDA vesicles to various external triggers is assessed to the conformational arrangement. Low pH, liquid ethanol addition and vapor forms of acetic acid and ethanol are used as external triggers. Results showed that the functionalization with DETA promotes the response of PDA vesicles to acetic acid molecules in both liquid and vapor form. Despite the stronger dispersion forces between PCDA-DETA lipids, a complete disappearance of the blue phase is observed in poly(PCDA-DETA) vesicles upon exposure to the acetic acid vapor and excess liquid ethanol. In contrast, UV-Vis spectra indicate the presence of a fraction of the blue phase in poly(TCDA-DETA) vesicle solutions after these exposures. This difference may be attributed to strain release occurring through mechanisms other than the complete twisting of the conjugated backbone, resulting in the persistence of blue phase vesicles in the poly(TCDA-DETA) system. The initial intermediate purple phase could contribute to this distinction. Furthermore, adding excess liquid ethanol leads to a color transition in both DETA-functionalized and monocarboxylic PDA vesicles, suggesting that the amine-modified head group functionality is independent of the color change ability but dependent on the level of color change. Moreover, the amount of liquid ethanol added proves to be a crucial factor in inducing conformational changes in the PDA vesicles' conjugated backbone.

DETA-functionalized electrospun fibers are tested in Chapter 5 to explore the applicability of solid-phase tools. PEO is used as a matrix polymer. Despite the color change observed upon adding excess liquid ethanol, the electrospun fibers do not exhibit a color change upon ethanol vapor exposure, similar to the results observed with ethanol bubbling in vesicle PDA forms. DETA-substituted PDA-based electrospun fibers in food spoilage experiments demonstrate a visual color change from blue/purple to red over time, indicating conformational transitions. However, the melting behavior in these experiments suggests that the humidity could be effective.

In conclusion, this master thesis has provided valuable insights into polydiacetylenes' supramolecular interactions and biosensing applications. The chemical modification of diacetylene monomers with *m*BzA and DETA functional groups has shed light on the influence of dispersion forces and enhanced head group interactions. The findings regarding the pH response, reversibility, and stimuli sensitivity of PDA vesicles contribute to understanding the underlying mechanisms in these systems and possible sensor applications. Furthermore, using electrospun fibers as solid-phase tools demonstrates their potential application for studying conformational changes in

PDA/PEO systems. However, additional experiments are required to explore the effect of humidity on these fibers. Overall, this research enhances the knowledge of polydiacetylene-based materials and contributes to the fundamental advancements in supramolecular chemistry and biosensing applications.

.

PUBLICATIONS RELATED TO THIS THESIS

- Hande E. Cingil, Gizem Beliktay, Eric M. M. Tan. A study on the conformation-dependent colorimetric response of polydiacetylene supramolecules to external triggers. *Materials Chemistry Frontiers*, **7(2)** (2023), 294–305, doi: 10.1039/d2qm01006b
- Gizem Beliktay, Tayyaba Shaikh, Emirhan Koca and Hande E. Cingil. The effect of photopolymerization time on the reversible colorimetric pH response of polydiacetylene vesicles. (Under revision)

BIBLIOGRAPHY

1. D.-H. Park, B. Kim and J.-M. Kim, *Bulletin of the Korean Chemical Society*, 2016, **37**, 793-794.
2. H. Peng, J. Tang, J. Pang, D. Chen, L. Yang, H. S. Ashbaugh, C. J. Brinker, Z. Yang and Y. Lu, *Journal of the American Chemical Society*, 2005, **127**, 12782-12783.
3. S. Kolusheva, T. Shahal and R. Jelinek, *Journal of the American Chemical Society*, 2000, **122**, 776-780.
4. C. Kim and K. Lee, *Biomacromolecules*, 2019, **20**, 3392-3398.
5. H. E. Cingil, G. Beliktay and E. M. Tan, *Mater. Chem. Front.*, 2023.
6. J. M. Lehn, *Angew. Chem., Int. Ed. Engl.*, 1988, **27**, 89-112.
7. J.-M. Lehn, *Angewandte Chemie International Edition in English*, 1990, **29**, 1304-1319.
8. P. D. Beer and P. A. Gale, *Angewandte Chemie International Edition*, 2001, **40**, 486-516.
9. G. Liang, H. Ren and J. Rao, *Nature chemistry*, 2010, **2**, 54-60.
10. H. E. Cingil, E. B. Boz, G. Biondaro, R. De Vries, M. A. Cohen Stuart, D. J. Kraft, P. Van der Schoot and J. Sprakel, *J. Am. Chem. Soc.*, 2017, **139**, 4962-4968.
11. H. E. Cingil, I. M. Storm, Y. Yorulmaz, D. W. te Brake, R. de Vries, M. A. Cohen Stuart and J. Sprakel, *Journal of the American Chemical Society*, 2015, **137**, 9800-9803.
12. E. V. Anslyn, *The Journal of organic chemistry*, 2007, **72**, 687-699.
13. J. W. Steed and J. L. Atwood, *Supramolecular chemistry*, John Wiley & Sons, 2022.
14. F. J. Hoeben, P. Jonkheijm, E. Meijer and A. P. Schenning, *Chem. Rev.*, 2005, **105**, 1491-1546.
15. S. Topal, O. Karakaya, E. Sezer, B. Ustamehmetoglu and T. Ozturk, *International Journal of Energy Research*, 2022, **46**, 21979-21988.
16. D. Gunturkun, R. Isci, B. Sütay, L. A. Majewski, S. Faraji and T. Ozturk, *European Polymer Journal*, 2022, **170**, 111167.
17. R. H. Friend, R. Gymer, A. Holmes, J. Burroughes, R. Marks, C. Taliani, D. Bradley, D. D. Santos, J.-L. Bredas and M. Lögdlund, *Nature*, 1999, **397**, 121-128.
18. K. M. Coakley and M. D. McGehee, *Chemistry of materials*, 2004, **16**, 4533-4542.
19. D. T. McQuade, A. E. Pullen and T. M. Swager, *Chemical reviews*, 2000, **100**, 2537-2574.
20. M. O. Sinnokrot and C. D. Sherrill, *Journal of the American Chemical Society*, 2004, **126**, 7690-7697.
21. B. Yoon, S. Lee and J.-M. Kim, *Chemical Society Reviews*, 2009, **38**, 1958-1968.
22. X. Qian and B. Städler, *Chem. Mater.*, 2019, **31**, 1196-1222.
23. M. A. Reppy and B. A. Pindzola, *Chemical Communications*, 2007, 4317-4338.
24. Y.-l. Su, *Reactive and Functional Polymers*, 2006, **66**, 967-973.
25. H. Sixl, in *Polydiacetylenes*, Springer, 2005, pp. 49-90.
26. H. Shin, B. Yoon, I. S. Park and J.-M. Kim, *Nanotechnology*, 2014, **25**, 094011.
27. A. V. Hall, O. M. Musa and J. W. Steed, *Crystal Growth & Design*, 2021, **21**,

3614-3638.
28. N. Traiphol, N. Rungruangviriya, R. Potai and R. Traiphol, *Journal of Colloid and Interface Science*, 2011, **356**, 481-489.
29. S. Okada, S. Peng, W. Spevak and D. Charych, *Acc. Chem. Res.*, 1998, **31**, 229-239.
30. K. P. R. Nilsson, A. Herland, P. Hammarström and O. Inganäs, *Biochemistry*, 2005, **44**, 3718-3724.
31. Q. Ye, X. You, G. Zou, X. Yu and Q. Zhang, *Journal of Materials Chemistry*, 2008, **18**, 2775-2780.
32. U. Jonas, K. Shah, S. Norvez and D. H. Charych, *Journal of the American Chemical Society*, 1999, **121**, 4580-4588.
33. Y. Tomioka, N. Tanaka and S. Imazeki, *The Journal of chemical physics*, 1989, **91**, 5694-5700.
34. J. M. Kim, E. K. Ji, S. M. Woo, H. Lee and D. J. Ahn, *Advanced Materials*, 2003, **15**, 1118-1121.
35. F. Fang, F. Meng and L. Luo, *Materials Chemistry Frontiers*, 2020, **4**, 1089-1104.
36. Z. Yuan and T. W. Hanks, *Polymer*, 2008, **49**, 5023-5026.
37. R. Chance, *Macromolecules*, 1980, **13**, 396-398.
38. M. Weston, R. P. Kuchel, M. Ciftci, C. Boyer and R. Chandrawati, *J. Colloid Interface Sci.*, 2020, **572**, 31-38.
39. R. Lécuiller, J. Berréhar, C. Lapersonne-Meyer and M. Schott, *Physical review letters*, 1998, **80**, 4068.
40. J. Wu, A. Zawistowski, M. Ehrmann, T. Yi and C. Schmuck, *Journal of the American Chemical Society*, 2011, **133**, 9720-9723.
41. M. N. Tahir, A. Nyayachavadi, J.-F. Morin and S. Rondeau-Gagné, *Polymer Chemistry*, 2018, **9**, 3019-3028.
42. A. D. Tjandra, M. Weston, J. Tang, R. P. Kuchel and R. Chandrawati, *Colloids Surf., A*, 2021, **619**, 126497.
43. M. Weston, A.-H. Pham, J. Tubman, Y. Gao, A. D. Tjandra and R. Chandrawati, *Mater. Adv.*, 2022.
44. M. Weston, A. D. Tjandra and R. Chandrawati, *Polymer Chemistry*, 2020, **11**, 166-183.
45. J. T. Wen, J. M. Roper and H. Tsutsui, *Ind. Eng. Chem. Res.*, 2018, **57**, 9037-9053.
46. S. R. Diegelmann and J. D. Tovar, *Macromol. Rapid Commun.*, 2013, **34**, 1343-1350.
47. D. G. Rhodes, D. A. Frankel, T. Kuo and D. F. O'Brien, *Langmuir*, 1994, **10**, 267-275.
48. M. Schott, *J. Phys. Chem. B*, 2006, **110**, 15864-15868.
49. R. W. Carpick, D. Y. Sasaki, M. S. Marcus, M. Eriksson and A. R. Burns, *Journal of Physics: condensed matter*, 2004, **16**, R679.
50. G. P. Camilloto, C. G. Otoni, G. W. R. de Almeida, I. R. a. N. de Oliveira, L. H. M. da Silva, A. C. d. S. Pires and N. d. F. F. Soares, *ACS Food Science & Technology*, 2021, **1**, 745-753.
51. A. J. Burris and Q. Cheng, *Langmuir*, 2021, **37**, 14920-14929.
52. E. Lopez, D. F. O'Brien and T. H. Whitesides, *Journal of the American Chemical Society*, 1982, **104**, 305-307.
53. L. Gros, H. Ringsdorf and H. Schupp, *Angewandte Chemie International Edition in English*, 1981, **20**, 305-325.

54. H. H. Hub, B. Hupfer, H. Koch and H. Ringsdorf, *Angewandte Chemie*, 1980, **92**, 962-964.
55. H. Menzel, S. Horstmann, M. D. Mowery, M. Cai and C. E. Evans, *Polymer*, 2000, **41**, 8113-8119.
56. Z. Yuan, C.-W. Lee and S.-H. Lee, *Polymer (Guildford)*, 2005, **46**, 3564-3566.
57. Q. Cheng and R. C. Stevens, *Langmuir*, 1998, **14**, 1974-1976.
58. J. Brédas, R. Chance, R. Silbey, G. Nicolas and P. Durand, *The Journal of Chemical Physics*, 1981, **75**, 255-267.
59. Q. Huo, K. Russell and R. M. Leblanc, *Langmuir*, 1999, **15**, 3972-3980.
60. H. Shin, F. Jannah, E. J. Yoo and J.-M. Kim, *Sensors and Actuators B: Chemical*, 2022, **350**, 130885.
61. N. Charoenthai, T. Pattanatornchai, S. Wacharasindhu, M. Sukwattanasinitt and R. Traiphol, *J. Colloid Interface Sci.*, 2011, **360**, 565-573.
62. J.-M. Kim, J.-S. Lee, H. Choi, D. Sohn and D. J. Ahn, *Macromolecules*, 2005, **38**, 9366-9376.
63. S. Hankin, M. Downey and D. Sandman, *Polymer*, 1992, **33**, 5098-5101.
64. C. Khanantong, N. Charoenthai, T. Phuangkaew, F. Kielar, N. Traiphol and R. Traiphol, *Colloids Surf., A*, 2018, **553**, 337-348.
65. T. Pattanatornchai, N. Charoenthai, S. Wacharasindhu, M. Sukwattanasinitt and R. Traiphol, *Journal of Colloid and Interface Science*, 2013, **391**, 45-53.
66. J. Lee, E. J. Jeong and J. Kim, *Chemical Communications*, 2011, **47**, 358-360.
67. A. Reichert, J. O. Nagy, W. Spevak and D. Charych, *Journal of the American Chemical Society*, 1995, **117**, 829-830.
68. X. Chen, S. Kang, M. J. Kim, J. Kim, Y. S. Kim, H. Kim, B. Chi, S.-J. Kim, J. Y. Lee and J. Yoon, *Angewandte Chemie International Edition*, 2010, **49**, 1422-1425.
69. Y.-l. Su, J.-r. Li and L. Jiang, *Colloids and Surfaces B: Biointerfaces*, 2004, **39**, 113-118.
70. H. Beckham and M. Rubner, *Macromolecules*, 1993, **26**, 5198-5201.
71. A. Chanakul, N. Traiphol and R. Traiphol, *Journal of Colloid and Interface Science*, 2013, **389**, 106-114.
72. L. Rougeau, D. Picq, M. Rastello and Y. Frantz, *Tetrahedron*, 2008, **64**, 9430-9436.
73. S. Toommee, R. Traiphol and N. Traiphol, *Colloids and Surfaces A: Physicochemical and Engineering Aspects*, 2015, **468**, 252-261.
74. S. J. Kew and E. A. Hall, *Analytical chemistry*, 2006, **78**, 2231-2238.
75. H. C. Fry, J. M. Garcia, M. J. Medina, U. M. Ricoy, D. J. Gosztola, M. P. Nikiforov, L. C. Palmer and S. I. Stupp, *Journal of the American Chemical Society*, 2012, **134**, 14646-14649.
76. M. Gou, G. Guo, J. Zhang, K. Men, J. Song, F. Luo, X. Zhao, Z. Qian and Y. Wei, *Sensors and Actuators B: Chemical*, 2010, **150**, 406-411.
77. R. Potai, K. Faisadcha, R. Traiphol and N. Traiphol, *Colloids and Surfaces A: Physicochemical and Engineering Aspects*, 2018, **555**, 27-36.
78. N. Traiphol, A. Chanakul, A. Kamphan and R. Traiphol, *Thin Solid Films*, 2017, **622**, 122-129.
79. A. Wu, C. Beck, Y. Ying, J. Federici and Z. Iqbal, *The Journal of Physical Chemistry C*, 2013, **117**, 19593-19600.
80. D. J. Ahn, E.-H. Chae, G. S. Lee, H.-Y. Shim, T.-E. Chang, K.-D. Ahn and J.-M. Kim, *Journal of the American Chemical Society*, 2003, **125**, 8976-8977.
81. B. Yoon, H. Shin, E.-M. Kang, D. W. Cho, K. Shin, H. Chung, C. W. Lee and

J.-M. Kim, *ACS applied materials & interfaces*, 2013, **5**, 4527-4535.
82. S. Wacharasindhu, S. Montha, J. Boonyiseng, A. Potisatityuenyong, C. Phollookin, G. Tumcharern and M. Sukwattanasinitt, *Macromolecules*, 2010, **43**, 716-724.
83. O. Mapazi, P. K. Matabola, R. M. Moutloali and C. J. Ngila, *Sens. Actuators, B*, 2017, **252**, 671-679.
84. N. Traiphol, K. Faisadcha, R. Potai and R. Traiphol, *J. Colloid Interface Sci.*, 2015, **439**, 105-111.
85. C. Jia, J. Tang, S. Lu, Y. Han and H. Huang, *Journal of fluorescence*, 2016, **26**, 121-127.
86. S. W. Lee, C. D. Kang, D. H. Yang, J. S. Lee, J. M. Kim, D. J. Ahn and S. J. Sim, *Advanced Functional Materials*, 2007, **17**, 2038-2044.
87. N. K. Karmakar, S. Pandey, R. K. Pandey and S. S. Shukla, *Applied Spectroscopy Reviews*, 2021, **56**, 513-529.
88. X. Wang, X. Sun, P. A. Hu, J. Zhang, L. Wang, W. Feng, S. Lei, B. Yang and W. Cao, *Advanced Functional Materials*, 2013, **23**, 6044-6050.
89. J. Lee, H. T. Chang, H. An, S. Ahn, J. Shim and J.-M. Kim, *Nature Communications*, 2013, **4**, 2461.
90. J. Yoon, S. K. Chae and J.-M. Kim, *Journal of the American Chemical Society*, 2007, **129**, 3038-3039.
91. D.-H. Park, J.-M. Heo, W. Jeong, Y. H. Yoo, B. J. Park and J.-M. Kim, *ACS applied materials & interfaces*, 2018, **10**, 5014-5021.
92. H. Jiang, Y. Wang, Q. Ye, G. Zou, W. Su and Q. Zhang, *Sensors and Actuators B: Chemical*, 2010, **143**, 789-794.
93. H. Bhattacharjee, A. Preziosi and G. Patel, *The Journal of Chemical Physics*, 1980, **73**, 1478-1480.
94. A. C. S. Pires, N. d. F. F. Soares, L. H. M. da Silva, M. C. H. da Silva, A. B. Mageste, R. F. Soares, Á. V. N. C. Teixeira and N. J. Andrade, *The Journal of Physical Chemistry B*, 2010, **114**, 13365-13371.
95. A. Potisatityuenyong, R. Rojanathanes, G. Tumcharern and M. Sukwattanasinitt, *Langmuir*, 2008, **24**, 4461-4463.
96. C. Kim, C. Hong and K. Lee, *Biosensors and Bioelectronics*, 2021, **181**, 113120.
97. E. Lebègue, C. Farre, C. Jose, J. Saulnier, F. Lagarde, Y. Chevalier, C. Chaix and N. Jaffrezic-Renault, *Sensors*, 2018, **18**, 599.
98. D. H. Charych, J. O. Nagy, W. Spevak and M. D. Bednarski, *Science*, 1993, **261**, 585-588.
99. D. H. Charych, W. Spevak, J. O. Nagy and M. D. Bednarski, *MRS Online Proceedings Library (OPL)*, 1992, **292**, 153.
100. A. A. Ismail, F. R. van de Voort and J. Sedman, in *Techniques and Instrumentation in Analytical Chemistry*, eds. J. R. J. Paré and J. M. R. Bélanger, Elsevier, 1997, vol. 18, pp. 93-139.
101. A. R. Hind, S. K. Bhargava and A. McKinnon, *Advances in colloid and interface science*, 2001, **93**, 91-114.
102. H. Günther, *NMR spectroscopy: basic principles, concepts and applications in chemistry*, John Wiley & Sons, 2013.
103. H.-H. Perkampus, *UV-VIS Spectroscopy and its Applications*, Springer Science & Business Media, 2013.
104. G. G. Guilbault, *Practical fluorescence*, CRC Press, 2020.
105. B. J. Berne and R. Pecora, *Dynamic light scattering: with applications to chemistry, biology, and physics*, Courier Corporation, 2000.

106. C. E. Hall, *Introduction to electron microscopy*, LWW, 1954.
107. G. S. Lee, T. Y. Kim and D. J. Ahn, *Journal of Industrial and Engineering Chemistry*, 2018, **67**, 312-315.
108. Z. Ma and J. Ren, *Colloids Surf., A*, 2007, **303**, 179-183.
109. J. Yoon, K. A. B. Azizan, H. O. Yoo, S. Okada and J. M. Kim, *Macromolecular rapid communications*, 2009, **30**, 981-985.
110. E. Shirai, Y. Urai and K. Itoh, *The Journal of Physical Chemistry B*, 1998, **102**, 3765-3772.
111. A. Saito, Y. Urai and K. Itoh, *Langmuir*, 1996, **12**, 3938-3944.
112. G. Ma and Q. Cheng, *Langmuir*, 2005, **21**, 6123-6126.
113. D. Seo and J. Kim, *Advanced Functional Materials*, 2010, **20**, 1397-1403.
114. Q. Cheng, M. Yamamoto and R. C. Stevens, *Langmuir*, 2000, **16**, 5333-5342.
115. P. J. Flory, *Principles of polymer chemistry*, Cornell university press, 1953.
116. M. Worboys, *Journal of Materials Chemistry*, 1998, **8**, 903-912.
117. T. Yokoyama, A. Masuhara, T. Onodera, H. Kasai and H. Oikawa, *The Journal of Physical Chemistry C*, 2011, **115**, 22121-22125.
118. G. Ma, A. M. Müller, C. J. Bardeen and Q. Cheng, *Advanced Materials*, 2006, **18**, 55-60.
119. A. Chanakul, N. Traiphol, K. Faisadcha and R. Traiphol, *J. Colloid Interface Sci.*, 2014, **418**, 43-51.
120. A. Chanakul, R. Traiphol and N. Traiphol, *Colloids and Surfaces A: Physicochemical and Engineering Aspects*, 2016, **489**, 9-18.
121. C. P. d. Oliveira, N. d. F. F. Soares, E. A. F. Fontes, T. V. d. Oliveira and A. M. M. Filho, *Food Chemistry*, 2012, **135**, 1052-1056.
122. K. W. Kim, J. M. Lee, Y. M. Kwon, T.-Y. Choi, J. Y. H. Kim, S. Bae and J.-A. Song, *Macromolecular Research*, 2018, **26**, 284-290.
123. N. Mino, H. Tamura and K. Ogawa, *Langmuir*, 1991, **7**, 2336-2341.
124. N. Ahmad Daud, B. W. Chieng, N. A. Ibrahim, Z. A. Talib, E. N. Muhamad and Z. Z. Abidin, *Nanomaterials*, 2017, **7**, 135.
125. W. Xue, D. Zhang, G. Zhang and D. Zhu, *Chinese Science Bulletin*, 2011, **56**, 1877-1883.
126. A. M. Alam, J. P. Yapor, M. M. Reynolds and Y. V. Li, *Materials*, 2016, **9**, 202.
127. J. L. Ordóñez, R. M. Callejón, A. M. Troncoso and M. C. García–Parrilla, *Journal of Food Composition and Analysis*, 2017, **63**, 139-147.
128. W. Du Toit, K. Lisjak, J. Marais and M. Du Toit, 2006.
129. J. L. Moreira and L. Santos, *Analytical and bioanalytical chemistry*, 2005, **382**, 421-425.